PhD-FSTC-2015-08
The Faculty of Sciences, Technology and Communication

DISSERTATION

Defense held on 11/02/2015 in Luxembourg

to obtain the degree of

DOCTEUR DE L'UNIVERSITÉ DU LUXEMBOURG

EN PHYSIQUE

by

Anna DJEMOUR
Born on 16 February 1988 in Cologne (Germany)

CONFINEMENT EFFECTS ON A LOW MOLECULAR WEIGHT LIQUID

Dissertation defense committee

Dr Roland Sanctuary, dissertation supervisor
Professor, Université du Luxembourg

Dr Christiane Alba-Simionesco
Director, Laboratoire Leon Brillouin, Saclay

Dr Andreas Michels, Chairman
Professor, Université du Luxembourg

Dr Patrick Huber
Professor, Technische Universität Hamburg-Harburg

Dr Jörg Baller, Vice Chairman
Post-Doc, Université du Luxembourg

Contents

1. Introduction

> The whole is greater than the sum of its parts
>
> *Aristotle*

Composite systems are becoming increasingly important in today's world. Such materials, especially when combined with nanostructures, can open up new levels of smart functionalities only seen in the composite. Nanoporous glasses in combination with glass forming resins are investigated as both components are ideal for the investigation of composites.

The development of nanoporous structures in the laboratory by C. Kresge, R. Ryoo and G. Stucky [1, 2, 3] is an important milestone in science as evidenced by its inclusion on the list of Nobel prize predictions for 2014 compiled by Sciencewatch [4]. Porous materials with nanometer sized pores with their large internal surface areas can be used to study confinement and adsorption effects (amongst others) and be employed in a large variety of industrial applications as catalysts, bio-sensors or molecular sieves.

Glass formers are omnipresent in nature and industrial applications whilst not being fully understood. This is nicely summarized by the following quote by the Nobel prize winner P.W. Anderson who said that "*the deepest and most interesting unsolved problem in solid state physics is probably the theory of the nature of glass and the glass transition.*[5]"

At high temperatures glass forming materials are in thermodynamic equilibrium, but as thermodynamic variables like the temperature or pressure are changed, their viscosity increases dramatically (i.e. the molecular structural rearrangements are increasingly impeded). The formed glass is amorphous without any long-range order though with solid-like mechanical properties. A qualitative description of the behavior at the glass transition is given by the notion of a characteristic length scale of subsystems of molecules which are clusters of particles that can relax collectively [6]. However this length scale can be difficult to determine experimentally.

One way to learn more about glass formers is to study the effect of confining them to small pores. As the confinement dimensions come within the range of the characteristic length scale, the glass transition can be hindered. However other effects in confinement such as the surface interactions need to be considered in the determination of the effect of the finite size.

The behavior of liquids in the pores is also interesting as the diffusion through the pores offers insight into liquid transport phenomena on very small scales [7, 8, 9, 10] besides the macroscopic inuence of the components on the composite [11, 12, 13, 14].

This work discusses the above phenomena in addition to the the temperature dependence of the flow of a glass former through the pores, probing the influence of the restricting geometry on the dynamics of the liquid which result from the changes in structure and molecular mobility.

In this thesis the investigated composite is made up of controlled pore glasses with a network of interconnected nanometer sized pores filled with the low molecular weight oligomer Diglycidyl Ether of Bisphenol A (DGEBA). The pore size and the chemical properties of the surface of the pores are varied to gain insight into the physics of the flow through the pores and the glass transition of confined DGEBA. The principal experimental techniques used to investigate the system are thermomechanical analysis (TMA), differential scanning calorimetry (DSC) and broadband dielectric spectroscopy.

After a short introduction into the theoretical and experimental background regarding fluids in porous systems, the glass transition and the possible dynamics in confinement, the materials and experimental methods used are set-out. The results of the characterization of the components are presented in chapter 4. Chapter 5 reports on the findings from the TMA measurements of the macroscopic thermal expansion of the pg/DGEBA system. The observation of a freezing of the flow through the pores is discussed for the first time. Additionally a core-shell model for the molecules in the untreated pores is presented. In chapter 6 the specific heat capacity of the confined DGEBA is analyzed. It will be shown that the glass transition in untreated pores is increasingly influenced by the surface interactions as the pore size is decreased. Surface treatment with an estimate of the characteristic length scale involved in the glass transition. The next chapter compares the results from TMA and DSC to be able to complete the picture of the complex behavior exhibited by the system. This is followed by the investigation of the glass transition over a large range of frequencies.

Finally the results presented in this thesis are briefly summarized in the context of their interpretation and the findings from ongoing research into confined glass formers.

2. Theoretical and experimental background

2.1 Liquids in pores

When nanoporous glass made up of a network of interconnected pores comes into contact with a wetting liquid, a large capillary pressure $p_{Laplace}$ acts on the fluid sucking it into the pores. The pores deform due to the difference between the gas pressure of the capillary condensation p_0 and the much higher vapor pressure at saturation p, as described by the Kelvin equation:

$$ln(p/p_0) = (V_M/RT) \cdot p_{Laplace} \tag{2.1}$$

$$p_{Laplace} = \frac{2\sigma cos(\Theta)}{r} \tag{2.2}$$

with molar volume V_M, gas constant R, surface tension of the fluid σ, contact angle between the liquid and the pore surface Θ and pore radius r. First a single molecule layer wets the pores followed by the bulk in a meniscal form. This was shown by Huber et al for water in porous glasses [9] and is analoguous to adsorption of gas molecules in pores. The subsequent uptake of the fluid increases monotonically and follows the $\sqrt{t}$ Lucas-Washburn Law [15, 16] (calculated from Hagen-Poiseuille flow), depending on the surface tension, viscosity and density of the fluid and the contact angle to the pores. Gravitational forces can be neglected in this calculation compared to the Laplace pressure in nanometer pores.

The deformation of porous structures is known as the Bangham effect with the interfacial energy lowered by the adsorption of a liquid at the pore walls [11, 17]. The negative Laplace pressure would then cause an expansion of the structure following the spontaneous imbibition of a fluid. Further expansion follows till the pressure equilibrates and the pores are filled. When this happens and the flow of the liquid through the glass is uninhibited, the liquid does not deform the pores anymore. However one has to take into account that especially for high surface interactions between the pores and

the filler, there is an immobile adsorbed layer of liquid present at the pore walls, which additionally influence the deformation.

Information about the adsorption and flow of a fluid in pores and the deformation of the pores can be obtained by simply measuring the mass uptake [18], from x-ray [19] and neutron scattering investigations [14, 20] and mechanical analysis by DMA [21, 22, 23].

2.2 Glass formers

This section gives a short introduction into the phenomena of materials that can transition into a glassy state. Glass forming materials exhibit a freezing of the molecular dynamics without the characteristic long range order of christallization when external parameters such as pressure, temperature or shear stress are varied. In this state the glasses are amorphous.

Most glass formers are either structural or ideal glass formers. The former need to be supercooled below the crystallization temperature becoming glassy at about $T_g = \frac{2}{3}T_m$. Their entropy is higher than in the crystalline state i.e. the glass state is not in equilibrium. Ideal glass formers do not crystallize and therefore the glass state could be described as their solid-like state.

Due to the lack of long range order and therefore structural characterization in the amorphous glass, the nature of this state and transition are still up to debate. This problem is complicated by the fact that at the glass transition time-dependent phenomena such as relaxations superimpose the changes of thermodynamic quantities such as entropy, density or thermal expansion. It is therefore unclear wether it is a phase transition or just a dynamic phenomenon. Additionally there are many different materials which can become glass-like, from the small water molecule to large proteins with significally differing other properties which makes it difficult to find common explanations.

The glass transition is evident in changes in many different physical properties such as the heat capacity, thermal expansion or density or in the observations of the dramatic increase of the viscosity and structural relaxation rates. It is therefore difficult to define the actual transition temperature as the glass transition is strongly dependent on the thermal history and the experimental method complicating the correlation of the glass transition temperatures observed in different physical quantities. In the specific heat capacity for example a step between the glassy and the liquid-like regime is observed experimentally, while in the thermal expansion or the density there is a kink in the slope of the curves seen at the glass transition. One also has to separate the dynamic, i.e. frequency dependent relaxation from the

thermal glass transition driven by kinetics as these can differ considerably.

Due to the problems outlined above, through decades of research into the mechanisms underlying the glass transition with many different proposed theories, the question of its nature is still not clearly solved.

However the most common ideas and approaches are shortly introduced here starting with the concept of the cooperative rearranging regions by G. Adam and J.H. Gibbs. This concept was extended in the notion of dynamical heterogeneities by Donth et al [24].

Cooperative Rearranging Regions (CRR)

Adam and Gibbs [6] proposed a molecular kinetic theory of cooperative rearranging regions where a subset of molecules can rearrange independently upon large enough energy fluctuations. Fragile glass formers show a non-Arrhenius behavior for the dielectric relaxations of glass formers near T_g. Gibbs et al therefore postulated that the increase in relaxation times is proportional to an increase of cooperativity of the molecular reorientations, i.e. a decrease in the number of possible configurations [25]. This means that more and more molecules have to behave cooperatively. The subsets/cooperative rearranging regions are then the smallest regions that can undergo a transition to a new configuration without influencing other regions at or outside their boundary.

These CRR's are negligibly small at temperatures $>> T_g$ and become larger as the transition region is approached with decreasing temperature. As their size ξ increases near T_g the reorientational mobility of each molecule implies the cooperative motion of more molecular neighbours which means the time needed for the reorientation increases more and more. Therefore the relaxation time τ increases dramatically till at a temperature T_0 the entropy S_0 with only a few or even 1 available configuration for the glass former meaning the whole sample or a macroscopic part is included in the cooperative rearranging region.

Quantitatively, the curvature of the Arrhenius plot of the α-relaxation determined from the empirical William-Landels-Ferry fit is related by Gibbs et al [6] to the configurational entropy of the system S_c for the relaxation times τ:

$$\tau = \tau_0 exp\left[\frac{C}{TS_C}\right],\ S_C \to 0 \Rightarrow \tau \to 0 \tag{2.3}$$

with C as a material specific constant. The characteristic length scale of the CRR can then be determined from the proportionality of the number of particles in a CRR to the configurational entropy $N \approx S_c^{-1}$:

$$\xi = 2\alpha S_c^{-1/3} \tag{2.4}$$

with the material specific parameter α. The resulting values give a lower limit for the size of the cooperative rearranging regions.

Dynamical Heterogeneities

Donth et al treated the notion of a characteristic length scale using the concept of independently fluctuating subsystems [24]. He extended the idea of CRRs for a kinetic view of the glass transition by evaluating the entropy of a smallest possible subset of molecules which is still representative of the whole system. The resulting size of the cooperative region is usually larger than the one calculated using the Adam-Gibbs method as it also includes an immobile part which causes the kinetic glass transition. This is because of the dynamical heterogeneities present in the cooled state where, on short time-scales, the reorientational mobility of each molecule is different from all neighbouring molecules. Compared to the dynamically homogeneous nature at high temperatures the mobility is similar only on long time-scales.

The characteristic size of these dynamical heterogeneites is difficult both from simulations and from experiments due to the long time-scales of the relaxations near the glass transition. Using the von Laue-Landau fluctuation approach, Donth relates the entropy fluctuations due to the temperature fluctuations:

$$\delta\bar{T}^2 = \frac{k_B T^2}{C_V} \tag{2.5}$$

to the heat capacity contribution of the dynamic glass transition Δc_p:

$$\delta\bar{S}^2 = k_B C_p \tag{2.6}$$

using the smallest volume V_s of subset of molecules that can represent the whole system, and $\delta\bar{T}^2$ the corresponding temperature fluctuations in this subsystem. This results in an equation for this volume as

$$V_s = k_B T^2 \frac{\Delta(1/c_p)}{\rho(\delta T)^2}, \tag{2.7}$$

with the step height $\Delta(\frac{1}{c_p}) = (\frac{1}{c_p})_{glass} - (\frac{1}{c_p})_{liquid}$.

The differences in the constant volume and constant pressure heat capacity c_v to c_p are neglected in this calculation. All quantities needed can be accessed using temperature modulated differential scanning calorimetry though the width of the temperature fluctuations $\delta\bar{T}^2$ needs to be corrected to the frequency dompain compared to the measured temperature domain of the dynamic glass transition according to K. Schröter [26].

2.3 Dynamics in Confinement

First experiments done by Jackson et al [27] on crystallizing molecules showed a decrease in melting temperature which was even suppressed in sufficiently small pores. The study of glass forming materials in confinement was undertaken as it was proposed as a way to confirm the idea of CRR's and determine their size ξ when molecules are confined on a length scale in the range of ξ [28]. In the latter case size effects around the glass transition temperature should appear when ξ is close to the size of the confinement. All the molecules in the confined space are involved in the dynamics and would therefore relax faster than in the bulk. This implies that the glass transition would be decreased compared to the bulk. Additionally the type of confinement should not influence the possible results for ξ as this is a property of the glass former.

Initial studies done by Mckenna et al [29] with differential scanning calorimetry (DSC) on salol in controlled pore glasses seemed to confirm this idea and proposed a formula for the decrease in T_g, (ΔT_g), as proportional to the inverse pore diameter $(1/d)$. However further studies with DSC, dielectric spectroscopy, neutron scattering or solvation dynamics (amongst others) in the last 20 or so years have shown that the picture of dynamics in confinement is far more diverse, for reviews see [30, 31, 32, 33].

Especially where thin films are employed for a 1-Dimensional confinement, there have been very conflicting results published from large decreases to large increases or even no effect on the glass transition. Several have postulated that this range of results is solely due to the manner of preparation of the samples, especially cleanliness and sample environment with no effect of the actual confinement. The molecular dynamics in the films are also largely dependent on wether the film is in contact with a surface on one or both sides of the thin film or is freestanding [34].

3-Dimensional confinement such as droplets in rubber or in hard spheres [35, 36] resulted in quite large decreases in glass transition temperatures. These consisted an easier system for the evaluation of dielectric spectroscopy results as the insulating matrix resulted in no dc-conductivity contribution at low frequencies so that the whole frequency range accessible could be analyzed.

For the confinement in porous systems such as porous glasses (with randomly or uniformly oriented channels), amounting to a 2-dimensional confinement, a depression in transition temperature was usually observed to a slightly smaller degree compared to 3-dimensional systems. There have, however also been results published with an increase in T_g or even two separate glass transitions as seen in [37].

Comparing the available literature one has come to the conclusion that in addition to size limitation effects, surface effects due to the interactions between glass-former and confining material need to be considered. These could be due to H-bonding and/or van der Waals forces. Especially for hydrophilic surfaces of the confining material, most investigations showed direct or indirect evidence of a significantly slowed or even immobilized surface layer. This means that the amount of actual material which can still be part of the collective motion is assumed to be less than the confinement size [38].

The surface layer could be distinguished for the droplets clearly in dielectric spectroscopy measurements [35], and is also seen as a reason for the conflicting results in thin films. As the confinement in only 1 dimension would be expected to have less of an effect on the glass former, other mechanisms such as through the surface layer might be so large as to hinder the cooperative motion much more strongly than expected leading to a total or even over-compensation of the expected confinement reduction of T_g .

The dynamic exchange between this interfacial phase and the inner bulk-like material [39] would also explain increases in glass transition temperature and further glass transitions observed in porous systems. The strength of the surface interactions generally depends not only on the hydrophilicity but also on the type of filler molecules (polar vs. nonpolar, OH-groups which can bond to the surface; liquids, polymers or liquid crystals) and on the morphology of the surface walls. Attractive surfaces would lead to thicker surface layers which, depending on the properties of the filler, would have a lower mobility [40, 41].

The dielectric spectroscopy results by the group of Kremer for various glass formers in random and oriented PG even showed evidence for three regions with a completely immobilized layer right at the surface, an interfacial part with reduced mobility and the liquid-like main part [33, 42, 39]. The third layer would not necessarily be seen using other methods as the two parts of the composite impact the total measurement result differently depending on the measurement method (in differential scanning calorimetry the two components are measured in parallel while in dielectric spectroscopy they are measured more in series).

Zheng et al amongst others suggested that the negative pressure between the glass former and confiner (due to the mismatch in thermal expansion coefficients between the two) would explain the depression of the glass transition temperatures [43]. However already in the initial results from Mckenna et al, they estimated that the negative pressure present in the pores is far too small near the glass transition to cause the observed changes in T_g. This was confirmed by investigations by Simon et al [44] and Koppensteiner et al [45] showing that, though the negative pressure is measurable, the iso-

choric conditions would have to be imposed at much higher temperatures than observed to cause a depression in T_g.

Changes in the molecular motion might also be attributed to reductions in the density of the confined material due to the size limitation. Changes in density were measured for confined tolene with neutron diffraction with lower densities than in the bulk for both native and silanized surfaces [40, 20]. This means that in pores even if an initial reduction in T_g is observed, when the values were corrected for the density, T_g is usually higher than in the bulk.

Further the confined glass transition region is usually broadened compared to the bulk due to the wider distribution of relaxation rates [29, 36, 46, 47, 39, 42].

If all the mechanisms such as finite size and surface effects involved can be quantitavely identified and separated from each other, a notion of the cooperativity length can be established. Varying results have been published between $1 - 3nm$ up to 12nm [48, 26]. These values are however strongly dependent on the method and calculations used.

3. Materials and Methods

3.1 Materials

3.1.1 Diglycidyl Ether of Bisphenol A (DGEBA)

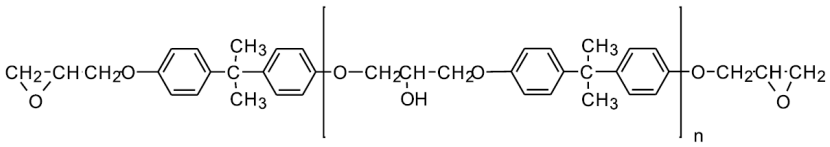

Figure 3.1: The DGEBA molecule $C_{21}H_{24}O_4$

In the present PhD project the glass former Di-Glycidyl Ether of Bisphenol A (DGEBA) was investigated in confinement. It is a low molecular weight oligomer with an almost ideal glass transition. The DGEBA variant used here is D.E.R. 331 from Dow Chemicals which is a product of epichlorohydrin and bisphenol A [49]. This epoxy resin is commonly used as a resin for applications such as adhesives and coatings. It is easily polymerized using curing agents such as Diethylenetriamine (DETA).

Generally, the molecular weight M_n of DGEBA is dependent on the degree of polymerization $n = 0.15$ of its molecular chain:

$$M_n = (340 + 248 \cdot \ n)\, g/mol$$

For D331 this results in a molecular weight of about 374 g/mol according to the manufacturer's specifications. The individual chains are therefore quite short, around 3nm in length.

3.1.2 Porous glass

Porous materials such as porous glasses consist of a network of interconnected channels out of silica glass (please refer to [50] for a review about porous glasses). Pore sizes smaller than 2nm are known as micropores, up to 50nm

they are commonally described as mesoporous or nanoporous while larger pores are macropores. The porous network is very rigid with a very small thermal expansion in the range of quartz glass.

Due to their large internal surface areas (up to $1000\,m^2/g$) Porous glasses have many uses as molecular sieves in chromatography of materials like polymers and proteins, as substrates for the sequential analysis and synthesis of DNA, as catalysators, as detectors (for example Tscherenkow detectors) or for nuclear waste immobilization.

Materials with an internal porous structure can occur naturally (e. g. zeolites with very small pores are useful for trapping water or oil) or can be manufactured by different processes such as spinodal decomposition or via the sol-gel transition. Different shapes of porous glass or porous glass powder are available with pore channels or pores with controlled sizes.

Spinodal decomposition includes a metastable phase separation in borosilicate glasses which is then followed by the acid leaching of the soluble sodium borate-rich phase, first observed by W.E.S.T̃urner et al [51]. The resulting porous structure is consolidated by drying at very high temperatures ($1200\,°C$). Both the process and the product are known as VYCOR, Corning's brand name for porous glass. Vycor typically has a low porosity (volume of the pores compared to the total volume) of around 30% and a narrow pore size distribution. The structure of Vycor was fully characterized by Levitz et al [52]. In the present thesis we used circular disks (diameter: 5 mm; thickness: 1-2 mm) of Vycor 7930 with a typical pore diameter of 4 nm. Further samples with pore sizes between 44 and 111nm were provided by Vitrabio who manufactured the porous glass using their own patented process Trisoplac based on the Vycor process [53].

In the sol-gel process, the parameters (such as the type of precursor and ratio of the precursor to water, or the gelation and drying temperatures) can be varied extensively thereby controlling pore size and pore size distribution. The precursor sol such as tetraethyl orthosilicate (TEOS) becomes a gel with a liquid and solid phase. Removing the liquid phase leaves a network of silica spheres attached to each other with the voids as pores. This usually results in a larger pore size distribution than for the Vycor glass. Sol-gel samples with pore diameters varying between 2.5 and 20nm were obtained from Angstrompore. The samples were available as circular discs with a diameter of about 10mm and around 3-4mm thick.

Generally porous glasses are very sensitive to fluctuations in temperature. If they are heated/cooled too quickly, microcracks appear in the glass breaking up the internal porous structure. Therefore samples were handled with care during all steps: heating/cooling rates were generally chosen much smaller than 5K/min.

3.1.3 Sample preparation

The various porous glass samples are first cleaned before any modifications or filling. They are very slowly heated under vacuum of $< 10^{-5}$ mbar up to 150 °C and kept at this temperature for at least 24 hours. Older samples, especially if left in air, started to appear brown due to organic material trapped inside . trapped inside the pores. Before using them for investigation, they had first to be rinsed in H_2O_2 and then to be heated under vacuum.

Silanization

The surfaces of the pore walls in silica porous glass are inherently hydrophilic due to the presence of hydroxyl groups on the surface. When filling the pores, this can lead to strong interactions between the filler and the pores. To hinder the hydrogen bonds forming between the filler molecules and the pore surfaces, the latter can be functionalized. This surface modification is done by grafting a silanizing agent onto the hydroxyl groups at the pore surfaces. Depending on the chemical properties of the agent, silanization can reduce the hydrophilic character of the surface.

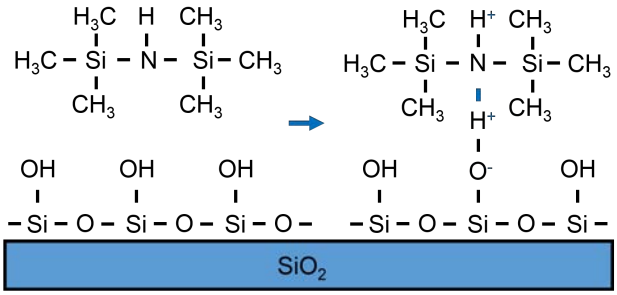

Figure 3.2: Schematic of the HMDS molecule attaching like an umbrella to the OH groups at the pore surfaces.

Hexamethyldisilizane (HMDS, molecular formula $C_6H_{19}NSi_2$) is used as the silanizing agent in many studies on porous glasses as it is a small molecule greatly enhancing hydrophobicity (see for example [47, 54, 21]). Small-sized silanes are used, so that the original pore diameters are not substantially reduced by the coating process. This is important to ensure comparability between the analysis of native (untreated) filled pores and silanized filled pores.

The silane atoms form hydrogen bonds with the OH-groups at the silica walls. Even if not all OH-groups bond with the silane, the umbrella-like shape of the HMDS molecule (shown in figure 3.2) means that neighbouring

OH-groups could be covered meaning a full layer of trimethylsilyl Si-$(CH_3)_3$ groups is present on the pore surface as a result of the grafting. To achieve the actual silanization, the cleaned porous glasses are completely immerged into the HMDS liquid under a closed hood for 24 hours at 55 °C. Finally, to get rid of un-reacted silane molecules, the porous glass samples are steamed with Choloroform for another 24 hours and cleaned (procedure according to G.Blum et al [55]).

Filling

The samples are filled with DGEBA in a vacuum chamber. This chamber is heated to 80 deg C and set under a vacuum of $< 10^{-5}$ mbar. The DGEBA is introduced into the chamber via a syringe. For glasses with large pores a high filling fraction can be achieved within 24 hours; several months are needed to fill the glasses with the smallest pores.

The filling fraction f is defined as the ratio of the volume of pores filled with DGEBA to the total volume of pores. Using the porosity $\phi = V_{pores} \cdot \rho_{PG}$, where ρ_{PG} represents the mass density of the porous glass sample and V_{pores} the volume of the pores, the filling fraction is obtained as

$$f = \frac{m_{filler}/\rho_{filler}}{m_{PG} \cdot \phi/\rho_{PG}} \tag{3.1}$$

with the masses of the porous glass m_{PG} and of the DGEBA filled into the pores m_{filler}, and the densities of the porous glass ρ_{PG} and of DGEBA ρ_{filler}.

3.2 Methods

3.2.1 Nitrogen adsorption/desorption

The surface and internal structure of porous glasses can be evaluated by measuring the adsorption and desorption isotherms of a gas in the samples. A comprehensive review of this technique can be found in the book by S.Lowell et al [56]. The following section gives a short overview.

A controlled amount of a gas such as Nitrogen, Helium or Argon is introduced into a bulb containing the sample. The gas pressure P -relative to the pressure in an empty reference bulb P_0 - diminishes as gas molecules are adsorbed onto the surface of the adsorbent till it reaches a dynamic equilibrium value i.e. a constant relative pressure. The amount of adsorbed gas can then be calculated from the difference in the gas pressure. By successively adding

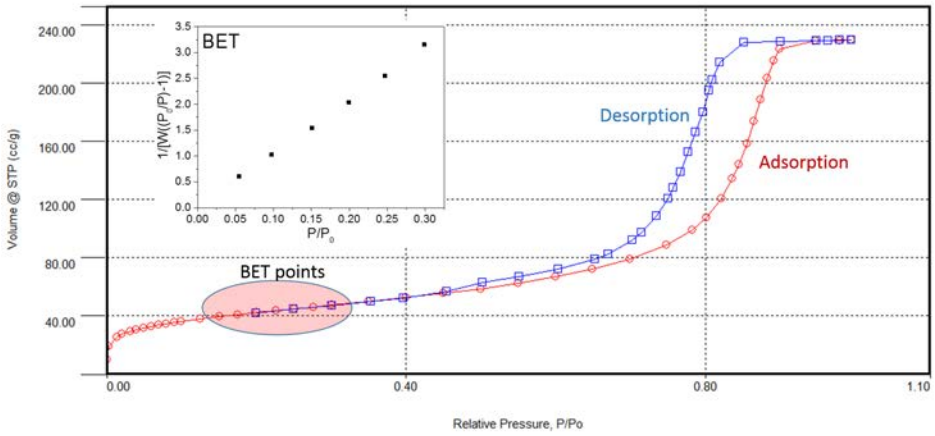

Figure 3.3: Nitrogen adsorption (red line) and desorption (blue line) isotherms for a Vycor porous glass. The volume of adsorbed gas is normalized for STP conditions. The points used for the analysis of the surface area are marked BET and are shown in the inset plotted for $\frac{1}{[W((P/P_0)-1)]}$.

more gas molecules into the bulb, a series of relative pressures P/P_0 between 0 and 1 at a constant temperature (77K, i.e. the boiling temperature of nitrogen) make up the adsorption isotherm. By lowering the relative pressure in steps, the volume of adsorbent is diminished and the amount of removed gas can be measured, resulting in a corresponding desorption isotherm.

The general shape of the isotherm can reveal the type of material such as porous vs. non-porous [57] while the shape of the hysteresis between the adsorption and desorption curves indicates the type of pores (cylindrical, slit-shaped, spherical, different wedge shapes, ink-bottle-shaped) [58].

Surface area by BET Analysis

Brunauer, Emmett and Taylor (BET) [59] extended Langmuir's ideas [60] for the calculation of the surface area S of a material when a single layer of molecules is adsorbed. They took into account that adsorbates do not form single layers of molecules onto the adsorbate but that in some areas there might be several molecules layered while in other places a first layer might not yet have formed, see figure 3.4 for clarification. Langmuir's equation for a single layer:

$$\frac{W}{W_m} = \frac{C \cdot (P/P_0)}{1 + C \cdot (P/P_0)} \tag{3.2}$$

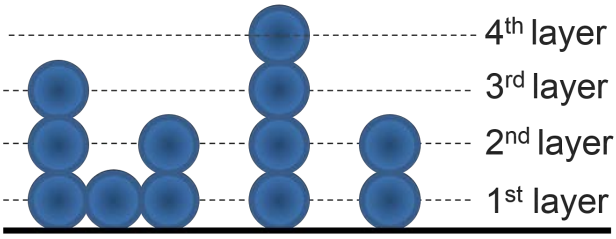

Figure 3.4: Demonstration of possible adhesion of molecules onto a surface, showing that some places on the surface might already be covered in several layers while no molecules have yet adhered to other points on the surface necessitating the multilayer BET formula for the surface area compared to Langmuir's equation.

therefore needed to be developed for multi-layer adsorption:

$$\frac{1}{W((P/P_0)-1)} = \frac{1}{W_m C} + \frac{C-1}{W_m C}\frac{P}{P_0} \tag{3.3}$$

with W representing the weight of the gas adsorbed at P/P_0 and W_m the weight of a monolayer of the adsorbate (covering the whole surface). C is a constant yielded by the adsorption and desorption rate equations at equilibrium indicating the magnitude of the adsorbate/adsorbent interaction.

In the plot of $\frac{1}{[W((P/P_0)-1)]}$ against the relative pressure for several values of P/P_0 (the linear regime is chosen here between 0.05 and 0.35) of the adsorption isotherm (see the inset marked BET in figure 3.3), the slope s and intercept i can be evaluated:

$$s = \frac{C-1}{W_m C}\ ,\ i = \frac{1}{W_m C} \tag{3.4}$$

leading to an expression for $W_m = 1/(s+i)$.

The surface area S per gram of porous glass can then be calculated using the molecular cross-sectional area σ_{gas} of the adsorbate, its molecular weight M, the Avogadro number N_A and the actual sample weight w:

$$S = \frac{W_m \cdot N_A \cdot \sigma}{M \cdot w} \tag{3.5}$$

In our experiments nitrogen is used as the adsorbate gas as its size is well defined, it is inert and additionally easily available and practical to handle.

Porosity

Other parameters describing a porous material like the porosity can be determined by looking at higher values of P/P_0 in the adsorption and the desorp-

tion curve. First, the total pore volume V_{pores} is determined from the amount of vapor adsorbed at a value of P/P_0 just below 1 assuming the pores are filled with liquid. However, this value can be problematic for smaller pores as the actually accessible pore volume (due to blocked pores) is usually less. Audonnet et al therefore recommended the use of the porous volume measured at the end of capillary condensation as this value stands for the actual volume which can be filled with the adsorbate [20]. The porosity ϕ can then be calculated using the specific density of the porous glasses: $\phi = V_{pores} \cdot \rho_{PG}$.

The average pore size for cylindrical pores is proportional to $2 \cdot V_{pores}/S$. For the pore size distribution analysis, the desorption isotherm is usually better suited. This is due to the lower P/P_0 values for the same adsorbent volumes, meaning one is closer to equlibrium (as seen in the nitrogen adsorption/desorption curves in figure 3.3). Classical macroscopic theories such as that developed by Barrett, Joyner and Hallenda (BJH theory) [61] look at the stepwise change in adsorbed gas volume to calculate the pore radii for each step ($r_p = r_c + t_i$, with the initial physically adsorbed layer t_i and the remaining radius r_c of capillary condensation).

However macroscopic theories usually underestimate the filling of the smaller pores necessitating a molecular level description. Density functional theory [62, 63] or Monte Carlo [64] simulations can be used in this case. The experimental isotherm is given by a Generalized Adsorption Isotherm (GAI) equation:

$$N(P/P_0) = \int_{W_{min}}^{W_{max}} N(P/P_0, W) f(W) dW \tag{3.6}$$

for different pore widths W and the pore size distribution $f(W)$. For a system of adsorbate/adsorbent (in this case Nitrogen/Silica), the set of $N(P/P_0, W)$ isotherms is obtained from Non-Local DFT of inhomogeneous fluids or Grand Canonical MC simulations. The equation can then be solved numerically.

Measurement

The nitrogen adsorption/desorption isotherms of the porous glasses used here were measured using a Nova2000e from Quantachrome Instruments. The sample is first degassed in the left sample holders (see figure 3.5) and can be heated to the required degassing temperatures using heating mantles. The bulb containing the sample is then placed in one of the right sample holders next to an empty reference bulb where P_0 is continuously measured. To ensure equilibrium and reliable values for P_0, a low pressure tolerance and high equilibration times were set. Typically, 30 adsorption and 29 desorption points (with each point taking about 20 minutes to measure depending on the sample) were measured with enough points for the BET surface area in

Figure 3.5: Nitrogen adsorption/desorption setup: Nova 2000e with 2 placements for degassing on the left and the sample holder with the empty reference holder above the nitrogen dewar on the right.

the linear regime (i.e. minimum 3, usually 6 relative pressures between 0.1 and 0.3) and a higher frequency of points between relative pressures of 0.6 and 0.9 as these are more valuable for the pore size distribution calculations. The measurements were made using Nitrogen gas as an adsorbent and cooled to 77K with liquid Nitrogen in a dewar. The isotherms were then evaluated using the Quantachrome Novawin Software. The results however are only exact if the minimum surface area of the measured sample is at least $10\,m^2/g$ which makes it difficult to analyze very small samples of porous glass. For those pore sizes where only smaller amounts are available, the results using the Nova2000e could not be trusted quantitavely, though different pore sizes could be compared qualitatively and the main results made available by the manufacturer were used. All samples were also filled with H_2O and weighed as a further confirmation of the porosity and thereby the possible filling fraction.

3.2.2 Contact angle

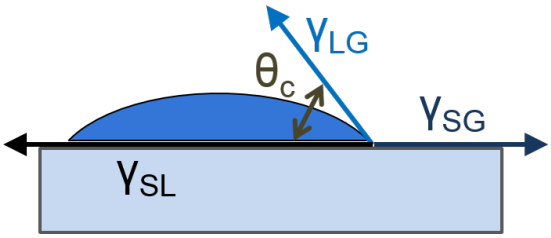

Figure 3.6: Scheme of a drop of liquid on a solid surface showing the surface energies γ_{LG}, γ_{SG}, γ_{SL} between the various interfaces (liquid-gas, solid-gas, solid-liquid) respectively, and the contact angle θ_C.

The angle where a liquid-gas interface meets a solid surface is known as the contact angle. This angle reflects the intermolecular interactions between the surface-liquid-gas combination when in thermodynamic equilibrium for a certain temperature and pressure. Young's equation [65] quantifies this relationship for the contact angle θ_C (see figure 3.6):

$$cos\,\theta_C = \frac{\gamma_{SG} - \gamma_{SL}}{\gamma_{LG}} \tag{3.7}$$

with the interfacial surface energy γ_{SG} between the solid and gas, γ_{SL} between the solid and liquid and γ_{LG} for the liquid-gas interface. When the solid is completely wetted by the liquid the contact angle is 0 with a strong interaction between the solid and liquid. This can be observed for example for water on a flat metallic or ceramic surface. A contact angle of $\theta < 90$ stands for a high wettability, which in the case of water as a liquid means that the solid surface is known as hydrophilic. A lower wettability characterized by a $\theta > 90$ implies a hydrophobic surface (for water). Contact angle measurements can therefore be used to check the effect of the silanization of a surface. This was done using a contact angle setup from OEG GmbH with the help of Marlena Filimon. A droplet of liquid is pipetted onto the surface and photographed with an iDS camera and evaluated for the contact angle with the setup's SURFTENS software.

3.2.3 Differential scanning calorimetry (DSC)

Differential Scanning Calorimetry (DSC) is the most commonly used calorimetric method allowing the determination of heat flows $HF = \frac{dQ}{dt}$ allows for determining heatflows generated by temperature gradients between the

sample and a reference. Depending on the situation these heatflows can correspond to latent heats (phase transitions like cristallization or melting, chemical reactions, amongst others) exchanged by the sample or to changes of the specific heat capacity of the investigated system. In DSC sample and reference pans are submitted to a temperature program $T_{oven} = T_0 + \beta \cdot t$ (β representing the heating/cooling rate), which yields a heatflow $HF = k \cdot \Delta T$ emerging between sample and reference. While ΔT is corresponding to the temperature difference between sample and reference, k is a characteristic constant of the instrument which has to been determined by calibration. In absence of phase transitions the heat capacity c_p of the sample can directly be determined from $HF = c_p \cdot \beta$. The interpretation of the heat flow signal gets more complicated when e. g. latent heat is exchanged by the sample and superimposes the evolution of the heat capacity. From inspection of the previous equation it can be understood that a large heating rate β is needed to resolve small changes in cp while the measurements are only sensitive enough to see at which temperature these changes happen when a small β is used. Obviously DSC cannot be exploited to determine c_p under isothermal conditions ($\beta = 0$).

Temperature modulated DSC

Temperature Modulated DSC (TMDSC) was developed as an extension of DSC by Reading et al [66]. For a review and further information please refer to [67]. In a TMDSC experiment, the oven temperature obeys to

$$T_{oven}(t) = T_0 + \beta t + A_T \cdot sin(\omega t) \tag{3.8}$$

with the amplitude A and the frequency ω of the temperature modulation. The heat flow emerging due to the temperature difference between sample and reference can be written as:

$$HF = \beta C_{p,\beta} + k \cdot A_T \cdot sin(\omega \cdot t - delta) \tag{3.9}$$

with A_T: amplitude of the time-dependent temperature difference ΔT between sample and reference, δ: phase shift angle between oven temperature and time-dependent temperature difference ΔT. In the frame of linear response theory the heat flow signal can be interpreted as an answer to the modulated oven temperature [68]:

$$HF[T,t] = \beta \cdot C_{p,beta} + \omega \cdot A_T \cdot /C_p^*(T,\omega)/cos(\omega \cdot t - \phi) \tag{3.10}$$

ϕ: phase shift angle between heat flow and heating rate ($\phi = pi/2 + \delta$).

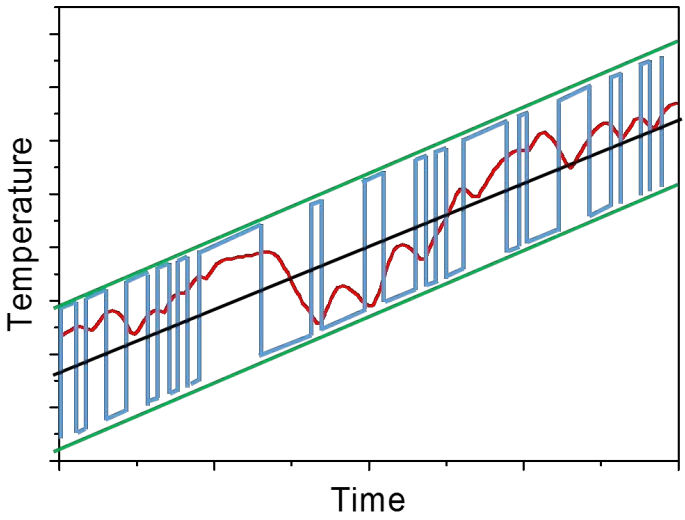

Figure 3.7: Temperature-time diagram of the TOPEM temperature program with the stochastically modulated temperature program (in blue), followed by the cell temperature (in red) the underlying heating rate (in black), and the amplitude of the modulation (in green).

Comparison of equations 3.9 and 3.10 yields modulus and argument of the complex specific heat capacity c_p^*:

$$c_p^* = \frac{C_p^*}{m} = \frac{k \cdot A_T}{\omega \cdot A \cdot m} \tag{3.11}$$

and $tan(\phi) = \frac{A_T}{A}$, m: mass of the sample.

c_p^* can be separated into the specific storage $c_p^{'}$ and loss heat capacities $c_p^{''}$:

$$c_p^* = c_{p,0} + \frac{\Delta c_p}{1 - i\omega\tau} = c_p^{'}(\omega) + i \cdot c_p^{''}(\omega) \tag{3.12}$$

The problem with TMDSC is that it is time-consuming. One needs 3 measurements for each frequency: one empty run, one calibration run with a known sample such as aluminium or sapphire and the actual sample measurement.

TOPEM

TOPEM analysis [68] yields the quasi-static heat capacity c_{p0} and the frequency-dependent complex heat capacity c_p^* without the need for additional calibration (TMDSC requires accurate and time-consuming calibration). In a single measurement c_p^* can be determined over a wide frequency range. This is

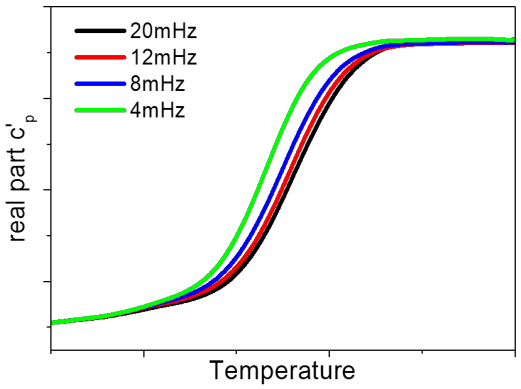

Figure 3.8: Temperature dependence of the specific storage heat capacity at different frequencies obtained from a single TOPEM measurement.

achieved by superimposing the linear temperature program $T_{oven} = T_0 + \beta \cdot t$ with a stochastic temperature profile T_{Topem}(see figure 3.7). Using this method the underlying heating rate β, the maximum perturbation A_{Topem} (of the time-dependent temperature difference ΔT between sample and reference) and the times between the pulses $\Delta t_{p,min}$ and $\Delta t_{p,max}$ can be varied. This temperature pulse needs to be small enough to ensure the sample response remains linear. The dynamic $T_g(\omega)$ is not significantly influenced by the underlying cooling rates, provided these are small enough ($\beta \ll 2\,K/min$) [69]. Though the quasi-static $c_{p,0}$ is actually measured dynamically at a frequency of 4mHz, the frequency is so low that it is very close to the thermal c_p due to the underlying heating rate β

Correction of heat capacity signals

Both the porous glass matrix and the DGEBA filler contribute to the measured heat flow signal. Using a simple mixing rule the specific heat capacity can be normalized to the contribution of the oligomer. With the DGEBA concentration x ($x = m_{DG}/m_{tot}$) and the specific heat capacity of the porous glass $c_{p,PG}$, one can calculate the specific heat capacity $c_{p,DG}$ of the DGEBA, the phase shift angle ϕ as well as the real and imaginary parts of $c^*_{p,DG}$:.

$$c_{p,DG} = \frac{c_{p,meas} - (1-x) \cdot c_{p,PG}}{x} \tag{3.13}$$

$$\phi_{DG} = \frac{\phi_{meas}}{x} \tag{3.14}$$

$$c'_{p,DG} = \frac{c_{p,meas} \cdot cos\phi - (1-x) \cdot c_{p,PG}}{x} = \frac{c'_{p,meas} - (1-x) \cdot c_{p,PG}}{x} \tag{3.15}$$

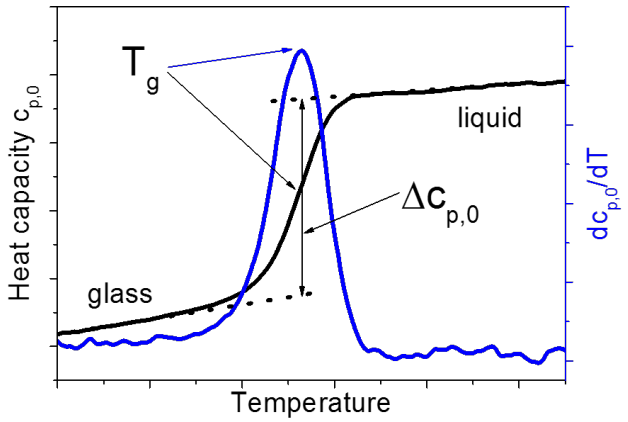

Figure 3.9: The quasi-static heat capacity of DGEBA (black line) and its temperature derivative (blue line) as a function of temperature.

$$c''_{p,DG} = \frac{c_{p,meas} \cdot sin\phi}{x} = \frac{c''_{p,meas}}{x} \tag{3.16}$$

Measurement

TMDSC and TOPEM experiments were carried out on a DSC 823e (Mettler Toledo) in the temperature range extending from -60C to +80 C. The heating rate $\beta = 0.3K/\text{min}$ was a compromise between fairly ensuring thermal equilibrium conditions and keeping the duration of an experiment lower than 24 h. TMDSC and TOPEM were measured on a DSC 823e from Mettler-Toledo between $-60C$ and $+80C$ with an underlying heating rate of $\beta = 0.3\,K/min$. This slow heating rate was a compromise between coming close to thermal equlibrium and limiting the total measurement time to < 24 hours. Experiments with a longer duration could become problematic due to the possible appearance of frozen water around and in the sample chamber of the calorimeter which could compromise the heat flow signal.

Fig. 3.9 illustrates how $c_p(T)$ and $dc_p/dT(T)$ are exploited to determine the glass transition temperature T_g and the relaxation strength Δc_p (step height) - magnitudes which are essential for the characterization of the glass transition undergone by DGEBA.

3.2.4 Thermo-mechanical analysis (TMA)

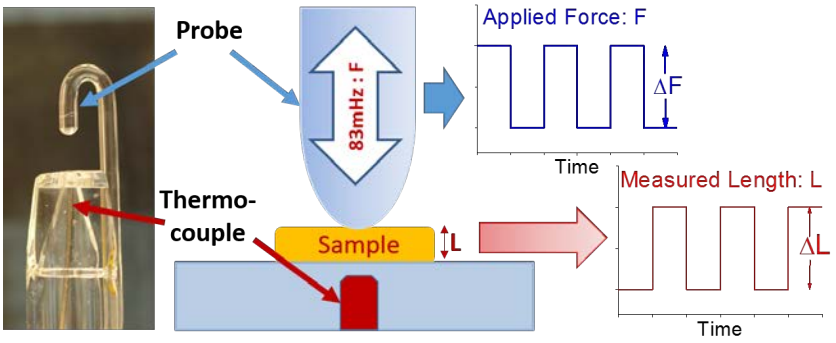

Figure 3.10: Photo and schema of the TMA setup showing the probe measuring the sample's height which can oscillate between 2 forces with a frequency of 83mHz. This applied force is shown in the blue curve which results in the length measurement shown in the red curve. The sample's temperature is measured with a thermocouple inserted under the sample in the sample stage.

Thermo-Mechanical Analysis (TMA) is a technique measuring the dimensional changes accompanying phase transitions as a function of the applied temperature. A TMA setup consists of the sample stage, a sensitive probe measuring the sample's height and a thermocouple measuring the temperature. The sample environment is enclosed in a furnace with nitrogen gas flow.

The main function is the analysis of the dilatometric expansion of the length or volume of a sample as a function of temperature. The linear expansion coefficient α can be determined by dividing the temperature derivative of the length by the length of the sample:

$$\alpha = \frac{dL}{dT} \cdot \frac{1}{L}$$

For an isotropic material, the volume expansion coefficient $\gamma$is then equals to $3 \cdot \alpha$. The force holding the probe down on the sample needs to be so small that the applied stress σ plotted against the measured strain ϵ of the sample is in the linear elastic regime. Larger stresses could incur irreversible deformations.

As mentioned above, phase transitions such as the glass transition are accompanied by a change in free volume v_f which manifests itself through a significant change in the slope of the thermal expansion curve. The glass transition temperature can then be determined from the intersection of linear

fits of the length expansion in the glass and in the liquid regime as shown in figure 3.11.

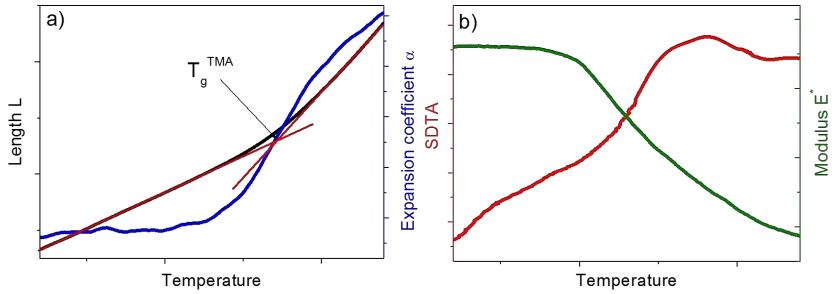

Figure 3.11: TMA measurements of DGEBA confined in a porous glass. Figure a): dilatometric expansion L (black curve) and the calculated linear expansion coefficient α (blue curve). The linear fits of the glass and liquid regions are marked in red. Figure b): the elastic modulus E^* is shown in green and the SDTA signal in red.

With the TMA/SDTA 841e setup from Mettler-Toledo used in this thesis it is also possible to vary the stress acting on the probe. During the measurements the force applied on the sample can be modulated between two different forces with a frequency of 83.3mHz seconds. This means that on top of the length change, the complex elastic Young's modulus $E^*(T)$ of the sample can be determined:

$$E^*(T) = \frac{\sigma}{\epsilon} = \frac{\Delta F/A}{\Delta L(T)/L} \tag{3.17}$$

with $\Delta F = F_1 - F_2$ the difference between the two applied forces, $\Delta L = L_2 - L_1$ the resulting difference in measured height (a lower force translates into a larger sample height and vice versa, see figure 3.10) and the area A where the force is applied. Further Single Differential Thermal Analysis (SDTA) of the sample is possible using Mettler-Toledo's STARE software which calculates the difference between the sample's temperature measured with a K-type thermocouple and the reference temperature. This analysis can help in the identification of thermal effects due to the heating/cooling of the sample. In total, 6 parameters can be extracted from a single TMA measurement with modulated force: the length L (as the mean of the varied measured length), the complex modulus E^*, the storage modulus (or real part) E', the loss modulus (or imaginary part) E", the phase δ, and the SDTA signal. All samples were measured in the same range as for DSC (between around $-60°C$ and $80°C$) and with the same heating/cooling rate of $0.3\,K/min$.

3.2.5 Broadband dielectric spectroscopy (BDS)

In dielectric spectroscopy, the impedance of a sample is measured as a function of the frequency of an applied electric field (ranging between 10^{-6} and 10^{12} Hz) [70]. The observed dielectric permittivity ϵ is based on molecular dipole moments and the reorientational dynamics of the dipoles and electric charges in the sample due to the applied electric field (established first by Debye [71]). The sample acts as a dielectric in a capacitor (sample is placed between two electrodes). The empty capacitor has a capacitance of $C_0 = \epsilon_0 A/d$ which becomes $C_s = \epsilon^* C_0$ when the sample is inserted. The actual values measured are the amplitudes U_0 and I_0 of the applied voltage $U^*(t) = U_0 e^{i\omega t}$ and current $I^*(t) = I_0 e^{i\omega t+\delta+\pi/2}$ and the phase lag δ. The impedance

$$Y^* = \frac{U^*(t)}{I^*(t)} = \frac{1}{i\omega\varepsilon^* C_0} \tag{3.18}$$

is, as the capacitor is described by a parallel circuit with ideal resistance R_s and capacitance C_s, equal to

$$Y^* = \frac{R_s}{i\omega C_s R_s + 1}. \tag{3.19}$$

The frequency dependent complex dielectric function for the permittivity then is:

$$\epsilon^*(\omega) = \epsilon'(\omega) - i\epsilon''(\omega) = \frac{C_s^*(\omega)}{C_0};\ \epsilon' = \frac{C_s}{C_0},\ \epsilon'' = \frac{1}{\omega R_s C_0} \tag{3.20}$$

The structural relaxations accompanying the transition from a liquid to a glass in glass-forming materials are characterized by the α-relaxation time (see the peak at higher frequencies than the conductivity signal marked in figure 3.12). Further dynamic processes present in glass formers are observed at shorter time-scales such as the β and γ processes. The relaxations corresponding to the peaks in the dielectric spectra can be fitted at each temperature using the Havriliak-Negami function [72]:

$$\epsilon^*(\omega) - \epsilon_\infty = \frac{\Delta\epsilon}{(1 + (i\frac{\omega}{\omega_0})^\beta)^\gamma}\ ;\ 0 < \beta \leq 1,\ 0 < \gamma \leq 1 \tag{3.21}$$

with the stretching parameters β and γ. This formula is an analytical combination of the Cole-Cole [73] and Davidson-Cole [74] stretched exponential functions describing non-Debye-type relaxations in the frequency domain. The resulting fitting parameters are used to describe the evolution of the relaxation processes over the temperature. Specifically, the frequency f of

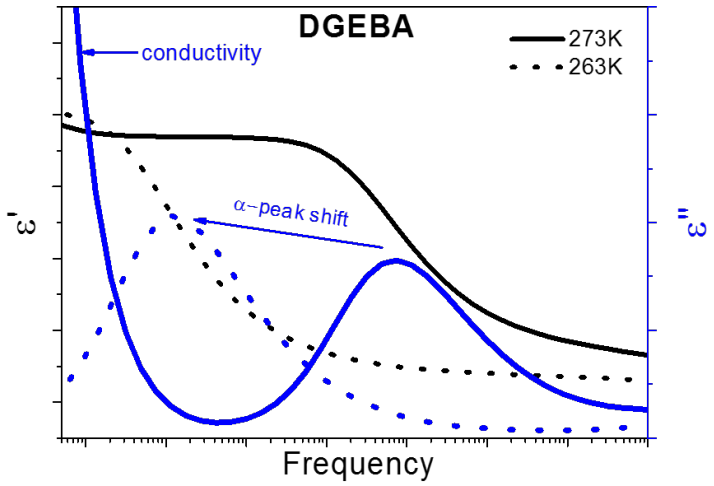

Figure 3.12: Dielectric spectroscopy spectra of DGEBA for 273 K (solid lines) and 263 K (dotted lines). ϵ' is depicted in black and ϵ'' in blue. The conductivity signal can be seen at low frequencies in ϵ'' while the α peak shifts towards lower frequencies with decreasing temperature.

the peak positions can be plotted in a $log(f)$ vs. $1000/T$ (inverse temperature) diagram showing the change in the relaxations accompanying the glass transition over many decades. This data extends the DSC data at very low frequencies over a much larger range of frequencies. Properties such as the activation energy and the fragility can be extracted from this plot. For the porous glasses, other fit parameters such as ϵ_∞ cannot be evaluated quantitavely as there is no apparent mixing rule to separate the signals of the pure porous glass and the DGEBA filler for dielectric spectroscopy. The samples were analyzed for this thesis using a Betasorb spectrometer from Novocontrol with an Alpha-A frequency analyzer and a Quatro Cryosystem. The spectrometer can measure in the frequency range from $3 \cdot 10^{-5}$ till $4 \cdot 10^{7}$ Hz through temperatures of $-160\,^{\circ}$C to $+400\,^{\circ}$C. The samples were sputtered with a thin layer of gold on each side for optimal contact to the external electrodes and then measured from $+50\,^{\circ}$C to $-150\,^{\circ}$C in steps of $2\,^{\circ}$C.

4. Characterization

The components of the system -porous glass and the epoxy resin DGEBA- under investigation are characterized thoroughly. The results are used as a basis for the results of the combined system.

4.1 Porous Glasses

The properties of the silica porous glasses were characterized with different methods. First the results from the nitrogen adsorption/desorption analysis with a quantitative analysis of the pores are presented. This is followed by images of the porous structure taken with AFM and SEM. To be able to take into account the contribution of the empty silica network in the analysis of the composite, the empty porous glasses are measured using TMA and DSC. Finally the impact of silanization is shown on silica surfaces.

BET

The method established by Brunauer-Emmett-Taylor, referred to by BET and introduced in chapter 3, is used to determine the porous structure of the glasses. Please refer to Section 3 for further details about the method. The nitrogen adsorption and desorption isotherms needed were taken using the Quadrasorb Nova 2000e. The samples were degassed and then measured with 30 P/P_0 adsorption points and 29 P/P_0 desorption points between 0 and 1. The results are summarized in table 4.1. The determination of the properties from nitrogen adsorption and desorption measurements such as the pore diameter and the total pore volume is strongly dependent on the range of measured relative pressures. The values and their errors are therefore calculated from the average of several data fits varying the relative pressure values used for the evaluations. Problems are also incurred for very small pores ($< 4nm$) and for samples with a surface area per gram of material of $< 10m^2$, i.e. small surface areas and/or small amounts of material.

Pore diameter $[nm]$	Porosity $[\%]$	Surface Area $[m^2/g]$	Total pore volume $[g/cm^3]$
4.5(5)	27(2)	156(24)	0.27(3)
10.3(11)	56(4)	445(19)	1.02(5)
18.7(18)	41.3(4)	182(13)	0.71(5)
44.4(32)	39.2(6)	59(8)	0.49(7)
57.6(41)	61.9(5)	52(7)	0.52(6)
86.7(53)	51.4(5)	47(6)	0.55(6)
111.7(64)	59.2(6)	70(8)	0.69(7)

Table 4.1: Properties of the porous glasses from Nitrogen adsorption and desorption isotherms.

As mentioned in the section about the BET method, the fit of the measured points for low pressures not only delivers the surface area but also a constant C which is related to the interaction strength between the adsorbate and the adsorbent. These values are compared for the native and silanized samples in table 4.2.

	4	10	20	44	55	87	111
native	47.7(12)	41.2(9)	77.5(17)	7.5(4)	8.3(6)	8.1(4)	7.6(5)
silanized	33.5(7)	15.6(6)	30.7(8)	6.5(4)	4.6(3)	4.9(3)	5.1(4)

Table 4.2: C-constant from BET-fits for the various pore sizes and surface treatment.

The determination of the C-constant from BET-fits are largely dependent on the range of data-points chosen. The range must be within the linear regime of the nitrogen adsorption. The errors of the values were determined by varying the fitting range within the linear regime. Comparing the C-values for the native and silanized pores, it is apparent that these are smaller for the pores which were treated. This indicates that the interactions with nitrogen and therefore probably other materials are hindered after surface treatment.

AFM & SEM

To get a clearer idea of the structure of the porous glass atomic force microscopy (AFM) and scanning electron microscopy (SEM) measurements were performed with the help of Marlena Filimon from the University of Luxembourg and Joerg Schmauch from the Saarland University. The height and phase diagrams obtained by AFM for the surface of a porous glass with 20nm-sized native pores are shown in figure 4.1.

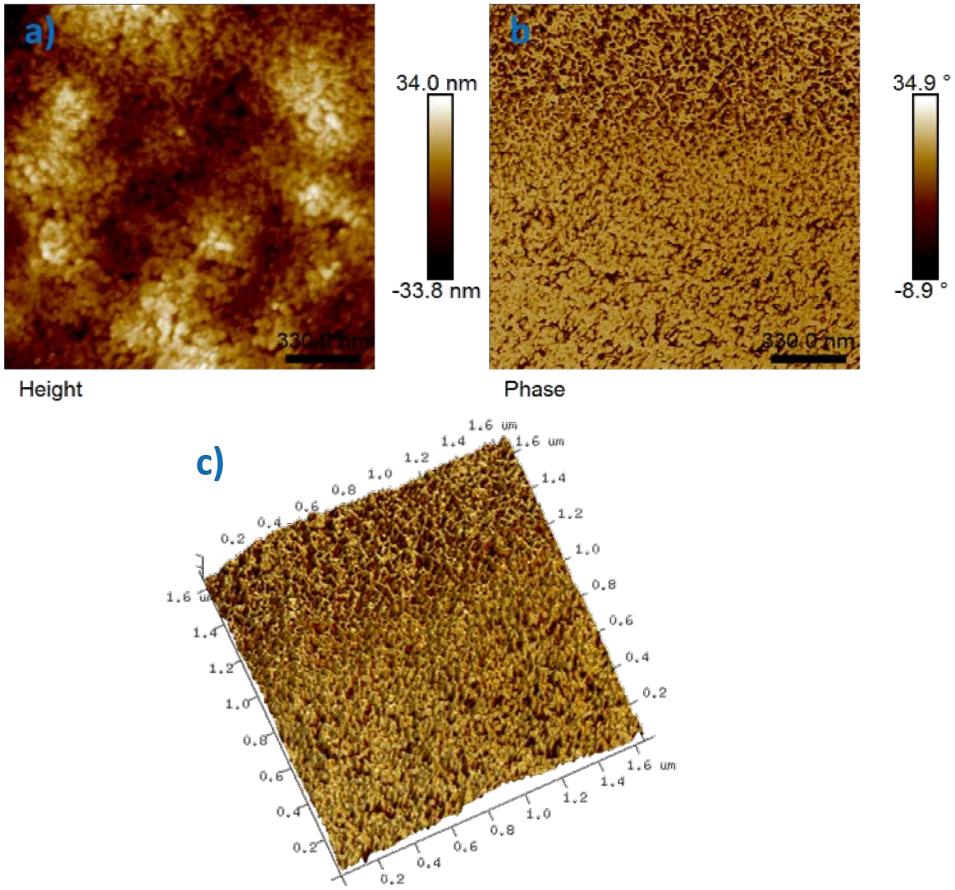

Figure 4.1: a) topography and b) phase diagrams of the surface of porous glass with 20nm pores using tapping mode AFM. A resulting 3-Dimensional model of the surface of the porous glasses is shown in figure c).

Combining the information of the two measurements, a 3-dimensional picture of the porous surface can be rendered (figure 4.1c)). One can see the pores and surface roughness of the porous glass.

Using SEM the view of the structure of the pores can be enhanced compared to AFM though the measurements are more destructive to the samples. Due to the bad conductivity of the porous glasses, the pores were coated with a few nm of platinum.

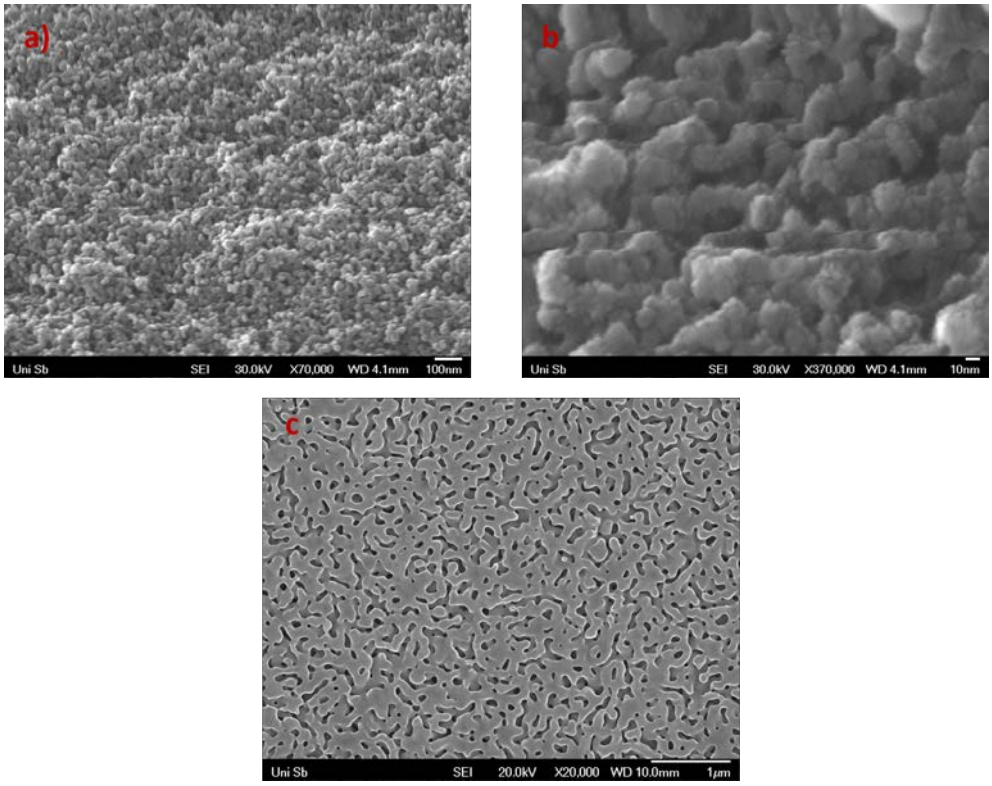

Figure 4.2: SEM micrographs of the surface of a porous glass with 20nm pores: a) 70000x magnification, b) 370000x magnification. c) Cut Cross section of 111nm pores at 20000x magnification.

In figure 4.2a) the surface morphology of the porous glasses with 20nm pores is shown at a magnification of 70000. The shape and repartition of the pores is much more defined compared to the AFM pictures. With a stronger magnification of 370000 times (figure 4.2b)) the shape and size can even be identified. The extent of the network of the pores is demonstrated in the picture of the cut Cross-section of porous glasses with 111nm pores in figure 4.2c) .

DSC & TMA

The specific heat capacity of the empty porous glasses measured with differential scanning calorimetry (DSC) can be fitted with a linear fit. This

is shown together with the thermal expansion for the 20nm porous glass in figure 4.3.

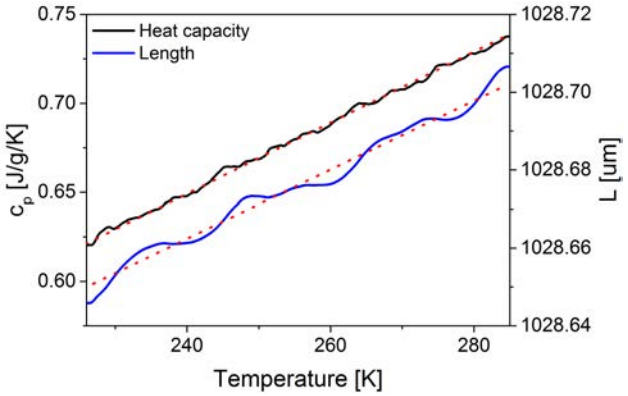

Figure 4.3: The specific heat capacity (black curve) and the length (blue curve) of an empty porous glass with 20nm-sized native pores as a function of temperature. The dotted lines correspond to linear fits to the experimental data.

Regarding the DSC measurements, the linear fits are used in section 6 for the correction of the specific heat capacity of the pg/DGEBA systems.

	4	10	20	44	55	87	111
intersection	0.27126	0.02015	0.17103	0.26634	0.20596	0.2628	0.19068
slope	0.00215	0.00218	0.00199	0.00172	0.00187	0.00182	0.00192

Table 4.3: Linear fit parameters (intersection: c_p value at T=0 and the slope) of the specific heat capacity of the empty porous glasses as a function of temperature.

The fits of the expansion yielded linear thermal coefficients for the porous glasses of around $(8 \pm 2) \cdot 10^{-7}[K^{-1}]$.

4.1.1 Contact Angle

For an indication of the wetting properties and of the impact of silanization on the surfaces of the pores, contact angle measurements were made. The nanopores are far too small to be able to do contact angle measurements with a microscope therefore flat silica slides were used as an approximation. The silica slides were silanized using the same procedure as set out in chapter 3 for the porous glasses. Small drops of DGEBA (which have a surface tension

of $0.047 N/m$) with approximately the same volume were placed on the native and silanized surfaces and photographed. The obtained pictures are shown in figure 4.4.

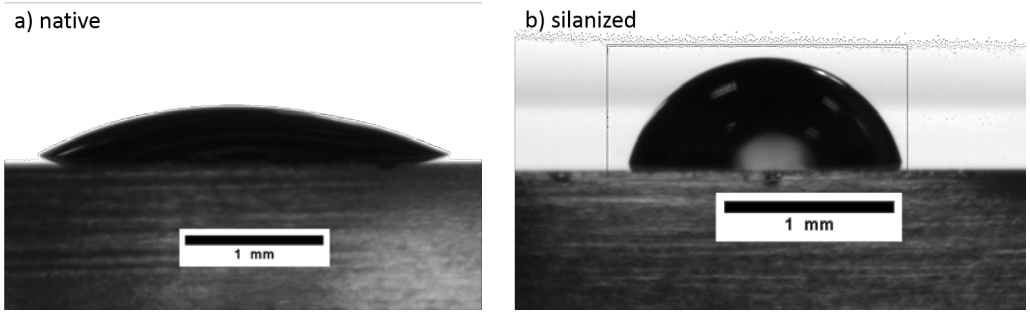

Figure 4.4: Image of a drop of DGEBA on a) an untreated silica surface and b) a silanized silica surface.

As can be seen in figure 4.4a) the DGEBA strongly wets the native surfaces resulting in a contact angle of (36 ± 3) deg. The value was determined from the average of the contact angle of 10 drops.

The drop of DGEBA on the treated surface (so that it is less hydrophilic) is shown in figure 4.4b). One can see that the silanization did not make the silica surface really hydrophilic as the contact angle is still below 90 deg with a value of (79 ± 5) deg. This means that surface interactions due to H-bonding is not completely hindered.

These values for the contact angle can only be taken as an approximation as the contact angle of liquids in very small cylindrical pores is usually higher than on flat surfaces. Li et al found that for various liquids in mesopores [75] the contact angle even increased in smaller pores. In pores the Young's equation relating the surface tensions of thegas-liquid-solid interfaces does not hold anymore as it does not take into account the geometry of the surface. Additionally the negative pressure in the pores and the different saturation of the liquid and the gas density can influence the contact angle of the liquids on pore surface walls.

4.2 DGEBA

The glass forming epoxy resin was characterized using DSC, TMA and dielectric spectroscopy and the results compared to literature.

DSC

The specific heat capacity of the bulk (unconfined) DGEBA was measured using the same parameters for the filled system with a heating rate of $0.3K/\text{min}$ (figure 4.5).

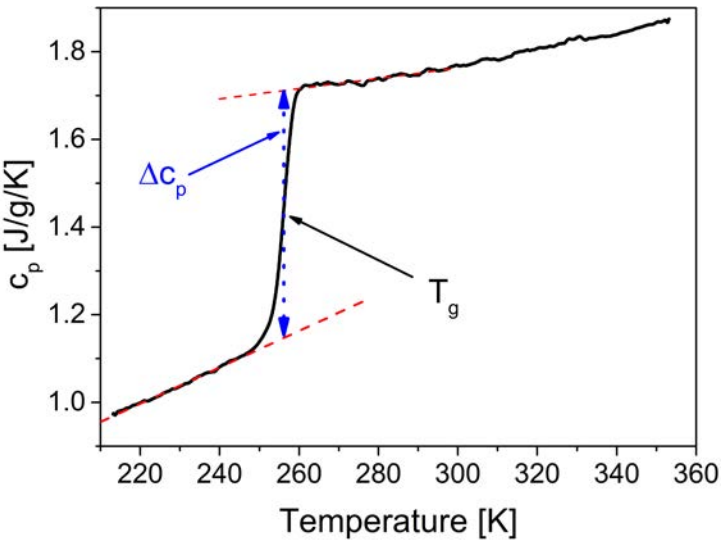

Figure 4.5: The specific heat capacity of DGEBA as a function of temperature

The step-like signature of the glass transition can clearly be observed followed by a liquid-like region at higher temperatures. The glass transition temperature could be determined (as the temperature corresponding to the inflection point of the $c_p(T)$ curve): $T_g = (256.1 \pm 0.3)\text{K}$. The step height at T_g between the heat capacity of the glass and liquid-like regions is $(0.56 \pm 0.02)\text{J/g/K}$. These values coincides with published measurements with the values 275K and 0.54J/g/K respectively for the same DGEBA variant D331 from Dow Chemicals [76, 77].

TMA

The thermal expansion of pure DGEBA using thermomechanical analysis (TMA) is measured with a dilatometric vial from Mettler Toledo. The liquid

DGEBA is filled into the vial, covered with mercury and topped off with a quartz piston. Figure 4.6 depicts the evolution of the adjusted length (adjusted to 0 at 220K and to 1 at 270K) of a DGEBA sample as a function of temperature.

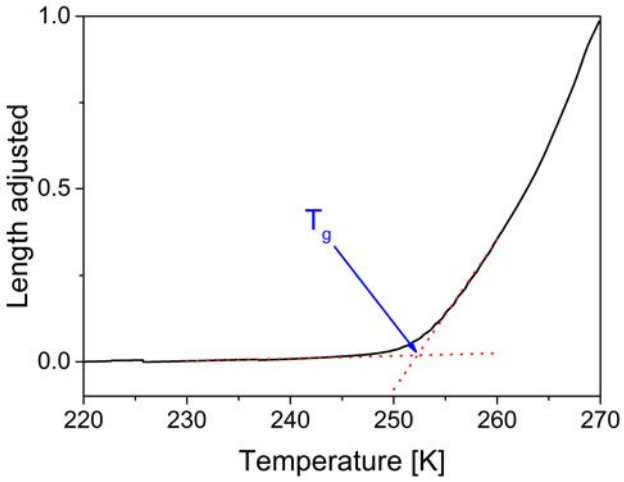

Figure 4.6: The expansion of DGEBA as a function of temperature adjusted to 0 at 220K and to 1 at 270K. The slope of the expansion in the glass and the liquid region are fitted (red lines). The glass transition temperature is marked at the intersection of these fits.

The measurement could only be performed at temperatures $T < 270K$ and a minimum force of 0.001N, as the DGEBA was otherwise too liquid slipping past the mercury and the piston. The glass transition temperature could be determined from the intersection of linear fits to the glassy and liquid branches of expansion as (252.3 ± 0.3)K. The expansion coefficients $\alpha_{glass} = (1.4 \pm 0.2) \cdot 10^{-4} K^{-1}$ and $\alpha_{liquid} = (5.5 \pm 0.3) \cdot 10^{-4} K^{-1}$ correspond to measurements of the expansion of DGEBA in literature [78].

DS

Dielectric Spectroscopy (DS) was used to investigate the frequency behavior of the complex dielectric constant of bulk DGEBA. opy cooling from 323K to 123K with a frequency run every 2K. The signal of the dielectric loss ϵ" is analyzed as the Kramers-Kronig formulae relate the loss ϵ" and storage ϵ', only one needs to be evaluated. The maxima of the relaxation peaks are easier to fit in ϵ". Cooling till around 225K any relaxations at lower frequencies are overshadowed by the large contribution from the dc-conductivity with ϵ" $= \sigma_{dc}/\epsilon_0\omega$. The α- relaxation was observed at higher temperatures over

the whole frequency range followed by the β and γ relaxations at lower temperatures. These relaxations were fitted with Havriliak-Negami peak functions. Thereby the relaxation frequency $f = 1/(2\pi\tau_{max})$ was determined as a function of temperature (with τ_{max} as the peak positions). The logarithm of the frequency is plotted versus the inverse temperature in an Arrhenius plot (see figure 4.7) .

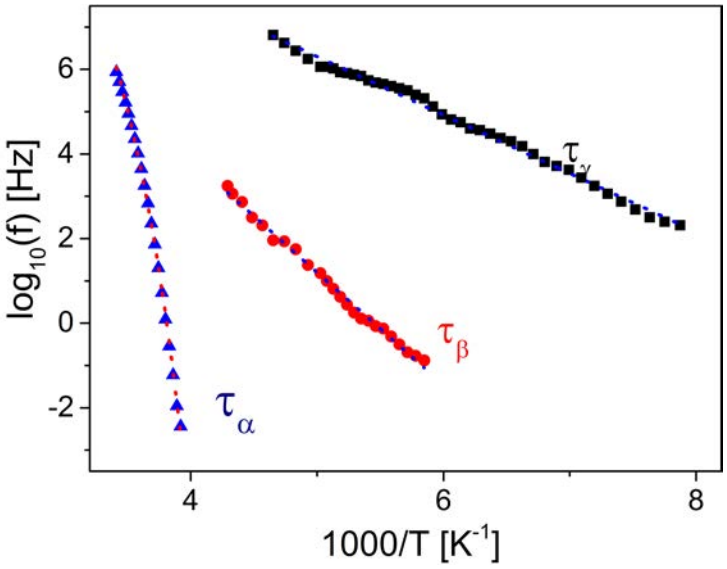

Figure 4.7: Dielectric spectroscopy results for pure DGEBA, showing the α (blue), β (red) and γ (black) relaxation times as a function of inverse temperature.

The α-relaxation can be fitted with a VFT-function while the β and γ-relaxations are fitted with Arrhenius fits. The measured frequency dependence coincide very well with the measurements by Corezzi et al on DGEBA [79].

5. Thermomechanical Analysis

The thermal expansion of the filled porous glasses was measured over a large temperature range to gain an insight into the effects of property changes of DGEBA on the confining rigid porous matrix. First studies by Koppensteiner et al, as discussed in chapter 2, showed a significant influence of glass formers on the confining material when measuring the thermal expansion of the system.

The present chapter treats the influence of pore size and surface treatment (by silanization) of the pore walls on the thermal expansion of DGEBA confined in porous glass matrices. The dilatation of the porous glass during the filling process is first investigated. This study is followed by the analysis of the thermal expansion of the porous glasses filled with DGEBA with special focus on the glass transition and flow behavior of DGEBA. The results are at first compared with findings from measurements on systems with silanized pores. Then differences yielded by cooling and heating runs are inspected: evidence for the occurrence of hysteresis between these two runs is provided.

5.1 Filling process

The swelling of a porous glass matrix was exemplarily measured while filling a matrix with 20 nm pores with liquid DGEBA. For that purpose an empty porous glass matrix was placed in the middle of a pan and liquid DGEBA was placed in the corners. The setup is shown schematically in figure 5.1. As DGEBA is still quite viscous at room temperature about (11-14 Pa·s), the pan was heated inside the TMA apparatus to 308K to ease the penetration of DGEBA into the glass matrix.

Figure 5.1: Scheme of the fill setup: the porous glass sample (grey) is placed in a pan (blue) with DGEBA drops at the corners. As the setup is heated the DGEBA flows toward the pores.

The tests were performed on the 20nm pores as these could be filled with DGEBA in an adequate amount of time and were available in larger quantities than other pore sizes. The sample expansion was measured using a force of 0.001N applied to the probe and is shown in figure 5.2.

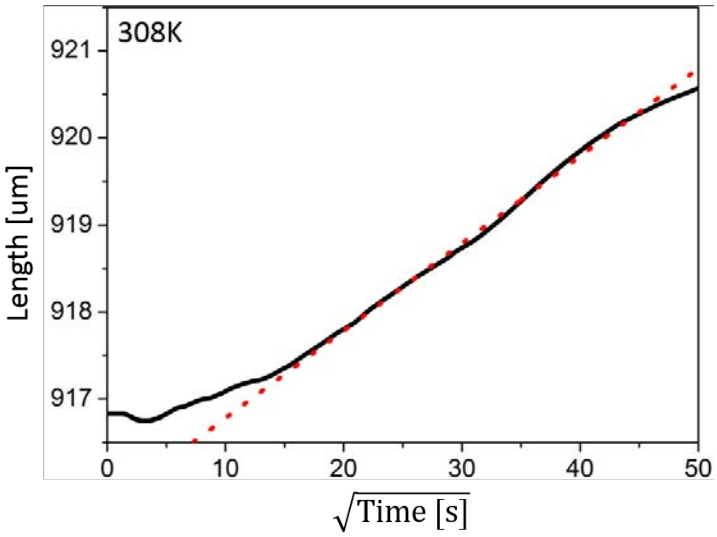

Figure 5.2: Time-dependent measurement of the expansion of porous glass during the filling with DGEBA. The linear fit of the data is marked in red.

Using neutron scattering Huber et al. [80] observed that the liquid molecules first attach to the pore walls and climb along these. The ascending motion of the molecules at the interface is followed by the bulk in the center of the pore. Thus a meniscus forms in the pores during filling. Finally the height of the swelling sample increases monotonically with the square root of time as shown in figure 5.2. This corresponds to a Lucas-Washburn $\sqrt{t}$ law describing the capillary rise of liquids [15, 16] in porous samples. Similar results have been observed for the uptake of liquids into porous systems by [23, 9].

5.2 Thermal expansion during heating

The linear thermal expansion of the filled porous glasses has been measured in the temperature range 230K to 340K. At first the results provided by heating runs are analyzed. In a second step, they are compared to the data obtained from cooling measurements.

Figure 5.3 shows the evolution of the sample height as a function of temperature for the whole bunch of native pg/DGEBA systems under investigation.

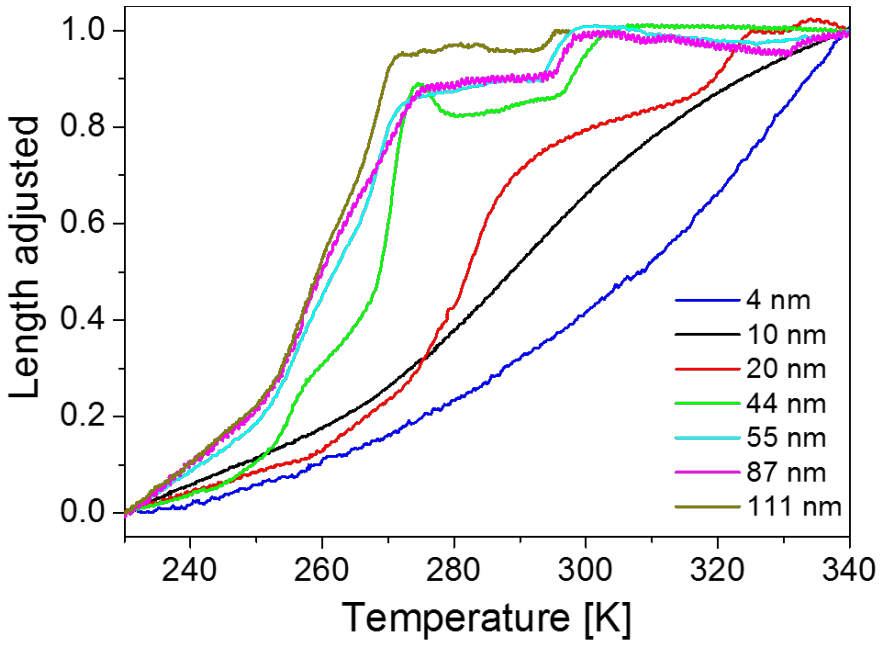

Figure 5.3: Linear thermal expansion of porous glasses filled with DGEBA for pore diameters between 4 and 111nm. All measurements are adjusted to 0 at 230K and to 1 at 340K.

The presented data of the untreated systems have been obtained upon heating. As the heights of the samples differ by up to a millimeter and the expansion effects are in the range of micrometers, the curves have been adjusted for better comparability: The length curves have been shifted vertically to 0 at 230K and then scaled to 1 at 340K.

Figure 5.3 reveals the complex thermal dilatation behavior of the composite systems, clearly documenting the influence of DGEBA on the porous matrix. All of the measurements have been carried out using the same procedure (heating rate of $0.3K$/min). Reproducibility was checked using several

samples of the same type (pore size) and repeating the measurement with the same sample several times.

In case of the samples with the largest pores, starting at the lowest temperature $T = 230K$, the adjusted length L_a linearly increases upon rising temperature. At the glass transition temperature T_g, the slope of $L_a(T)$ changes to a larger value. This transition is increasingly smeared-out with decreasing pore size ($d \leq 40nm$), T_g being shifted to higher temperatures. To understand the thermal expansion of the filled porous glass, one has to take into account interactions between the filler and the matrix. Beside geometrical contraints, these interactions hinder expansion or contraction of the filler as a reaction to temperature changes.

While T continues to increase, the pg/DGEBA samples keep expanding until, at a temperature which generally depends on the pore size of the investigated system, the slope abruptly drops to a dramatically lower value (similar to the one of the unfilled systems). For the sample with pore size d=10nm, only the beginning of this slope change can be observed. For the 4nm system the latter is not visible within the observed temperature range. This behavior can be explained by a change of the influence of the thermal expansion of the filler on the thermal expansion of the whole sample. A close inspection of e. g. the $L_a(T)$ curve corresponding to the sample with 111nm-sized pores (see figure 5.3 reveals that, between 270K and approximately 293K, the adjusted length only modestly increases: apparently, in this temperature range, a large fraction of DGEBA molecules can freely flow when temperature changes. In the following the event occurring at $T > T_g$ and generally characterized by a dramatic slope change of the respective $L_a(T)$ curve will be named flow transition.

In case of the pg/DGEBA samples with the largest pores, the $L_a(T)$ curves show a further anomaly in the form of a step at around 295K. The step separates two regimes with reduced slope of the curves. The physical origin of this step will be discussed after inspection of the $L_a(T)$ curves obtained for the pg/DGEBA systems with silanized pores. In case of the sample with 20nm-sized native pores the step height is more pronounced and occurs at a higher temperature (around 320K). At temperatures higher than those at which the step-like increase in $L_a(T)$ is observable, the samples show practically no thermal expansion, i.e. the behavior of the filled samples has become independent of DGEBA which can freely flow when temperature is changed. The step-like transition does not take place in the samples with 10nm- and 4nm-sized pores within the temperature range passed through in the course of the experiments.

A general observation is: for sufficiently small pore sizes, the smaller the pore size, the higher the temperatures at which the various transitions take

place.

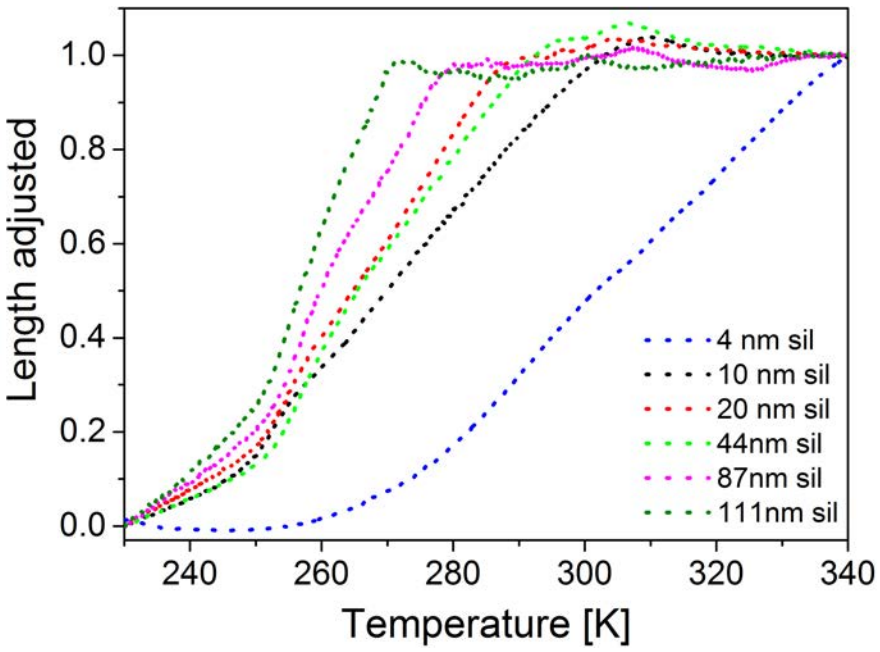

Figure 5.4: Linear thermal expansion of silanized porous glasses filled with DGEBA for pore diameters between 4 and 111nm. All measurements are normalized to 0 at 230K and to 1 at 340K.

Figure 5.4 shows the $L_a(T)$ curves obtained for the various pg/DGEBA samples with silanized pores. The data obtained for the 55nm silanized sample are left out of this analysis due to large fluctuations dominating the measurement. Inspection of table 5.1, where all the identified transition temperatures are listed, allows the comparison of the glass transition temperatures measured for the systems with native and silanized pores respectively. For pore sizes $d \geq 44nm$, the glass transition temperatures of both types of systems practically coincide with T_g of pure DGEBA. When $d < 44nm$, the glass transition temperatures of the silanized systems are always smaller than the one of the untreated samples.

Again with the exception of the 4nm system, the flow transitions found in the case of the samples with silanized pores, occur for each of the investigated surface treated systems at characteristic temperatures higher than the respective T_gs. There is a trend of the flow transitions to occur at higher temperatures, the lower the pore size. Regarding the 4nm systems and the 10 nm untreated system the event seems to take place outside the temperature range passed through during the measurements. It is important to point to a substantial difference between the results of the measurements carried

out on samples with silanized and native pores respectively: while the flow transitions of the former occur when the adjusted lengths of the samples take the value 1, the dramatic slope changes of the $L_a(T)$ curves corresponding to the filled porous glasses with native pores always occur at L_a values smaller than 1. The small step-like anomalies discussed for the samples with native pores cannot be resolved in the graphs obtained for the systems with surface treatment.

The latter finding opens up a window for the understanding of the step-like anomaly! In the samples with native pores, H-bonding as well as other types of interfacial forces with physical origin lead to attractive interactions between DGEBA and native pore wall surfaces. At high enough temperatures the thermal agitation of the DGEBA molecules is so high that, on the time average, the interfacial interaction between the filler and the porous glass can be neglected. DGEBA inside the pores can adjust its density to temperature changes within the timescale imposed by the experiment and most importantly without affecting the porous matrix, i. e. it can flow like a liquid through the pores. Thus, at sufficiently high temperatures, the evolution of the $L_a(T)$ curve is exclusively controlled by the thermal expansion of the glass matrix which is very low. When decreasing the temperature below $T_{flow}^{(2)}$ (see figure 5.3 and table 5.1), thermal agitation can no longer prevent that interfacial forces hinder the flow of a fraction of DGEBA molecules located in the vicinity of the pore wall surfaces. The considerable slope change of $L_a(T)$ between $T_{flow}^{(2)}$ and $T_g^{(2)}$ documents the forces exerted by the shell layer of filler molecules on the glass matrix. $T_g^{(2)}$ corresponds to the glass transition temperature of the shell layer. At temperatures smaller than $T_g^{(2)}$, the slope of $L_a(T)$ becomes much smaller than in the range $T_g^{(2)} < T < T_{flow}^{(2)}$, since the thermal expansion coefficient of glassy DGEBA is much lower than the one of liquid DGEBA ($\alpha_{glass} = 1.6 \cdot 10^{-4} K^{-1} < \alpha_{liquid} = 5.5 \cdot 10^{-4} K^{-1}$ for DGEBA).

The DGEBA molecules which are not immobilized in the glassy shell layer can freely move through or inside the pores to adjust their bulk density to the temperature changes. The situation changes at temperatures $T_g < T < T_{flow}^{1}$: although the material in the core stays liquid, the macroscopic flow of core DGEBA freezes. As a result the core exerts forces which are transmitted by the shell layer to the porous glass matrix: the slope of the $L_a(T)$ curve dramatically increases. Core DGEBA finally vitrifies at T_g.

In the samples with silanized pore surfaces H-bonding should play a minor role. When this kind of chemical interaction is the main one responsible for the formation of shell layers (as discussed above), one can understand that the transitions associated to the shell layer are completely absent or at least

so weak, that they can no longer be resolved.

The just described model will be corroborated by results from calorimetry in a later section. The table 5.1 gives an overview on the characteristic temperatures T_g, T^1_{flow}, $T^{(2)}_g$ and $T^{(2)}_{flow}$ as they could be determined for the various investigated samples.

For each sample the characteristic temperatures of the various transitions were evaluated by determining the intersection of linear fits of the regions above and below each kink. All transition temperatures are marked in figure 5.5. Additionally for an estimate of the amount of material which can be attributed to the shell layer, the step height ΔL (see figure 5.5) was evaluated and listed in table 5.1.

Pore size	T_g $[K]$	T^1_{flow} $[K]$	$T^{(2)}_g$ $[K]$	$T^{(2)}_{flow}$ $[K]$	ΔL
4nm	267.7(48)				
4nm silanized	249.7(36)				
10nm	266.0(32)				
10nm silanized	245.1(6)	304.4(7)			
20nm	260.4(28)	289.0(7)	318.2(8)	324.9(8)	0.122(5)
20nm silanized	249.7(5)	286.9(6)			
44nm	250.4(5)	271.9(7)	295.8(6)	302.4(6)	0.127(4)
44nm silanized	251.3(4)	294.2(7)			
55nm	251.4(4)	271.3(5)	293.4(7)	297.5(6)	0.096(4)
87nm	251.5(5)	274.3(6)	293.4(6)	298.3(7)	0.092(4)
87nm silanized	251.6(4)	279.7(6)			
111nm	251.3(4)	270.5(5)	293.3(7)	298.3(6)	0.040(5)
111nm silanized	251.5(5)	270.6(6)			

Table 5.1: Transition temperatures for the glass and flow transitions at lower and higher temperatures and the step height between the upper transitions ΔL determined for the range of pore sizes and surface treatments. The errors are estimated from several fits of the glassy and liquid-like slopes in the thermal expansion.

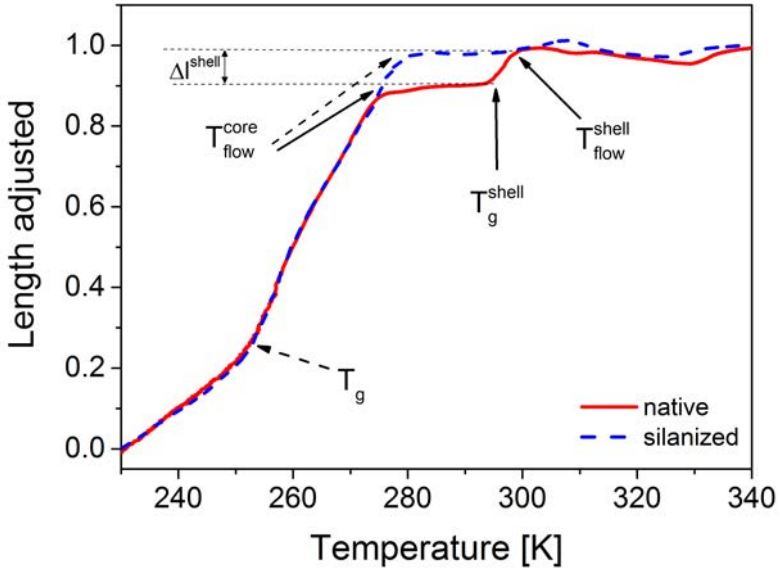

Figure 5.5: Linear thermal expansion of the native (red solid curve) and silanized (blue dashed curve) porous glasses with pores of 87nm filled with DGEBA. The various transitions T_g and T^1_{flow} for both systems, and T^2_g and T^2_{flow} for the native pores are marked. The evaluation of the step height ΔL of the shell in the native pores is indicated.

5.3 The glass transition

Figure 5.6 shows the glass transition temperatures T_g as a function of the pore size for samples with native and silanized pores respectively. As a reminder: pure DGEBA has a glass transition temperature $T_{g,DGEBA} = 252.3K$. For the systems with the largest pores ($d \geq 44nm$), irrespective of the surface treatment, T_g fairly corresponds to $T_{g,DGEBA}$. Obviously the confinement by the pores and interaction between DGEBA and porous matrix does not influence on the molecular dynamics of the core DGEBA here.

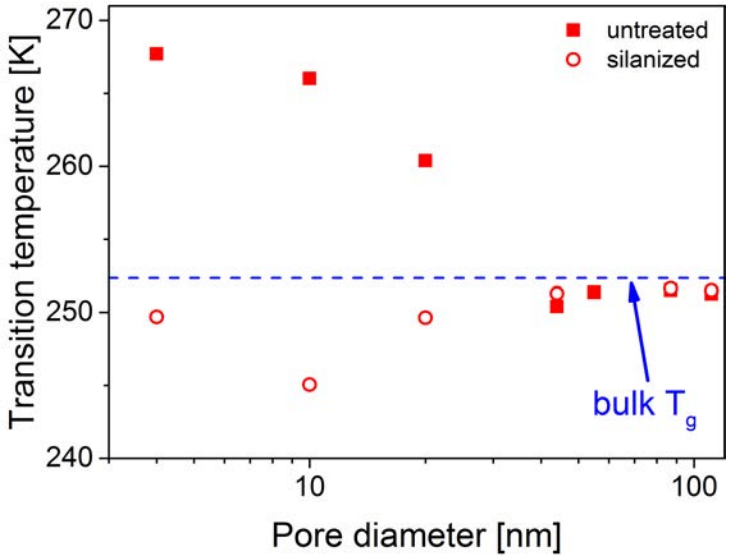

Figure 5.6: The glass transition temperatures T_g are shown for the untreated filled porous glasses (solid squares) and for the silanized filled porous glasses (open circles). T_g for the bulk DGEBA is marked by the blue dashed line.

For samples with native pores smaller than 44nm, T_g increases with decreasing pore size. This behavior changes with surface treatment: when $d \leq 44nm$, a modest tendency of T_g to drop below $T_{g,DGEBA}$ can be identified. However, while the glass transition temperatures of the 20nm and 10 nm samples seem to systematically deviate from $T_{g,DGEBA}$, T_g of the 4nm sample approaches the bulk value again. Taking into account the complexity of several curves obtained by TMA and the fact that dilatometric measurements bear many experimental uncertainties, one should avoid the over-interpretation of the results.

The changes introduced by silanization indicate that the surfaces of the pores play a large role in hindering the molecular dynamics of DGEBA inside the native pores, probably by means of van der Waals interactions and H-bonds between the polar DGEBA and the silanol groups at the surface of the porous silica glass. The slowing down of the α-process of the glass former by interfacial interactions results in a shift of the glass transition to higher temperatures in the systems with small enough pores. Why not in the systems with larger pores? A first response could be that in the samples with smaller pore sizes, the surface to volume ratio becomes so high that a substantial fraction of DGEBA molecules is in contact with or in the immediate vicinity of the pore wall surfaces. Hence a larger part of filler molecules feels the influence of interfacial interactions than in case of the systems with

larger pores.

In the silanized samples, H-bonding which plays a strong role in the samples with native pore is supposed to become less important. Even in the systems with the lowest pore sizes molecular dynamics are rather similar to those in pure DGEBA. With full trust in the measurements one can even state that the molecular dynamics become accelerated (with respect to pure DGEBA) when the pore size drops below 44nm. Such a behavior is known from literature [29, 81, 39]: when the confinement scale approaches the length scale of the regions with dynamic heterogeneity, the molecular dynamics becomes faster, when there are no other processes affecting the behavior of the glass former (such as the above described surface interactions).

5.3.1 Second glass transition

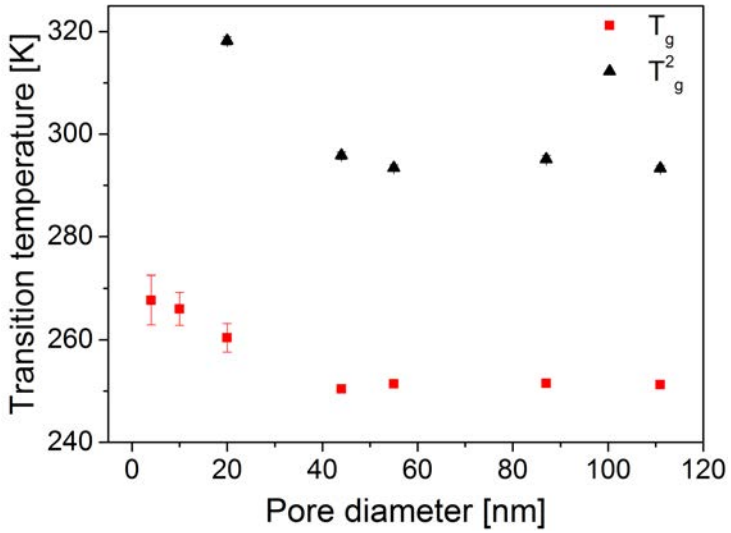

Figure 5.7: The two separate glass transition temperatures (lower in red, those at higher temperatures in black) shown as a function of the pore sizes for native pores (closed symbols) and treated pores (open symbols).

Figure 5.7 shows the evolution of the glass transition temperature T_g^2 associated to the shell layer as a function of the pore size d in addition to $T_g(d)$ already represented in figure 5.6. As already mentioned, the second flow transition occurs when, upon cooling, the flow of DGEBA molecules located in the immediate vicinity of the pore walls is hindered as a result of interfacial interactions. At the shell formed by the affected molecules freezes.

As in the silanized systems the interfacial interactions are considerably reduced, one does not expect the second flow transition to occur. Logically the corresponding glass transition takes place neither. In the untreated samples the molecular dynamics of DGEBA within the layer adhering to the pore surfaces is considerably slowed down compared to bulk DGEBA. As a consequence the shell layers becomes glassy at much higher temperatures than bulk DGEBA. For the samples where the shell glass transition could be identified, the values of T_g^2 are around 300K except for the case of the 20nm-sized native pores. In the latter sample the shell glass transition occurs almost 20K above the transition observed in the systems with larger pore sizes.

5.3.2 The flow transitions

In section 5.2 the flow transitions were introduced to describe important slope changes observed in the $L_a(T)$ curves at temperatures higher than T_g (see figures 5.3 and 5.4 for the samples with native and silanized pores respectively). The first of these flow transitions, occurring at the temperature T_{flow}^1=$T_{flow}^1(d, surface\,treatment)$, is observed for both types of investigated samples. As already mentioned it takes place when the macroscopic flow of bulk DGEBA inside the pores is hindered (increase of viscosity e. g.) and the mismatch of thermal expansion coefficients between DGEBA and the porous glass matrix can no longer be balanced (pure DGEBA has an expansion coefficient about 3 powers of magnitude higher than the empty porous glass, see values given above). Below T_{flow}^1, DGEBA stops to equilibrate its density after temperature changes. In the samples with native pores a second flow transition occurs when, e. g. upon cooling, the mobility of DGEBA molecules in contact with or located near the pore walls is restricted as a result of interfacial interactions which are particularly pronounced for the native pores. At $T_{flow}^2 = T_{flow}^2(d)$ the $L_a(T)$ curves obtained for the samples with native pores abruptly change from practically zero slope at $T > T_{flow}^2$ (shell layer can freely flow inside the porous glass when temperature changes) to a high slope value for $T_g^2 < T < T_{flow}^2$, where T_g^2 represents the temperature at which the shell layer freezes.

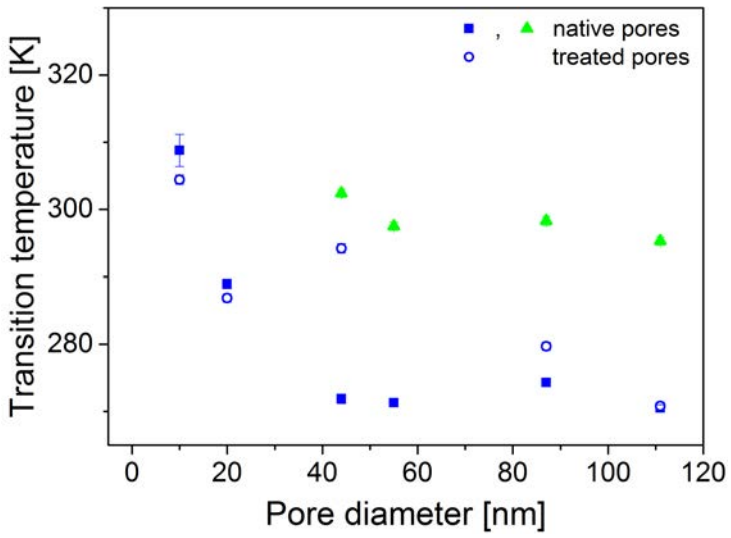

Figure 5.8: The transition temperatures T^1_{flow} (in blue) and T^2_{flow} (in green) identified with flow transitions shown as a function of the pore sizes for native pores (closed symbols) and treated pores (open symbols).

In figure 5.8 the flow transition temperatures T^1_{flow} and T^2_{flow} (listed in table 5.1) are plotted as a function of the pore size for both types of samples. Obviously, for the systems with larger pores ($d \geq 44nm$), both flow transition temperatures are independent of the pore size (as a reminder: the shell flow transition is only observed on the untreated samples). Analogous to the glass transition temperature T_g, T^1_{flow} and T^2_{flow} increase with decreasing pore size in case of pores with sizes $d < 44nm$.

5.4 Cooling versus heating

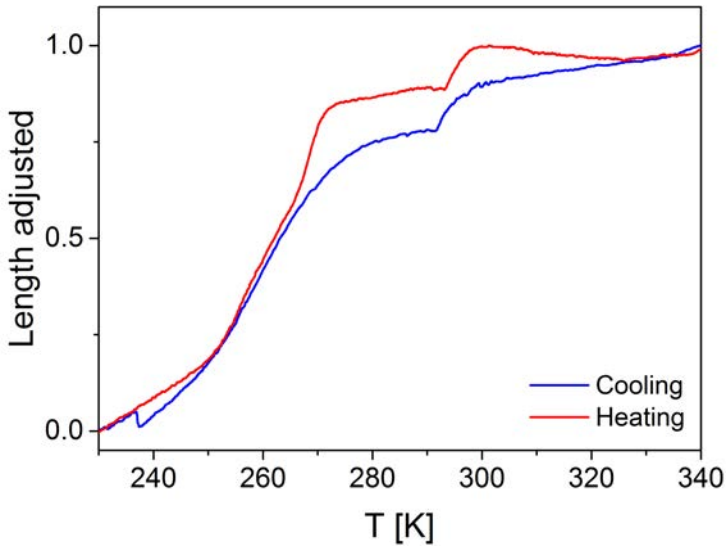

Figure 5.9: The adjusted linear thermal expansion of the native filled 55nm pores is shown during cooling (blue) and heating (red).

Figure 5.9 provides evidence for the existence of an hysteresis revealed by the $L_a(T)$ curves measured upon heating and cooling on pg/DGEBA sample with native 55nm-sized pores.

In the sample the first flowing transition (T^1_{flow}) occurs at lower adjusted length values and at a higher temperature upon cooling than upon heating. Moreover the respective transitions occurring while reducing the temperature are much less abrupt (i.e. well-defined) than in case of the heating measurements. The freezing of the flow seems to happen more gradually as the temperature is decreased during the measurement.

The glass transition of the shell layer and the corresponding flow transition also occur at higher temperatures upon cooling than upon heating. Again the L_a values at the two transitions are larger upon heating. This pronounced hysteresis behavior is possibly associated with aging of the change in density of the confined DGEBA.

5.4.1 Undercooling at low Temperatures

Looking at the heating and cooling measurements more closely at low temperatures, some of the bulk material seems to stay liquid for longer than expected during cooling, causing a larger contraction of the material. This

can be seen for the filled 55nm porous glass in figure 5.9 around 240K and much more pronounced in the $L_a(T)$ curves obtained for the 20nm- and 10nm-sized surface-treated pores shown in figure 5.10.

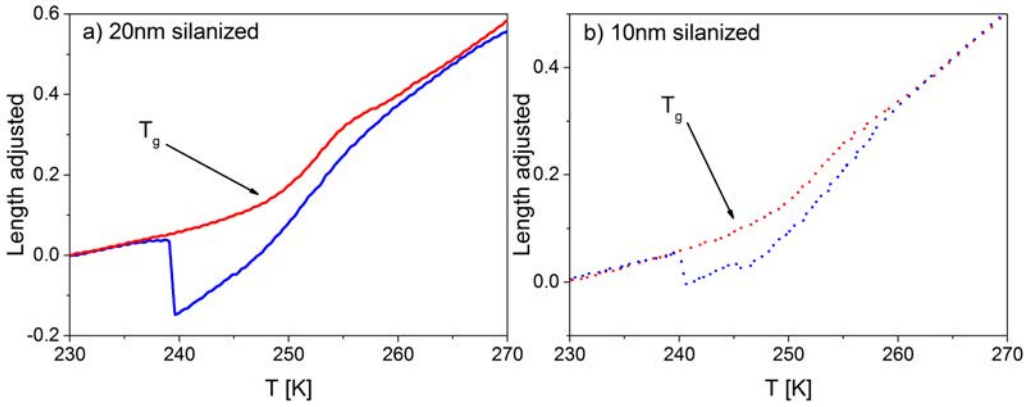

Figure 5.10: The cooling (blue curves) and heating (red curves) measurements of the length around the glass transition are plotted for the 20nm silanized pores in figure a) and for the 10nm silanized pores in figure b).

Apparently, at temperatures $T < T_g$, stress on the porous structure is suddenly released, so that the slopes of the respective $L_a(T)$ curves obtained upon cooling take the values of the glass-branches measured upon heating. The fact that the cooling and heating runs superimpose almost perfectly after the release of internal stresses, is a very nice confirmation of the reliability of the length data. For the 10-nm sample the phenomenon occurs in several stages (figure 5.10b)). Cyclic measurements on the same sample reveal that the observed hysteresis changes, disappears and reappears. The undercooling of the glass transition of core DGEBA upon cooling is possibly due to the large mismatch of expansion coefficients of the confining and confined components (the respective expansion coefficients differ by three orders of magnitude, see above).

5.4.2 Young's Modulus

TMA measurements delivered information on both the temperature dependence of the length changes, and on the complex Youngs modulus. When applied to a sample, a stress field oscillating at 83mHz yields a strain response at the same frequency (under linear response conditions). With the knowledge of stress, strain and the phase shift angle between the two signals, the storage (E) and loss (E) moduli of the investigated pg/DGEBA composite

can be determined. The temperature evolutions of E and E are exemplarily shown in figure 5.11 for the sample with 55nm-sized native pores.

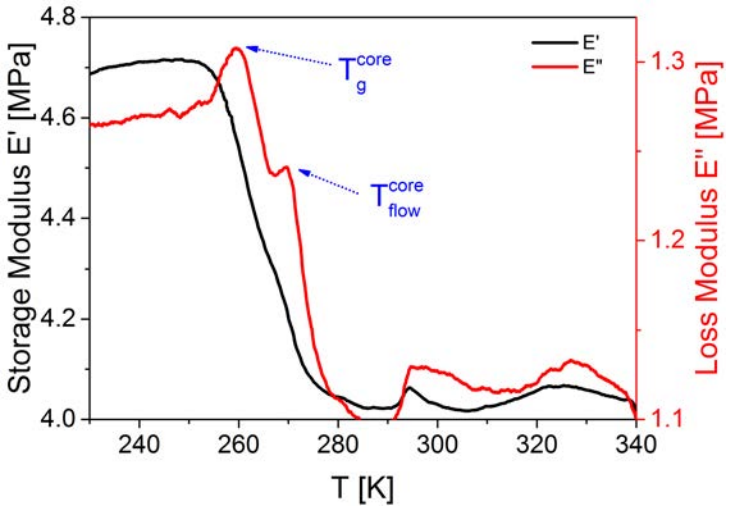

Figure 5.11: The storage E' (black curve) and the loss modulus E'' (red curve) are depicted for the 55nm native porous glasses.

The large step-like change in the storage modulus E at $T < 280K$ reflects the bulk flow and glass transitions of DGEBA inside the pores. In the same range of temperatures, the first loss peak at about 270K corresponds to the flow transition whereas the second, more pronounced maximum of the loss modulus at approximately 260K has to be associated to the glass transition. Clearly the bulk flow transition has a large impact on the filled porous glass properties.

The loss modulus peaks corresponding to the bulk glass transition were evaluated for all of the samples to determine T_g. Figure 5.12 shows the evolution of T_g obtained from measurements of Youngs modulus as a function of the pore size for samples with native and silanized pores respectively.

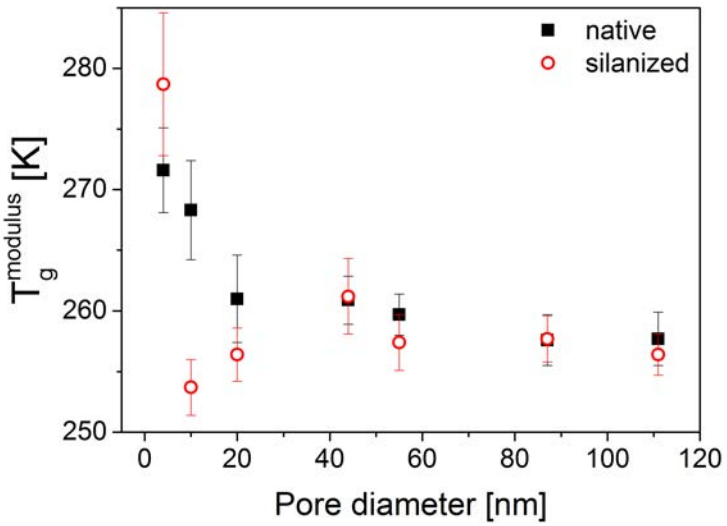

Figure 5.12: The glass transition temperature of the core from the modulus at 83mHz is plotted as a function of the pore diameter for native (black squares) and silanized porous glasses (red circles).

Obviously, for both the systems with native and silanized pores, the glass transition temperature shows the same behavior as the one determined from thermal expansion or calorimetric measurements. However, compared to the results from thermal expansion, the T_g values determined from E(T) are slightly higher. This difference is due to the kinetic character of the glass transition: Youngs modulus is measured at 83mHz, whereas the length changes are determined statically using a temperature ramp.

5.5 Summary

The Thermo-mechanical analysis of nanoporous glasses filled with the glass former DGEBA reveals a complex picture of the behavior of these composite systems. In case of samples with native pores (hydrophilic pore wall surfaces) two distinct glass transitions can be observed. This experimental feature suggests the model of a faster core and slower shell layer of DGEBA molecules in the pores. For these porous systems with untreated "hydrophilic" surfaces the interactions of the filler molecules with the pore walls induces a large up-shift of the glass transition of core DGEBA at low enough pore sizes. In contrast to these findings, silanization of the pore wall surfaces considerably reduces the interactions between the filler molecules and the porous glass matrix: compared to bulk DGEBA, the glass transition temperature practically does not change when the pore size decreases. At the lowest pore

sizes one even observes a modest tendency towards acceleration of molecular dynamics.

The most important and also completely novel result from the thermomechanical analysis is the discovery of flow transitions in both types of systems (samples with native and silanized pores). A flow transition occurs when macroscopic flow of DGEBA through the pores is frozen. It manifests itself by an abrupt slope change of the length versus temperature curves at a characteristic temperature T^1_{flow}. The latter transition results from a mismatch of the thermal expansion coefficients of the filler and the nanoporous matrix: DGEBA which can no longer adjust its density to temperature changes, exerts forces on the porous glass matrix below the flow transition. Despite the hindrance of macroscopic flow of the filler through the pores, DGEBA stays liquid at temperatures larger than its proper glass transition temperature. Both the glass transition and the flow transition are confirmed in the measurements of the elasticity at a frequency of 83mHz.

In the systems with native pores a second flow transition occurs at temperatures $T^2_{flow} > T^1_{flow}$. This transition is associated to the hindrance of flow of a shell layer in contact with the pore walls. H-bonding and possibly other physical interactions between DGEBA molecules situated at or in immediate vicinity to the pore walls oppose the free movement of filler particles within a shell layer when temperature changes. At T^2_g these shell layers freeze: core DGEBA continues to flow practically freely. As a consequence, in the temperature range $T^1_{flow} < T < T^2_g$, the interaction between the filler and the pore walls is considerably reduced.

6. Specific heat capacity analysis of confined DGEBA

Temperature modulated differential scanning calorimetry was used to investigate the evolution of the specific heat capacity of DGEBA under confinement. In analogy to the previous TMA analysis, first the results obtained from heating runs are shown and analyzed to be later compared to the data provided by experiments realized upon cooling. The effects of surface interactions and confinement on the main glass transition are investigated. This is followed by an analysis of two additional transitions which occur at temperatures higher than T_g and which are not observable in the specific heat capacity evolution of bulk DGEBA (and might be related to the flow and shell glass transitions seen in TMA). The comparison of results obtained from cooling and heating runs yields evidence for the existence of a hysteresis loop emerging in the $c_p(T)$ curves at higher temperatures. A special section is dedicated to the discussion of the porous glass/DGEBA (pg/DGEBA) systems with the smallest pore size. The present chapter is closed by an analysis on relaxation strengths, transition widths which are determined for the main glass transition of all of the investigated systems followed by the estimation of the characteristic length scale of the CRR's in confined DGEBA.

Figures 6.1 and 6.2 show the temperature evolutions of the specific heat capacities of various pg/DGEBA samples together with the $c_p(T)$ curve obtained for pure DGEBA (solid line). While the data shown in figure 6.1 have been obtained on samples with native pores, the curves depicted in figure 6.2 correspond to results measured on systems with surface-treated (silanized) pores. All the specific heat capacity data shown in these figures corresponds to a temperature modulation frequency of 4 mHz and are measured upon heating.

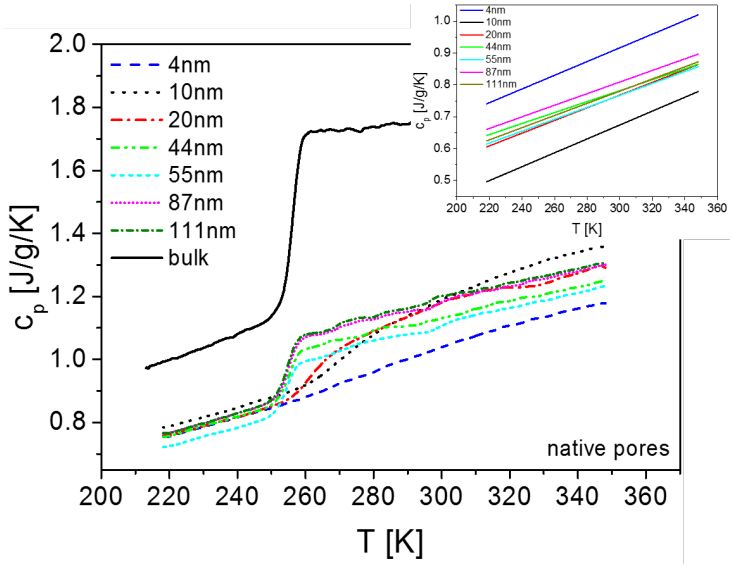

Figure 6.1: Heat capacity measurements of all native filled samples (dotted lines) compared to the bulk DGEBA (solid black line) during heating. The inset shows the linear fits of the heat capacity of the empty pores.

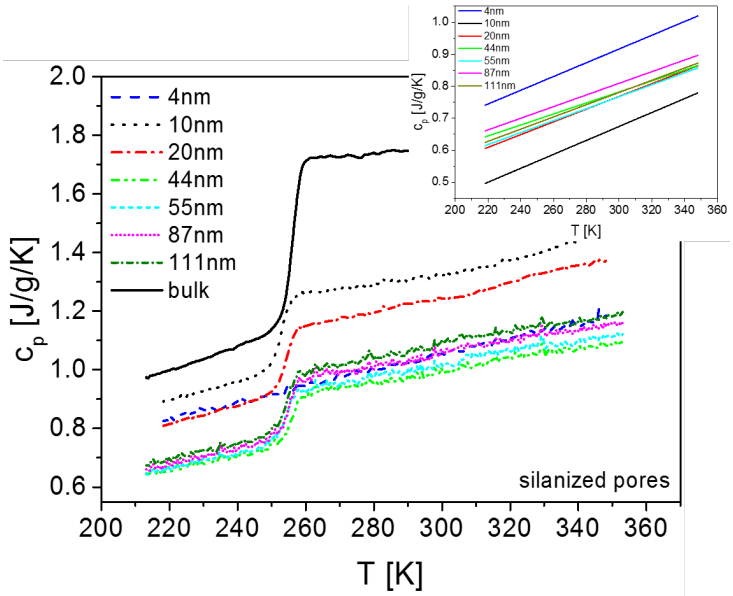

Figure 6.2: Heat capacity measurements of all silanized filled samples (dotted lines) compared to the bulk DGEBA (solid black line) during heating. The inset shows the linear fits of the heat capacity of the empty pores.

The c_p data are normalized for the further analysis in the following sections (figures 6.3 and 6.4) with respect to the DGEBA content of the respective samples using the ratio $m_{DGEBA}/(m_{pg}+m_{DGEBA})$, m_{pg} representing the mass of the empty porous glass. To allow for a better comparison, the $c_p(T)$-curves corresponding to the different pg/DGEBA samples have been shifted along the c_p-axis so that their respective inflection points (marking the glass transition) coincide with the one of the $c_p(T)$-curve obtained for pure DGEBA.

Porous glasses with native pores

While for systems using glasses with large pores (pore size $d = 111$; 87; 55; 44nm) the specific heat capacity shows a similar behavior as pure DGEBA (solid line in figure 6.3), significant changes can be observed for samples involving glass matrices with pore sizes smaller than 44nm ($d = 20$; 10; 4nm). For the samples with larger pores the glass transition regimes practically coincide with the one of pure DGEBA, whereas the $c_p(T)$ branches corresponding to the glassy and liquid regimes respectively slightly deviate from the bulk behavior.

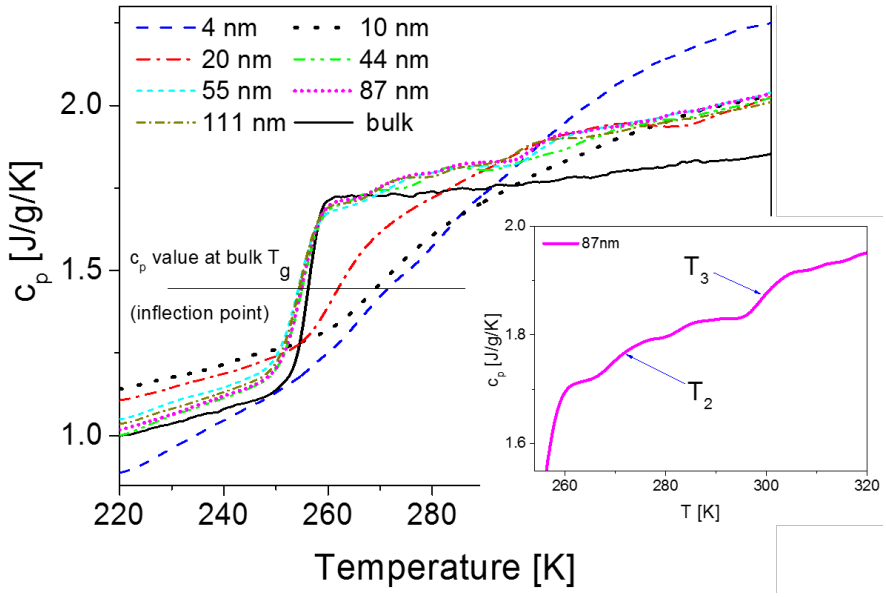

Figure 6.3: Corrected heat capacity measurements of all native filled samples (dotted lines) compared to the bulk DGEBA (solid black line) during heating from around 220K to around 345K. All curves are shifted on the y-axis to correspond to the DGEBA c_p value at the respective glass transition temperatures. The inset shows the evolution of c_p for the 87nm pore size at temperatures above the glass transition.

In the glassy regime the slopes $\left.\frac{dc_p}{dT}\right|_{pg/DGEBA}$ are slightly lower than in bulk while in the liquid regime there are several other changes visible. At temperatures around 270K and 300K respectively two further transitions seem to occur (these are marked in the inset of figure 6.3). These interesting effects will be dealt with in more detail in chapter 7 in comparison with the TMA measurements.

In contrast, for samples with pore sizes smaller than 44 nm the glass transition regimes no longer coincide with the one of pure DGEBA: the transition regime are considerably broadened and the glass transition temperature shifted to higher values. The smaller the pore size the larger is T_g. Interestingly the $c_p(T)$ curves corresponding to the 20nm-sized pores (red curve in figure 6.3) and the 10nm-sized pores (black dotted curve in figure 6.3) also merge with the liquid state branches obtained for the filled samples with larger pore sizes at approximately 290K and 320 K respectively. In the following the features exhibited by the liquid state branches of the $c_p(T)$ curves corresponding to the pg/DGEBA samples will often be addressed as $c_p(T)$-modulation.

Compared to the samples with 10nm-sized and 20nm-sized native pores, the glass transition of the 4nm samples (dashed blue line) occurs at a higher temperature. The transition is dramatically broadened and the step height Δc_p anomalously large even compared to pure DGEBA. Moreover, in contrast to the samples with larger pore sizes, the slope $\left.\frac{dc_p}{dT}\right|_{pg/DGEBA}$ of the glassy regime branch is comparable to the bulk value. Regarding the big Δc_p value of the 4 nm curve (resulting from the anomalous behavior of the 4 nm-sample in the glassy and liquid state) it has to be stressed that the mass of the DGEBA inside the glass matrix (d=4 nm) is only 15% of the empty porous glass. As a consequence of this rather modest fill-factor which is due to the low porosity of the glass substrate ($\approx 30\%$) the filled and empty samples differ only little one from the other. This makes the calculation of the difference yielding the specific heat capacity of the filled-in material erroneous.

Porous glasses with silanized pores

At first glance (in figure 6.4), in the systems with pore-sizes larger than 20nm, neither confinement nor silanization of the surfaces seem to take substantial influence on the molecular dynamics in DGEBA: the glass transition regimes practically coincide with the one of the filler.

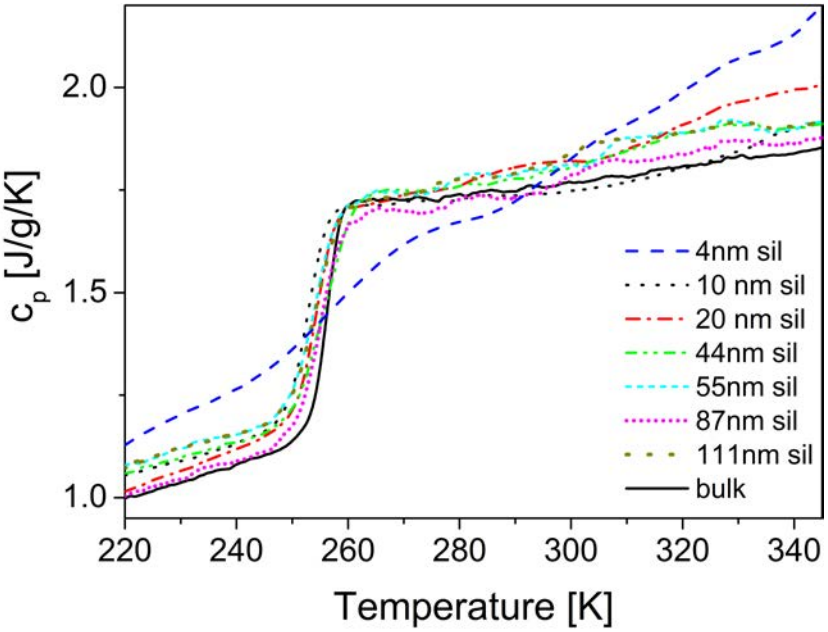

Figure 6.4: Corrected heat capacity measurements of all silanized filled samples (dotted lines) compared to the bulk DGEBA (solid black line) during heating from around 220K to around 345K. As above all curves are shifted on the y-axis to correspond to the DGEBA c_p value at the respective glass transition temperatures.

The behavior of the 4nm sample (strong broadening of the glass transition compared to the other samples) is particular and will be discussed later. With decreasing pore size the fraction of DGEBA molecules in the vicinity or in contact with the pore walls increases. Apparently the weakening of interfacial interactions (H-bonding) as a result of surface treatment leads to an increase of molecular mobility and hence to the same or slightly lower glass transition temperature as in pure DGEBA. The argument stating that in the glass matrices with silanized pore walls confinement practically has no influence on the molecular dynamics of DGEBA (with the exception of the 4 nm system) also allows for understanding the absence of broadening of the glass transition regimes (in contrast to the pg/DGEBA systems with native pores). Moreover, in contrast to the finding on the samples with native pores, the slopes of the $c_p(T)$-branches corresponding to the glassy and liquid regimes are rather comparable to the respective slopes obtained for the bulk.

6.1 The glass transition and more in confined DGEBA

This section discusses the quantitative impact of confinement on the observed transitions. As explained in chapter 3.2.3 and shown for the case of the bulk (unconfined) DGEBA, the transitions were evaluated by looking at the temperature derivative of the heat capacity: $\frac{dc_p}{dT}$ (as the peak maxima correspond to the inflection points at T_g in c_p). This approach is best suited to glass transitions which show a complex behaviour, e.g. due to broadening (for instance see $c_p(T)$ curves for pg/DGEBA systems with native pores ($d \leq 20nm$). As described before (see chapter 3), the main peak exhibited by the $\frac{dc_p}{dT}$-curve is fitted to a Gaussian for each investigated pg/DGEBA sample. The fits yield the glass transition temperatures which are represented as a function of the pore size in figure 6.5. The values are listed in table 6.1.

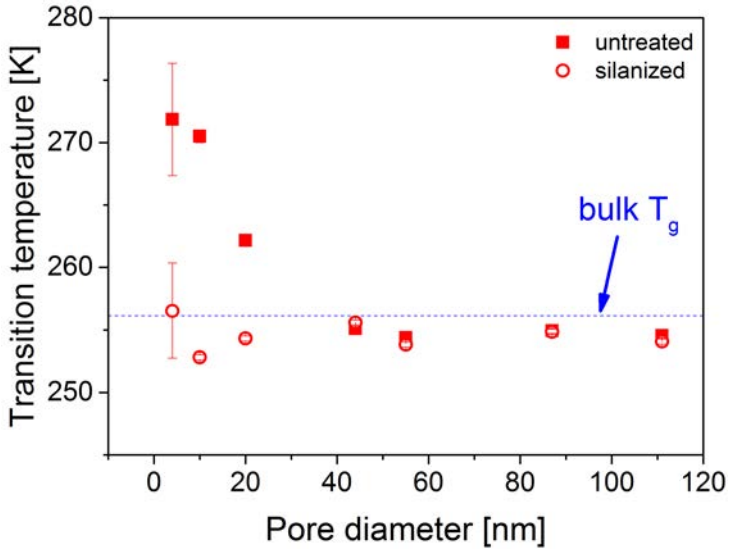

Figure 6.5: The glass transition temperatures determined from c_p are shown as a function of pore diameter. Solid squares mark the untreated pores compared to the open circles for the treated pores.

For the native pores (solid squares in figure 6.5), there is a clear increase of the glass transition temperature for pore sizes $d \leq 20nm$. In these systems the molecular dynamics are significantly slowed down compared to pure DGEBA and the pg/DGEBA samples with larger pore sizes (where T_g is independent of pore size). In pg/DGEBA systems with silanized pores (open circles in figure 6.5), T_g is practically independent of the pore size. All together these experimental facts allow to conclude that in the systems with

native pores, H-bonding of DGEBA molecules to the pore walls with far-reaching effects into the pore volumes, is responsible for the increase of the glass transition temperature, when the pore size is chosen sufficiently small. These observations and conclusions correspond to the results provided by many investigations described in literature and carried out on other systems of glass formers and porous matrices [30, 82]. In the systems with larger pores ($d \geq 40nm$) the surface to volume ratio is so small that the influence of interfacial interactions on the molecular dynamics of the major part of bulk DGEBA is negligible: T_g is independent of the pore size.

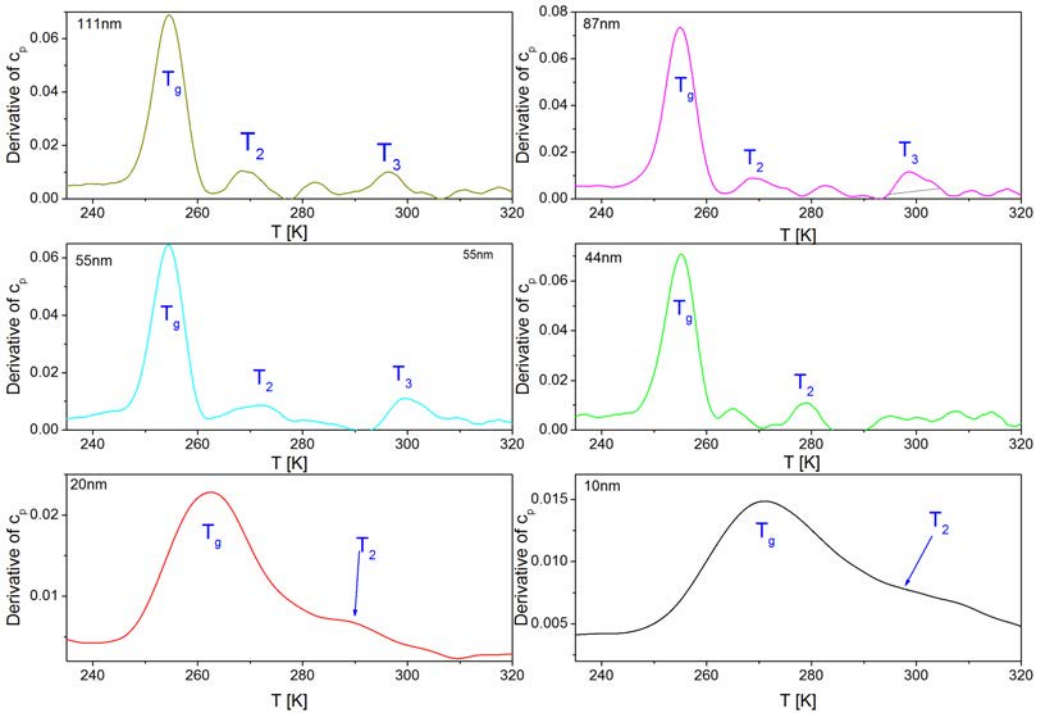

Figure 6.6: The temperature derivative of the heat capacity for the untreated pores: 111nm, 87nm, 55nm, 44nm, 20nm and 10nm. The large peak marks the main glass transition of the confined DGEBA with up to two small further peaks marking the further transitions T_2 and T_3.

Figure 6.6 shows for the pg/DGEBA untreated samples that, at temperatures higher than T_g , up two further transitions occur (the curves for the 4nm pores are shown in section 6.3). The temperatures T_2 and T_3 corresponding to the relative maxima of $\frac{dc_p}{dT}(T)$ are represented together with the main glass transition temperature T_g of all of the investigated samples in figure 6.7. The corresponding values are listed in table 6.1. It was not possible

to evaluate the two smaller peaks (at T_2 and T_3) for all of the investigated samples as they were sometimes too broadened and too small with respect to the background, so that they could not be resolved (as shown for the case of the 44nm pores in figure 6.6).

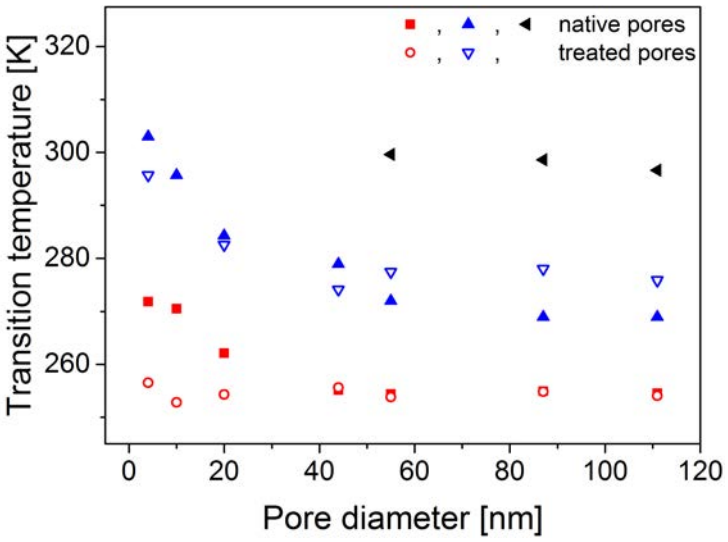

Figure 6.7: All the transition temperatures determined from the temperature derivative of the heat capacity are shown as a function of pore diameter. Solid symbols mark the untreated pores compared to the open symbols for the treated pores. The results marked in red are the maximum temperatures of the main peak associated with the main glass transition. The evolution of the 2nd identified peak is shown in blue while the third one is marked in black.

Pore size	T_g $[K]$		T^2 $[K]$		T^3 $[K]$	
	native	silanized	native	silanized	native	silanized
4nm	271.9(45)	256.5(38)	303(50)	295.7(33)		
10nm	270.5(5)	252.8(2)	295.7(8)			
20nm	262.1(4)	254.3(2)	284.3(7)	283.5(3)		
44nm	255.1(2)	255.6(2)	278.9(3)	274.2(5)		
55nm	254.4(2)	253.8(2)	272.1(3)	277.4(4)	299.6(3)	
87nm	255.0(2)	254.9(2)	269.0(3)	278.0(4)	298.6(3)	
111nm	254.6(2)	254.1(2)	268.9(3)	275.9(5)	296.6(3)	

Table 6.1: Transition temperatures determined for the range of pore sizes and surface treatments. The values are the peak maxima of gaussian fits of the temperature derivative of the respective heat capacity measurements. The errors were estimated from the results of several fits.

6.2 Cooling versus heating

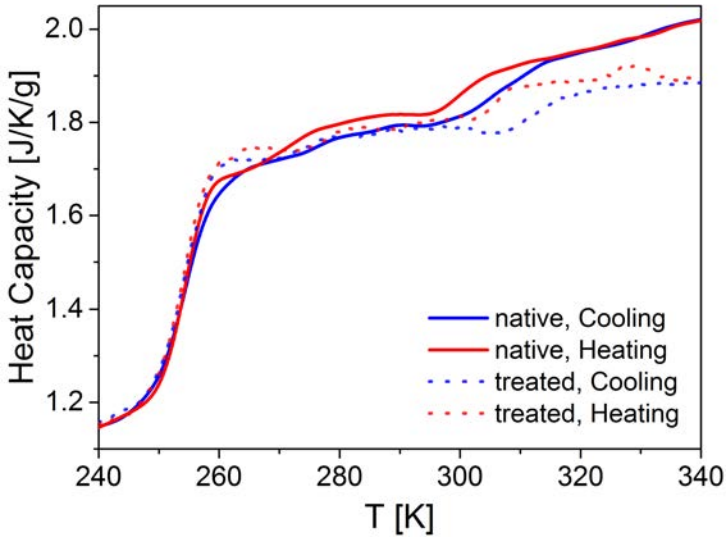

Figure 6.8: Heat capacity of the 55nm pores during cooling (blue curves) and heating (red curves) for the native pores (solid lines) and silanized pores (dashed lines).

It is of interest to see if there is any change while cooling the confined DGEBA to heating it up through the transitions. The $c_p(T)$ curves obtained during cooling and heating are exemplarily shown in figure 6.8 for pg/DGEBA samples with native and surface-treated pores ($d = 55nm$) respectively.

At the lowest temperatures there is no discernible difference in behavior between heating and cooling. This underligns the quality of the measured data. However, analogous to the results provided by TMA, at temperatures higher than T_g, there is a hysteresis visible between the cooling and heating runs.

DGEBA epoxy resins such as D332 (also from Dow Chemicals) can crystallize around 305K, especially when impurities are introduced. The hysteresis could therefore be an indication that some of the confined DGEBA crystallizes in the pores. However crystallization could be confirmed neither by DSC measurements (latent heat) nor by x-ray diffraction experiments.

To shed more light on the hysteris, the temperature evolution of the derivative of the specific heat capacity is shown in figure 6.9 (exemplarily for the pg/DGEBA sample with native pores ($d = 55nm$)).

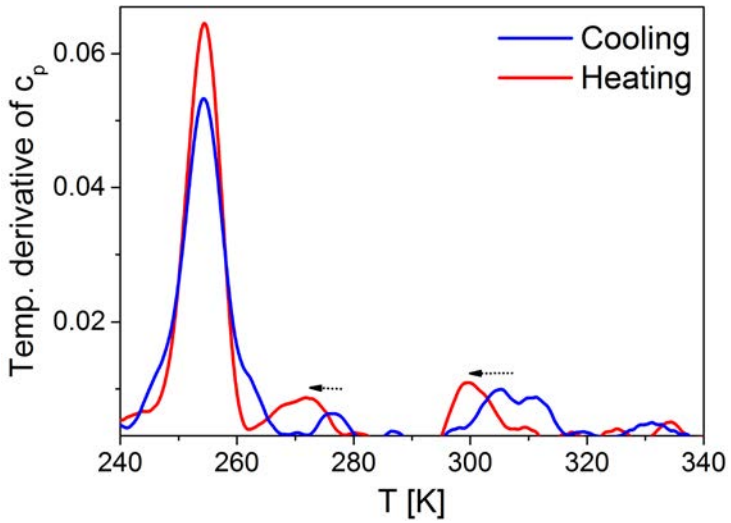

Figure 6.9: Comparison of the temperature derivative of the heat capacity during cooling (blue curve) and heating (red curve) for DGEBA confined in untreated 55nm pores.

Obviously the transitions occurring at higher temperatures ($T > T_g$) are slightly shifted towards lower temperatures while switching from cooling to heating. Thus the flow of DGEBA through the pores seems to be freezing in at higher temperatures and melting at slightly lower temperatures corresponding to an inverted undercooling. This is affecting the transitions of the shell layers. The hysteresis behavior described here above is reproducible from sample to sample and on a same sample over several measurement cycles. Possible explanations such as aging are discussed in comparison with the TMA results in chapter 7.

6.3 Small filler ratios and small pores

Accuracy of c_p values

For very small amounts of DGEBA filled into the porous glass matrix, the normalization of c_p to the resin content can cause problems as the heat capacities of both the porous and DGEBA are very similar: small differences in weight can cause large changes of the quantitative values calculated for the specific heat capacity.

This was especially the case for the samples with the smallest pores ($d = 4nm$) where the glass had a small total volume spanned by the pores. Even though the filling fraction was approximately 75%, the mass ratio m_{DGEBA}/m_{pg} (m_{DGEBA}: mass of DGEBA; m_{pg} : mass of empty porous glass) was only around 0.15.

To clarify the situation, figure 6.10 compares:

- The original (without normalization) $c_p(T)$ curves (solid lines) obtained for the pg/DGEBA samples with native pores ($d = 4nm$ and $d = 20nm$);

- The corresponding properly corrected $c_p(T)$ curves (dotted lines) and finally

- The $c_p(T)$ curve (dashed line) determined for the sample with 4nm-sized native pores after applying a correction which considers the sample as if it had the specifications of the 20nm sample, i.e. a much larger ratio m_{DGEBA}/m_{pg} .

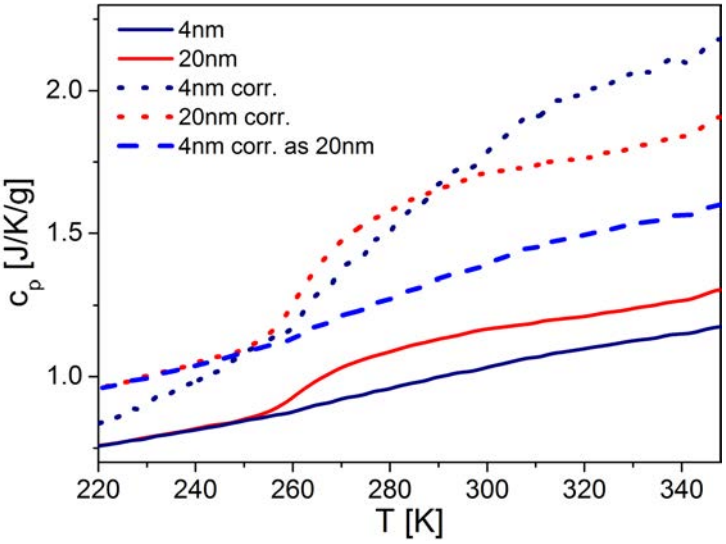

Figure 6.10: Heat capacity of 4nm (blue curves) and 20nm (red curves) native filled glass showing the original measurements (solid lines) and corrected for the heat capacity of the mass of the empty porous glasses (dotted lines). Additionally, the 4nm corrected heat capacity was calculated using the values for 20nm (dashed line).

Considering the $c_p(T)$ curve for the sample with $d = 4nm$ before correction (blue line in figure 6.10), one might argue that the glass transition is completely hindered by the confinement imposed by the small pores, as the curve almost seems linear. However after normalization to the DGEBA content, a glass transition can clearly be discerned though largely broadened. Finally, after correction taking a higher m_{DGEBA}/m_{pg} ratio (ca. 50%) into account, the glass transition can still be observed with a substantially reduced relaxation strength.

The comparison of the three curves allows to understand that in cases where $m_{DGEBA} \ll m_{pg}$, small errors occurring during the weight determination can induce large fluctuations of the specific heat capacity of DGEBA and overestimations of the relaxation strength.

Determination of Δc_p

In case of the properly corrected specific heat capacity of the system with 4nm-sized native pores it also looks as if the step height Δc_p of the glass transition is much larger than the one for samples with larger pores (see figures 6.3 and 6.4). Such an observation would contradict results reported in literature [29, 81] stating that Δc_p diminishes with decreasing confinement

size results fitting well into the theoretical model allowing for the calculation of the size of cooperative rearranging regions (CRR) [48, 83]. The reduction of Δc_p results from the fact that at very small pore sizes (i. e. with confinement getting more and more substantial) the fraction of DGEBA molecules involved in the main glass transition at T_g is dramatically reduced. As a matter of fact when the pore sizes diminishes, the pore surface to pore volume ratio grows and an increasing number of filler molecules interacts with the pore surfaces interaction leading to shell layers with proper (generally slowed down) molecular dynamics. For a sound evaluation of the relaxation strength Δc_p one has to take into account the evolutions of the liquid and glass branches of the $c_p(T)$ curves. As shown in chapter 3, Δc_p is generally calculated as the difference of the heat capacity values yielded by linear extrapolations (linear fits) of the liquid and glassy regime branches of $c_p(T)$ at the transition temperature T_g. This procedure is problematic in the case of the pg/DGEBA samples: as already discussed, at temperatures $T > T_g$, further transitions occur, overlap and lead to the complex $c_p(T)$-modulation observed in the liquid state of all of the investigated pg/DGEBA systems. In the next paragraph a procedure will be described which allows for an unambiguous determination of the relaxator strengths Δc_p for most of the samples, however as explained above, the large range of error for the 4nm samples means the value for Δc_p is extremely speculative and only an indication of the actual Δc_p in these pores.

Determination of transition width

Another problem is the determination of the transition width which very strongly depends on the temperature range selected for the evaluation. Here again the $c_p(T)$-modulation observed in the liquid state of all of the investigated pg/DGEBA systems but especially for the 4nm samples impedes a straightforward evaluation. In the next paragraph a method which allows for circumventing this problem will be presented.

Role played by the weight of DGEBA filled into the pores

The samples with 4nm-sized pores could usually be filled with up to 4.5mg of DGEBA. Such a weight is normally enough to ensure a good heat flow signal when performing calorimetry. This assumption was tested with a measurement realized on a pure DGEBA sample with a mass of 1.8mg. The test measurement did not reveal a substantial deviation from results obtained in experiments involving larger DGEBA masses. However here the bad conductivity of the porous glass (with a mass around 30mg) means that the error

due to a low mass of glass forming material is much larger than for the case of the pure bulk.

Excepting the problem caused by a very small amount of DGEBA in the pores, there are other features to be considered for playing a role in the systems with the smallest pores. Figure 6.11 shows the $c_p(T)$-curve of DGEBA filled into a porous glass matrix with silanized 4nm-sized pores (solid black curve) together with the temperature evolution of its derivative (dashed red curve).

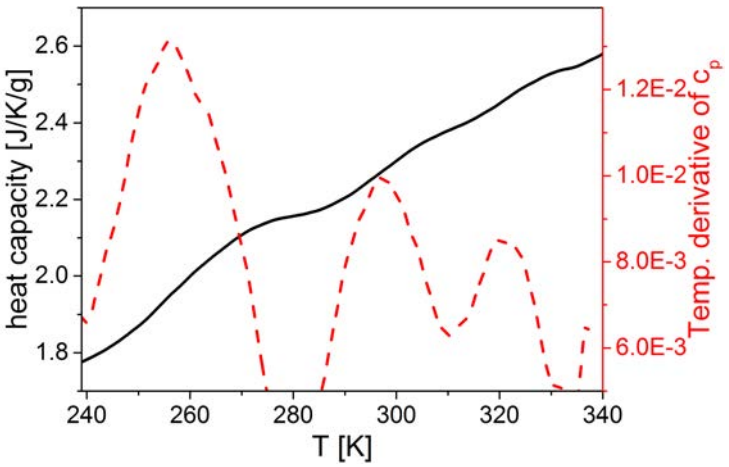

Figure 6.11: The heat capacity (black solid curve) and its temperature derivative (red dashed curve) are shown for DGEBA confined in silanized 4nm pores.

While normally a well-defined glass transition with dominant strength would be expected to occur as described for the surface-treated systems with larger pore sizes, three distinct transitions with approximately the same relative strength can be observed.

There are at least two reasons behind this specific behavior. Firstly, as the pore size is not so much larger than the DGEBA molecule, the number of DGEBA molecules contributing to relaxation processes is significantly reduced. Secondly, in both the porous glasses with large and small pore sizes the distribution of pore sizes is polydisperse. Though the silane agent is quite small, surface treatment can enhance the polydispersity by reducing pore volumes. Creation of bottleneck pores is possible too. The smaller the pore size the larger the surface to volume ratio: the fraction of DGEBA molecules involved in interfacial interactions increases. Hence, in the pg/DGEBA systems, downscaling of pore size is expected to reduce the ratio of the relaxation strengths associated to the DGEBA core and the DGEBA shell respectively.

Also, in porous glasses with smaller pore sizes, the morphology and roughness of the pore walls come into play much more strongly: an increasing number of molecules can be trapped by the surface.

6.4 Further information from c_p

6.4.1 Step height in c_p during the glass transition

In addition to the transition temperatures supplementary information can be gathered from the heat capacity measurements. Especially the step-like change in cp characterizing the transition of the samples from the glassy to the liquid state (and vice versa) is a reliable indicator for the amount of material involved in the main glass transition.

As explained in the previous section Δc_p is generally obtained as the difference of the c_p values deduced at T_g from linear extrapolations of the $c_p(T)$ branches corresponding to the liquid and the glassy regime respectively. However as all of the pg/DGEBA samples, whether surface-treated or not, exhibited further transitions at temperatures $T > T_g$ (shell layers) which partly overlapped with the main glass transition, the accuracy of linear fits of the $c_p(T)$ branches corresponding to the respective liquid phases is very poor. To still gain a fair approximation of the relaxation strength for DGEBA under confinement, the difference between the linear extrapolation of the glassy regime branch of $c_p(T)$ at T_g and $c_p(T_g)$ is evaluated. Assuming that the transition is symmetrical Δc_p then corresponds to the double of the latter difference.

The determination of Δc_p is exemplarily illustrated in figure 6.12 for the pg/DGEBA samples with native pores of sizes 4 nm and 20 nm respectively.

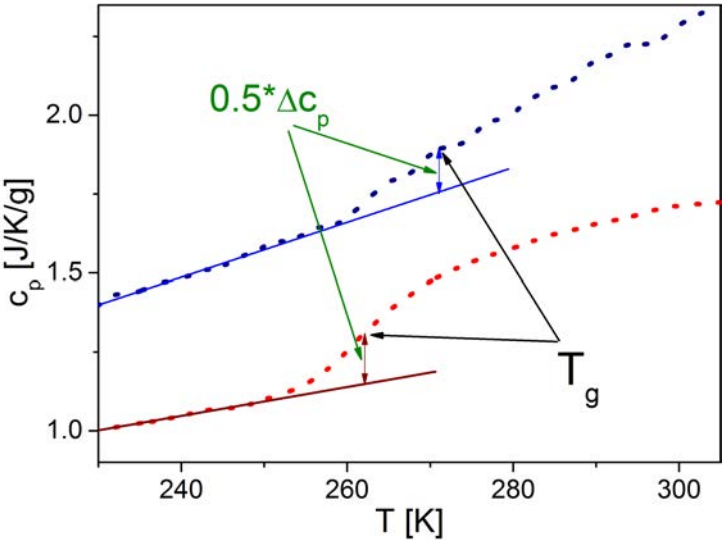

Figure 6.12: Heat capacity of DGEBA confined in untreated 4nm (blue dotted curve) and 20nm (red dotted line) pores. The 4nm curve is shifted on the y-axis. The c_p curve is fitted with a linear fit in the glassy regime. At T_g the difference in c_p between the curve and the linear fit is marked as $0.5 \cdot \Delta c_p$.

Here, as discussed above and shown in figure 6.12, the determination of Δc_p for the 4nm pores cannot be trusted quantitatively, but only used in the context of a general decrease of Δc_p for decreasing pore sizes.

The Δc_p values evaluated for all of the investigated pg/DGEBA systems are shown in figure 6.13 together with the relaxation strength corresponding to pure DGEBA All values are listed in table 6.2. The error bars in figure 6.13 were determined taking into account the scattering of the transition temperatures.

Δc_p $[J/K/g]$	4	10	20	44	55	87	111
native	0.25(9)	0.25(4)	0.33(4)	0.50(2)	0.49(2)	0.51(2)	0.50(2)
silanized	0.18(8)	0.50(2)	0.51(2)	0.52(2)	0.53(2)	0.53(2)	0.53(2)

Table 6.2: Step height Δc_p calculated as twice the step height in c_p between glassy c_p and c_p at T_g^1 for the range of pore sizes.

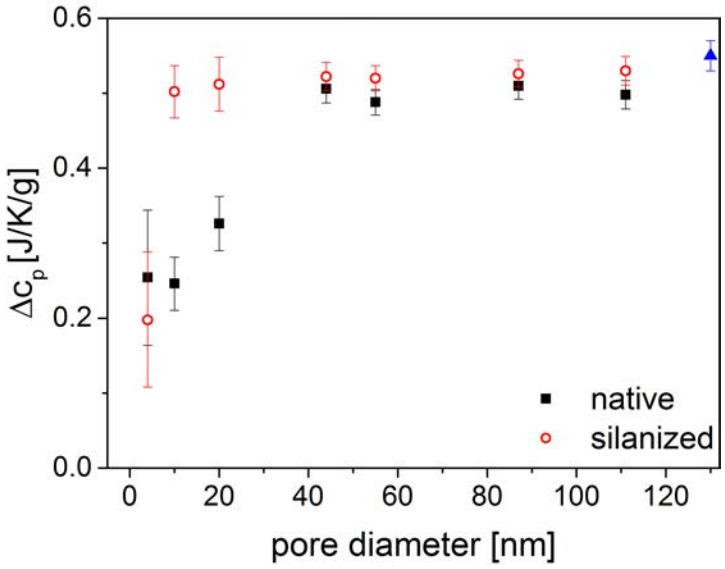

Figure 6.13: Δc_p plotted depending on the confining pore size for the untreated (closed black squares) and treated (red open circles) pores. The blue symbol marks the step height for bulk DGEBA.

For the untreated samples with pore sizes $d > 20nm$ there is a systematic, slight and more or less constant decrease of Δc_p with respect to the relaxation strength obtained for pure DGEBA (blue symbol in figure 6.13). This observation is in line with the previous conclusion that in the investigated untreated pg/DGEBA systems there is a small portion of DGEBA molecules forming a shell layer at the pore walls. As these shell layers become glassy at much higher temperatures than T_g these molecules do not contribute to the main glass transition anymore. In case of the systems with native pores ($d \leq 20nm$), Δc_p diminishes with decreasing pore size (and surface-to-volume ratio). This corresponds to the observations on the main glass transition which is increasingly slowed in the smallest pores. The values for the silanized samples are within the range of error of the pure unconfined DGEBA though maybe slightly decreased that could be due to some molecules still trapped at the lubricated surface and possible imperfect silanization. As expected for the surface-treated samples with pore sizes 10 nm and 20 nm respectively Δc_p approximately keeps the value determined for the systems with larger pore sizes ($d > 20nm$). This is no longer the case for the sample with silanized pores ($d = 4nm$): decreases at a value which is considerably smaller than the relaxation strength obtained for the sample with a pore size d = 10 nm fitting the observations on this sample shown in figure 6.11 with several smaller glass transitions. However the

non-monotonous behavior of Δc_p at 4nm should not be over-estimated: the larger error bar and other elements in these pores need to be considered as discussed above.

6.4.2 Size of the shell layer

In the pg/DGEBA systems with native pores the step height Δc_p at the glass transition of core DGEBA decreases with increasing surface to volume ratio (see figure 6.13). The direct determination of the step height Δc_p^{shell} associated to the glass transition of the shell layer from the $c_p(T)$ curves was generally not possible: the effect is too small and moreover overlapping with the other (flow) transitions. Therefore the assumption is made that Δc_p^{shell} approximately corresponds to the difference $\Delta c_p^{shell} \approx \Delta c_p^{bulk} - \Delta c_p$ between the step height Δc_p^{bulk} associated to the glass transition of bulk (unconfined) DGEBA and the step height Δc_p associated to the glass transition of core (confined but not in shell) DGEBA. With the knowledge of Δc_p^{shell} , the thickness of the shell layer d_{shell} can be estimated with the following equation according to Mckenna et al [38, 84]:

$$d_{shell} = \frac{d_{pores}}{2}\left[1 - \left(\frac{\Delta c_p}{\Delta c_p + \Delta c_p^{shell}} = \frac{\Delta c_p}{\Delta c_p^{bulk}}\right)^{0.5}\right] \tag{6.1}$$

Using Δc_p from the previous section, d_{shell} can be determined. The values are listed in table 6.3.

Pore size	d_{shell} $[nm]$	Volume fraction of shell
4nm	0.65(13)	0.546(317)
10nm	1.69(13)	0.561(123)
20nm	2.37(24)	0.418(94)
44nm	0.67(22)	0.061(62)
55nm	1.83(25)	0.129(49)
87nm	1.99(41)	0.089(39)
111nm	3.16(56)	0.111(35)

Table 6.3: Values for d_{shell} and the volume fraction of the shell layer calculated from Δ_p^{core} for the range of pore sizes. The errors were calculated using standard deviation.

Obviously the values, listed in table 6.3, strongly fluctuate. However if one considers the volume of the shell layer relative to the total pore volume, the calculated shell thickness seems to make sense. Under the assumption of

cylindrical pores with volume $V = \pi \cdot r^2 \cdot l$ the volume fraction of the shell layer can be calculated using the pore sizes and shell thicknesses. The values are listed in table 6.3 and plotted versus the pore size in figure 6.14.

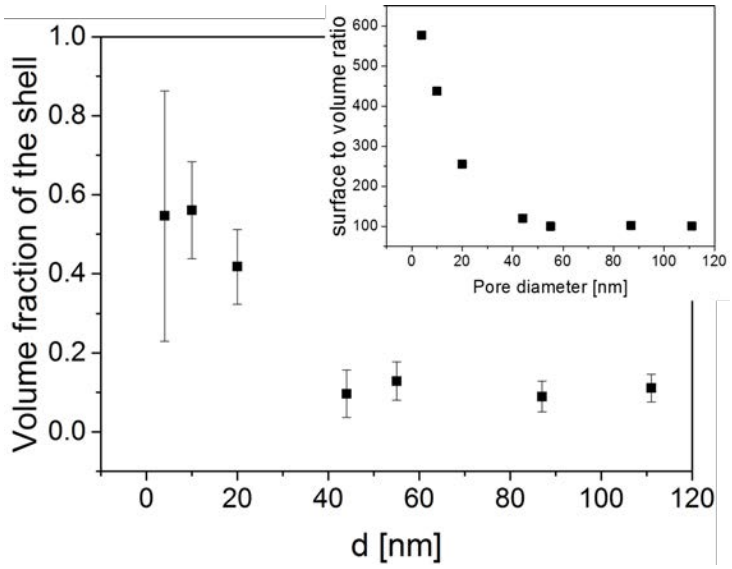

Figure 6.14: The volume fraction of the shell layer in the native pores compared to the total pore volume is plotted depending on the confining pore size for the pores. Inset: Surface to volume ratio as a function of pore size.

As expected the volume fraction occupied by the shell layer increases from approximately 10% (large pore sizes) to about 60% when the pore size is reduced below 20nm (again taking into account the large errors for the results of the 4nm systems). This evolution is in line with the growth of the surface to volume fraction of the pores with decreasing pore size. It also helps to understand why, at sufficiently low pore sizes, interfacial interactions dominate the molecular mobility and cause the increase of both the core and the shell glass transitions.

Similar results for the thickness and volume of the shell layer were observed by Mckenna et al [38] for the small molecule o-terphenyl and mixtures of o-terphenyl with polystyrene confined in porous glasses.

6.4.3 Broadening of the glass transition

Analogous to the evaluation of Δc_p , the modulation of the $c_p(T)$ values obtained for the liquid state of the pg/DGEBA samples, also impacts the

fits of the $\frac{dc_p}{dT}(T)$ peaks (see chapter 4 for the corresponding fit carried out for pure DGEBA) with the following Gaussian function:

$$y(T) = y_0 + \frac{A}{w \cdot \sqrt{\frac{\pi}{2}}} \cdot exp\left(-2 \cdot \left(\frac{T - T_g}{w}\right)^2\right) \tag{6.2}$$

with a constant A, the peak maximum T_g and the width w.

While the peak position can be defined rather unambiguously, the transition width $\delta T = w$ varies strongly depending on the temperature range used for the fit. As a matter of fact, in case of the pg/DGEBA systems, the right side of the peak ($T > T_g$) does not fit a Gaussian due to the mentioned $c_p(T)$-fluctuations caused by the upper transitions. C. Schick proposed a method to circumvent this problem by only fitting the peak to about 80% [85]. However his method was determined to circumvent the fluctuations in $c_p(T)$ due to vitrification on the left side of the glass transition fitting the glass transition peak mainly on the right side at higher temperatures. In the pg/DGEBA systems however, the fluctuations on the right side due to the flow transitions and the shell layer in the native pores are so large that the method proposed above was used for the left side neglecting the problem of further fluctuations at lower temperatures. This is exemplarily illustrated in figure 6.15 for the sample with native pores (d=55 nm): the main peak was fitted with a Gaussian only between the marked red lines.

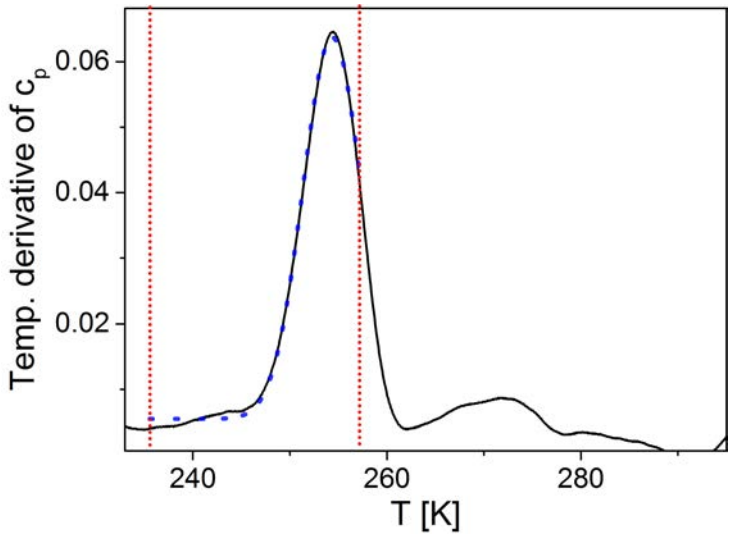

Figure 6.15: Gaussian fit (blue dotted curve) of the temperature derivative of the heat capacity (black curve) for 55nm native pores. The main peak was fitted within the temperature range delimited by the red lines.

While the left side of the peak ($T < T_g$) is completely within the evaluated range to establish the assumed correct background and height of the peak, the right side of the peak is only fitted to a temperature just above T_g to eliminate any distortion.

All the curves were evaluated in the same way leading to figure 6.16] where the transition widths are represented versus pore sizes (for the values see table 6.4). The peak width corresponding to pure DGEBA (marked in blue) is added for comparison. It was determined using the same partial temperature range as for the systems with confinement. As the curve obtained for neat DGEBA shows no asymmetry, the integral peak could also be fitted by a Gaussian. Both fits yielded the same value for the transition width. This finding shows that one can rely on the approach used here for the determination of the peak width.

Peak width w $[K]$	4	10	20	44	55	87	111
native	30.3	17.8	15.7	6.0	6.0	5.8	5.7
silanized	17.0	7.1	6.8	8.1	7.4	7.0	7.4

Table 6.4: The peak widths w identified from the Gaussian fits according to equation 6.2 for the investigated systems.

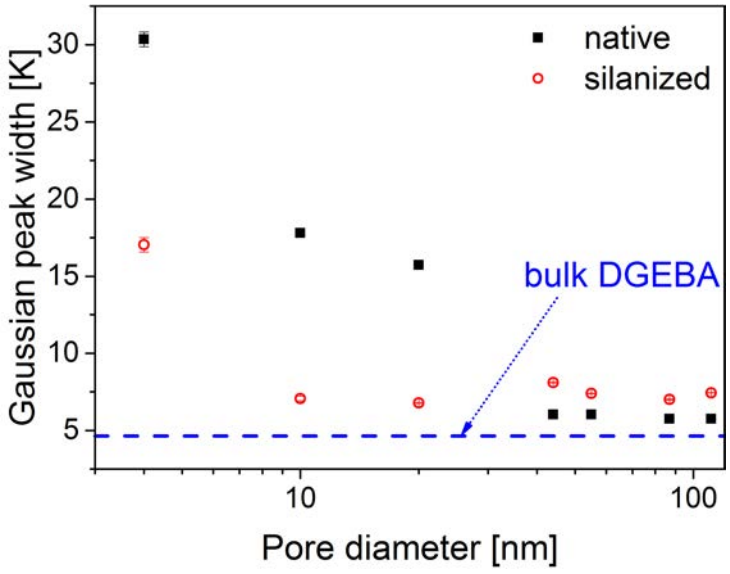

Figure 6.16: Fitted transition peak width plotted depending on the confining pore size for the untreated (closed black squares) and treated (red open circles) pores. The blue line marks the result for bulk DGEBA.

While for samples with large enough pore sizes Δc_p is equal to or drops to values slightly smaller than the relaxation strength measured for pure DGEBA , the transition widths of the pg/DGEBA systems ($d > 40nm$) are systematically and slightly larger compared to $\delta T = w$ determined for the neat resin. With decreasing pore size the width of the transition grows especially in the systems with native pores. In the samples with surface treatment only the transition width of the sample with the smallest pore size (d=4 nm) substantially deviates from the value evaluated for the systems with large pores.

6.4.4 Size of cooperating rearranging regions

The combination of the above results obtained from calorimetry for the transition temperature, step height and step width can be used to determine the possible length scale of the cooperative rearranging regions (CRR) involved in the glass transition as outlined in chapter 2. The most commonly accepted formula relating these factors is:

$$V = \frac{4}{3}\pi\xi^3 = \frac{k_B \cdot T_g^2 \cdot \Delta(1/c_p)}{\rho \cdot (w/2)^2} \tag{6.3}$$

with the Boltzmann constant k_B, the density ρ and $\Delta\,(1/c_p) = 1/c_{PG} - 1/c_{DGEBA}$.

Here only the results for DGEBA confined in silanized pores are used, as in the systems with native pores, interfacial interactions dominate the molecular dynamics so much, that the CRR sizes could not be compared to the value corresponding to bulk DGEBA. The ξ-values found for confined DGEBA are plotted in figure 6.17 as a function of the pore size.

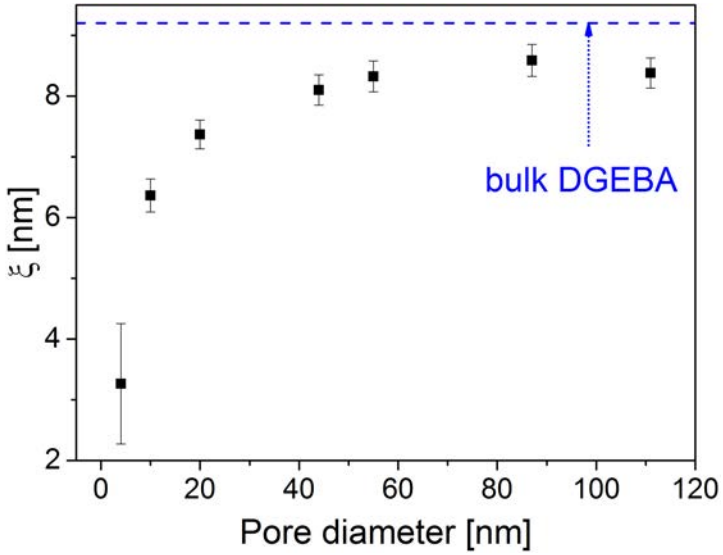

Figure 6.17: The calculated size of the CRR's ξ is plotted against the confining pore diameter for the silanized pores. The bulk value is marked in blue.

In case of the largest pores ($d \geq 44nm$), the characteristic lengths are comparable to the CRR size evaluated for bulk (unconfined) DGEBA and do not change very much. With confinement getting more important ($d < 44nm$), the characteristic length of the CRRs starts to decrease. At the smallest pore sizes, ξ finally takes values within the range of the pore sizes themselves: around 6nm in the system with 10nm-sized silanized pores and approximately 3 nm in the sample with 4nm sized pores (though this value has a very large error as discussed above).

From the theory dealing with dynamic heterogeneities in glass formers [24, 28] it is known that an acceleration of molecular dynamics has to be expected, when the length scale of confinement comes within the range of ξ. Thus, for the systems with the largest pores, confinement is expected to have no influence on the α-process of DGEBA. This is actually the case: results obtained from TMA e.g. confirm that, at pore sizes $d \geq 44nm$ the glass transition temperature of bulk DGEBA does not change with confinement. There is however a slight trend towards acceleration of molecular dynamics (decrease of T_g) which can be observed for the samples with 20nm- and 10nm-sized surface-treated pores (see figure 5.6). In these samples the characteristic length of the CRRs reaches values within the range of the pore sizes. Regarding the 4nm sample it has to be stressed once more that the characterization of the glass transition is very inaccurate due to the strong broadening of the transition.

The values represented in figure 6.17 seem to give a good approximation for ξ as they are in the range of length scales determined for other glass formers from experimental work and theoretical molecular dynamics simulations as presented in chapter 2. Donth et al for example saw similar dependencies of ξ on the pore size for a variety of glass formers [48, 83] though leading to slightly smaller characteristic lengths in the range of 2-3nm while others found values for ξ in the range of 6-12nm.

6.5 Summary

The dynamics of the confined DGEBA investigated with heat capacity measurements show evidence of additional phases compared to the bulk behavior. In the native porous glasses up to 3 separate transitions could be distinguished. The strongest transition is identified with the glass transition of a large part of the confined DGEBA molecules. For native pores, this transition is shifted to higher temperatures than in the bulk. The upshift of the glass transition temperature is increased with decreasing pore size. With surface treatment this upshift is suppressed, and the glass transition corresponds to the bulk measurements or is even slightly faster.

In the native pores, the step in heat capacity (Δc_p) through the glass transition decreases and the transition peaks are increasingly broadened with decreasing pore size. This result of the surface influence is negated with silanization so that the bulk behavior is approached.

In the silanized pores the characteristic length of the cooperative rearranging regions could be determined and showed a slight dependence on the pore size. This fits the picture of the CRR's for the glass transition where the increase in cooperativity with decreasing temperature is hindered in confinement.

Two extra phases at higher temperatures are seen at increasing temperature with decreasing pore size. The upper transition (at T_3) is probably evidence of a layer of DGEBA molecules at the pore walls forming a slowed shell around the core volume (T_g). The volume fraction of the slowed shell in the native pores could be approximated as more than 40% in the 10 and 20nm pg/DGEBA systems and around 10% in the larger pores $d \geq 40nm$. This third transition is negligible in the silanized pores as expected. The volume of the shell compared to the core confined DGEBA explains the large influence of surface effects propagating into the interior core confined DGEBA. In the smallest pores of 4nm size the surface boundaries and large surface to volume ratio mean that probably less than half the volume of DGEBA in the pores is involved in the core glass transition. The slowed molecules

in the shell play such a large role that a wide range of relaxation rates of the glass former appear even in the silanized pores. However the results in both 4nm pore sizes can only be treated as an estimation as there are large errors involved in the determination of the heat capacity for these samples. The second transition (at T_2) is tentatively identified with the flow transition seen in the dilatation results.

For both of these last transitions there was a hysteresis visible between cooling and heating measurements indicating there might be something like an aging effect involved. The shell layer becomes liquid at a lower temperature than it's glass transition during the cooling of the confined DGEBA. The flow of the DGEBA also melts earlier during heating than it's freezing upon cooling.

In the next chapter these results and those from thermomechanical analysis (chapter 5) are compared to clarify the observations on the dynamics of DGEBA filled in porous glasses.

7. Relaxation time-scales and further results

Results from thermo-mechanical analysis (TMA) and calorimetry (DSC-TOPEM) are compared in this chapter to get a better picture of the behavior of DGEBA confined in nanoporous glass matrices. After comparing the results provided by the two types of measurements, the glass transitions and flow transitions are evaluated quantitatively in the context of the proposed core-shell model of the glass former in the pores. This is followed by a discussion of the frequency dependency of the dynamic glass transition: broadband dielectric spectroscopic data added to the results from temperature modulated calorimetry allow for getting an overview on molecular dynamics in DGEBA extending over a large spectrum of time scales.

7.1 Comparison of TMA and DSC

Up to two glass transitions and two transitions called flow transitions could be identified from thermomechanical analysis of the filled porous glasses (chapter 5). These results corroborate the validity of the core-shell model which describes the behavior of the glass former in the native pores in an appropriate manner. With differential scanning calorimetry (TOPEM) up to three transitions passed through by confined DGEBA could be identified (chapter 6). The most important is clearly the glass transition of core (bulk) DGEBA in the pores. The two further transitions have so far been associated to changes in the flow behavior of the DGEBA molecules and to the glass transition of a shell layer formed by the filler molecules. Ideally this shell layer should not play any role in the systems with surface-treated pores (to ease the comparison with the native pores and the bulk DGEBA, the DGEBA in confined silanized pores is also denoted as core DGEBA though without a corresponding shell).

In figure 7.1 the evolutions of the length and specific heat capacity as a function of temperature are compared exemplarily for a sample with 55nm-

sized native pores.

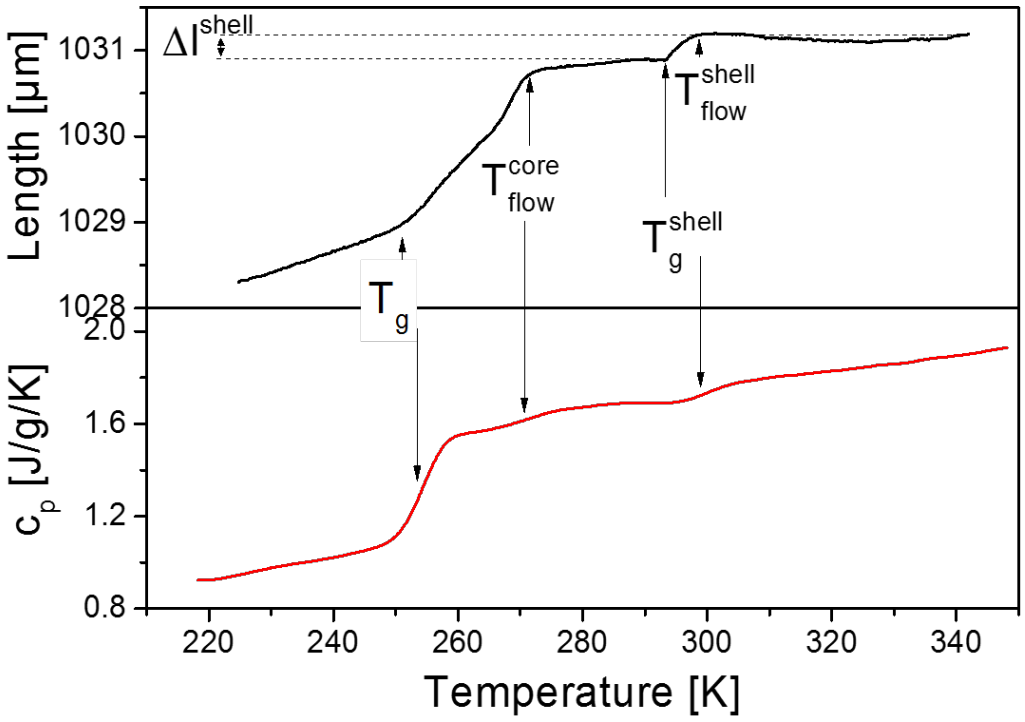

Figure 7.1: The expansion and the heat capacity of the 55nm native sample are plotted as a function of temperature. The various transitions observed in the course of the measurement are marked with arrows.

The main features (core glass transition, shell layer glass transition, flow transition of bulk DGEBA) observed in the thermo-mechanical experiment also show up in the $c_p(T)$ curve in similar temperature regions. Regarding the lack of coincidence of the marked characteristic temperatures it has to be stressed that the calorimetric measurements were dynamic measurements with a probe frequency of 4mHz whereas the thermo-mechanical experiments were static measurements using a temperature ramp. As a consequence the characteristic temperatures obtained from the evaluation of the $c_p(T)$ curves generally lie at higher temperatures than the corresponding transition temperatures evaluated from the length curves. The shell layer flow transition cannot clearly be distinguished in the $c_p(T)$ curve. This can be due to the fact that the amount of DGEBA in the shell layer is small.

7.1.1 Quantitative analysis of the core glass transition

The glass transition of the core DGEBA is the most pronounced event to be observed in both, the evolution of the specific heat capacity and the evolution of the adjusted length as a function of time. It is therefore the most accessible transition to analyze the influence of decreasing pore sizes and surface treatment. The dependence of T_g on the pore size yielded by DSC and TMA is plotted in figure 7.2 (results from sections 5 and 6, listed in tables 5.1 and 6.1).

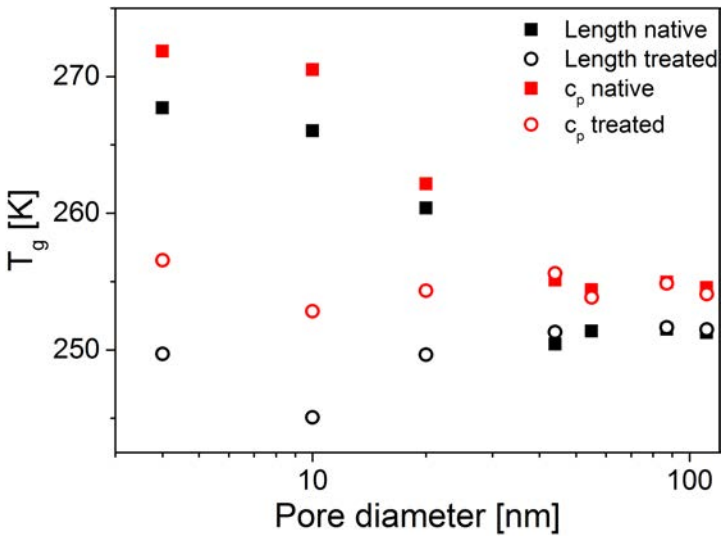

Figure 7.2: The core glass transition temperatures measured in TMA (Length: black symbols) and DSC (c_p: red symbols) are plotted for the range of pore diameters on a logarithmic scale. Solid squares mark the results for untreated (native) porous glasses compared to the treated (silanized) pores (open circles).

A logarithmic scale is chosen for the pore sizes. This representation allows for a better comparison of the results obtained at small and large pore sizes. Obviously TMA and DSC measurement provide glass transition temperatures of bulk DGEBA which qualitatively follow the same behavior when the pore size changes.

Both methods thus confirm that in the systems with native pores, the molecular dynamics of core DGEBA start to slow down when the pore sizes are sufficiently small($d < 44nm$). The lower the pore size, the larger is the surface to volume ratio characterizing the nanoporous structure. As a consequence, with decreasing pore size, the fraction of filler molecules in contact with or in vicinity to the pore wall becomes increases. Hence, at

the lowest pore sizes, an important part of core DGEBA inside the pores is sensitive to interfacial interactions or at least their direct effects.

Both methods also confirm that in the systems with silanized pores, T_g is practically independent of the degree of confinement. Interestingly the dependencies of the glass transition temperature on the pore size yielded by TMA as well as DSC exhibit the same fine structure at the lowest pore sizes. Obviously T_g tends to decrease below the glass transition temperature of unconfined DGEBA, when the pore size changes from 44nm to 10 nm. The observed acceleration of molecular dynamics is possibly due to the fact that at the lowest pore sizes the confinement length scale approaches the one of cooperative rearranging regions. Similar findings have been observed in literature for several materials [29, 86]. Regarding the glass transition temperature found for the system with 4nm-sized silanized pores it has to be stressed that the transition is extremely broadened. An accurate determination of T_g is difficult.

7.1.2 The flow transitions

Looking once more at the adjusted length versus temperature curve in figure 7.1, the most striking event to be observed is certainly the transition from a regime ($T_{flow}^{core} < T < T_g^{shell}$) where core DGEBA can flow rather freely through the pores to a regime ($T_g < T < T_{flow}^{core}$) where the macroscopic flow of core DGEBA is hindered (DGEBA still staying in a liquid state). As already mentioned, this transition, which is characterized by an important slope change clearly visible in $L_a(T)$, is due to the mismatch of the thermal expansion coefficients of core DGEBA and the porous glass ($\alpha_{DGEBA} \approx 5.5 \cdot 10^{-4} K^{-1}$ and $\alpha_{Porousglass} \approx 8 \cdot 10^{-7} K^{-1}$). As $T_g < T < T_{flow}^{core}$, bulk DGEBA, which can no longer adjust its density to temperature changes within the experimental timescale, exerts forces on the porous glass causing it to expand or contract (depending on the sign of the heating rate) much more than expected for an empty porous glass. From a thermodynamic point of view the transition implies a change from constant volume conditions ($T_g < T < T_{flow}^{core}$) to constant pressure conditions ($T_{flow}^{core} < T < T_g^{shell}$) during measurements of the specific heat capacity. This paradigm shift manifests itself in the $c_p(T)$ curve (see figure 7.1) by a modest kink which fairly coincides with the emergence of the bulk flow transition observed in the $L_a(T)$ curve. The second peak seen in the temperature derivative of $c_p(T)$ (figure 6.6 in section 6) seems to correspond to the core flow transition though this is not true for all investigated samples especially the 4nm pores where no corresponding flow transition temperature was observed in TMA (figure 5.3) and therefore the peaks solely correspond to glass transitions of core and shell layers. The

temperatures T_{flow}^{core} extracted from both methods are plotted in figure 7.3 for the samples with native as well surface-treated pores.

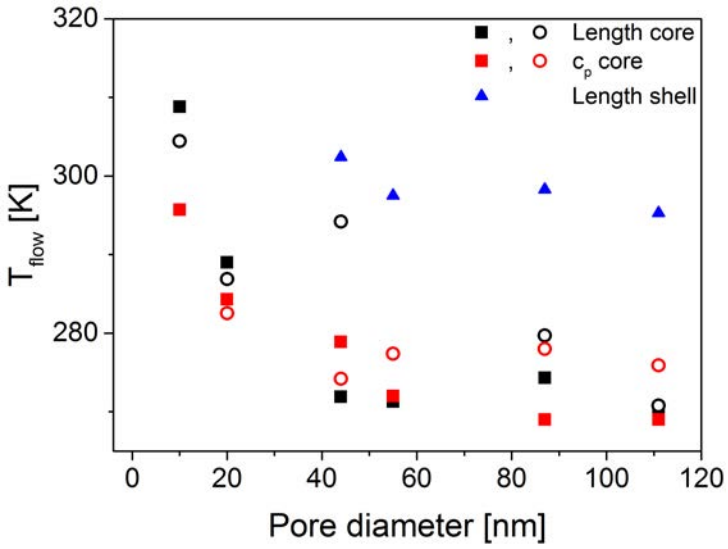

Figure 7.3: The flow transition temperatures identified from the expansion are plotted dependent on the pore size: T_{flow}^{core} as black squares and T_{flow}^{shell} as blue triangles. The flow transitions seen in c_p are plotted in red (circles). Results from untreated porous glasses as solid symbols, treated porous glasses as open symbols. Results from c_p without corresponding values from the length measurements are circled in blue.

Irrespective of the experimental method, the core flow transition temperature remains approximately constant (around 275K) for pore sizes larger than 20nm. For the systems with smaller pores ($d \leq 20nm$), the core flow transition could still be observed for the 20 nm- and just be suspected for 10nm-sized pores. In the latter systems T_{flow}^{core} increases with the confinement. Again the influence of surface properties of the porous glass is negligible or at least cannot be resolved. To conclude, the bulk flow transition is seen at similar temperatures in untreated and in treated porous glasses. Interestingly this experimental finding is in contrast to the behavior of the glass transition temperatures of bulk DGEBA with changing confinement: as already described, T_g increases with the confinement in the systems with native pores and practically keeps the value found for unconfined DGEBA in the samples with silanized surfaces (with even a modest trend to acceleration of molecular dynamics). It follows that only in the untreated samples a reduction of the pore size causes an increase of the viscosity of bulk DGEBA (due to the ef-

fect produced by interfacial interactions). Hence viscosity changes cannot be made the main responsible for the increase of T_{flow}^{core} at the lowest pore sizes. However flow through porous structures does not only depend on the viscosity of the liquid but also, and in much more pronounced way, on the pore size (Hagen-Poiseuilles law). The smaller the pore size, the slower the flow of DGEBA through the glass, the more time the filler needs to adjust its density to the temperature changes. As the pore size appears in Hagen-Poiseuilles law as d^4, its influence on the flow behavior surely plays a dominant role compared to the viscosity (which appears as η^{-1} in the same law). Relying on this explanation it can be understood that in the systems with the smallest pores, the bulk flow transition occurs at higher temperatures, irrespective of surface treatment.

For sake of completeness, figure 5.8 also shows the pore size dependency of the temperature T_{flow}^{shell} (blue triangles) corresponding to the shell layer flow transition. T_{flow}^{shell} could only be reliably determined for the systems with native pores using results from TMA. At large enough pore sizes ($d > 44nm$) the shell flow transition is independent of the pore size and occurs at a temperature exceeding T_{flow}^{core} by about 30K. In case of higher confinement, the shell layer transition could only be observed for 20nm-sized pores. For systems with still smaller pores the impact of the shell layer is shifted outside the range of the measurement. Analogous to the behavior of the bulk flow transition, the shell layer flow transition is shifted towards higher temperatures at low enough pore sizes.

7.1.3 Glass transition of the shell

From figure 7.1 it is known that both, TMA and DSC provide evidence for the existence of the shell layer glass transition. As already mentioned this additional glass transition occurs when the flow of the shell layer resulting from interfacial interactions between untreated pore walls and DGEBA molecules freezes. The glass transition temperatures T_g^{shell} have been evaluated from the length curves and partly also from the $c_p(T)$ data ($d \geq 55nm$). Figure 7.4 compares the respective results for different pore sizes.

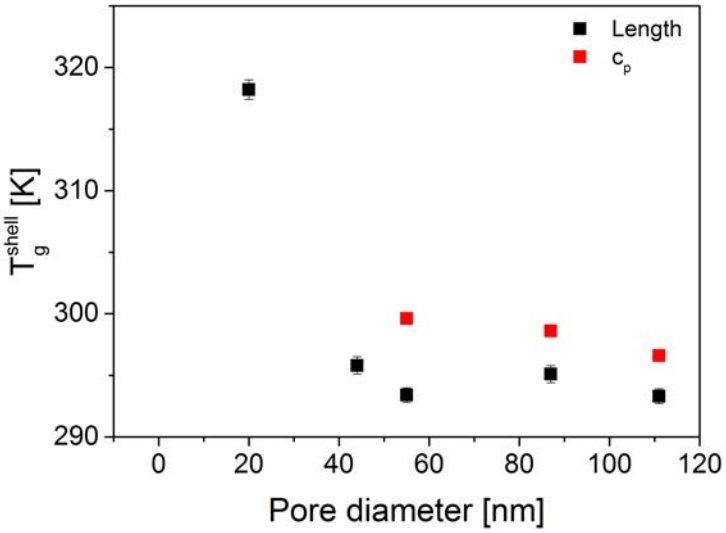

Figure 7.4: The glass transition temperature of the shell layers dependent on pore size is plotted for the expansion measurements (black symbols) and from heat capacity (red symbols). .

For the largest pore sizes ($d \geq 55nm$), T_g^{shell} is fairly constant. Obviously the transition temperatures obtained from calorimetric measurements are systematically higher than those evaluated from TMA data. This result does not surprise. As already explained, one has to take into account that c_p has been measured at a frequency of 4mHz while the length changes have been determined statically using a temperature ramp. Analogous to the behavior of the glass transition of bulk DGEBA ($T_g(d)$), only the T_g^{shell} value corresponding to the sample with 20nm-sized pores is increased.

7.2 Hysteresis

Combining the information from TMA and DSC is also helpful for the discussion of the hysteresis seen for the respective cooling and heating measurements.

Figure 7.5 allows the comparison of the behavior of the temperature derivative of the specific heat capacity with the evolution of the sample length of the pg/DGEBA system with 55nm-sized native pores.

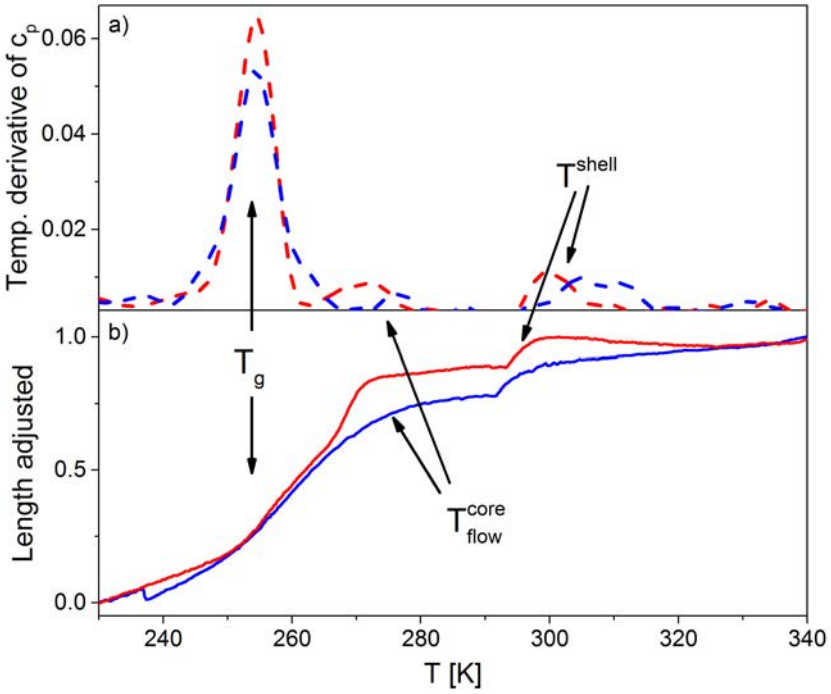

Figure 7.5: Plot of the temperature derivative of the heat capacity (figure a), dotted curves) and the expansion (figure b), solid curves) of the 55nm porous glasses for the cooling (blue curves) and heating measurements (red curves).

Obviously differences between cooling and heating measurements emerge around all of the glass and flow transitions. The length change at the flow transitions, especially at the bulk flow transition, seems to occur more gradually upon cooling than upon heating the sample. Moreover one can learn from the evolution of $\frac{dc_p}{dT}(T)$, that upon cooling the main glass transition (core DGEBA) is also slightly broadened. Aging could be a possible explanation though a much larger effect on the glass transition would be expected [87]. A simpler reason for the hysteresis might lie in the fact of the bad thermal conductivity of the porous glasses. The measurements are based on the assumption that the sample temperature is equal throughout the whole sample. However as the applied temperature is decreased, the filled porous glasses are cooled first at the extremities followed by the interior of the sample resulting in a temperature gradient within the samples. The transitions are therefore broadened.

7.3 Frequency dependence of the glass transition

Further information related to the glass transition can be gained from its frequency dependence. As temperature modulated DSC is limited to low frequencies in the mHz range, and the TMA (available at the laboratory) only allows to measure Youngs modulus at a fixed frequency (83mHz), dielectric spectroscopy was used to considerably extend the frequency range for the investigation of relaxation phenomena occurring in confined DGEBA. Dielectric measurements were performed at temperatures lower than 323K. Since at higher temperatures the electric conductivity of DGEBA starts to dominate the samples response to the applied electric fields.

The maxima of the imaginary part of the complex dielectric constant (loss peak maxima) are fitted with Havriliak-Negami functions as shown in chapter 3. The resulting values can be used to construct an Arrhenius diagram where $log_{10}(f) = log_{10}(\frac{1}{2\pi\tau_{max}})$ is represented as a function of $\frac{1000}{T}$.

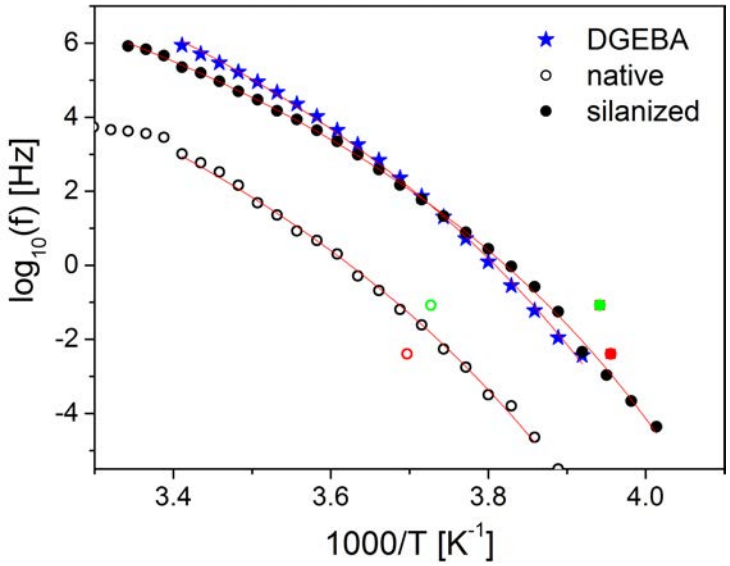

Figure 7.6: Arrhenius plot of the dielectric relaxations seen in the 10nm native (open circles) and treated pores (solid circles) compared to the bulk DGEBA (blue stars). VFT fits of the α peak are plotted in red. The results from DSC (red symbol) and TMA (green symbol) are added to the plot.

Figure 7.6 allows to compare the Arrhenius diagrams corresponding to the α-processes in unconfined DGEBA, the pg/DGEBA sample with 10nm-sized

native pores and the pg/DGEBA sample with 10nm-sized surface-treated pores.

It is well known [79] that unconfined DGEBA obeys to the empirical Vogel Fulcher Tammann law. Obviously both, the pg/DGEBA systems with native and silanized pores show a similar behavior. The corresponding VFT-fits are represented in figure 7.6. Regarding the activation plot of the sample with 10nm-sized native pores, the deviation of the Arrhenius diagram from the VFT-trace could correspond to the cross-over of the α and β-processes. What already was insinuated by results obtained from low-frequency calorimetric and TMA measurements is confirmed by dielectric spectroscopy for a broad range of frequencies: the molecular dynamics of the pg/DGEBA system with silanized pores are very close to those of unconfined DGEBA whereas the molecular dynamics of the sample with native pores (same pore size) are slowed down. It has to be stressed that the data from calorimetry and TMA only qualitatively fit to the activation plots obtained from dielectric spectroscopy. Most likely a mismatch of the temperature scales used in dielectric spectroscopy, calorimetry and TMA is responsible for the differences between the relaxation frequencies obtained by the various methods at a same temperature.

7.4 Summary

Only the comparison of the thermal expansion and differential scanning calorimetry results enables the complete identification of the different thermodynamic processes involved of the system of DGEBA confined in porous glasses. The model of a core and shell of DGEBA molecules especially in the pores with untreated surfaces could be confirmed. Both core and shell in the liquid-like regime undergo a flow transition where the equlibration of the negative pressure on the pore walls by the flow of the DGEBA through the pores is hindered below a certain temperature (within the timescale of the measurements). This flow transition is dependent on the confinement scale as the effect of the thermal expansion mismatch becomes more important with increasing surface-to-volume ratio (in decreasing pore diameters). However the increased negative pressure does not noticeably affect the glass former as the molecular dynamics in the native pores are dominated by the H-Bonds and van der Waals forces between the DGEBA molecules and the pores. These interfacial interactions result in significantly slowed relaxations which could be confirmed with dielectric spectroscopy.

In the silanized pores the glass transition is significantly decreased and comparable to the behavior of the bulk DGEBA with a possible slight size effect seen in the smaller pores resulting in slightly faster dynamics as the confinement comes within the range of the characteristic length associated with the cooperative rearranging regions at the glass transition. The frequency dependencies of the relaxations of confined DGEBA follow the expected behavior with slowed dynamics for the native systems and bulk-like or even slightly increased dynamics in the silanized pores.

8. Conclusions & Outlook

A wide variety of interesting phenomena has been observed in the investigation of the confinement of DGEBA in porous glasses depending on the pore size and the surface chemistry. This composite has been researched using thermomechanical analysis, calorimetry, and dielectric spectroscopy to gain insight into the flow and the glass transition of a confined glass former. Several competing effects play a role in the behavior of confined DGEBA and of the total system.

During the filling process of the untreated pores a Lucas-Washburn $\sqrt{t}$ dependence of the swelling of the pores is confirmed. In these native pores filled with DGEBA a significant influence of surface interactions was observed. This led to a broadened glass transition with decreasing pore size for a part of the DGEBA filled into the pores. The rest of the resin is identified as having adhered to the pore walls forming a significantly slowed surface layer with slowed glass dynamics. The volume of the shell layer was calculated to be up to around 50% of the confined DGEBA in the smallest untreated pores. This fact explains how the surface interactions, due to the formation of H-bonds, propagate far into the core, reducing the molecular dynamics as the pore size is decreased.

The shell layer practically disappeared for the pores which were treated with silane. The dynamics of the glass transition in the treated pores approached bulk behavior or is even slightly slowed as expected from finite size effects. Using these results a value for the inherent length scale of the glass dynamics was estimated which is within the range of estimations for various other materials from around $1-3nm$ [48, 81, 86] to $6-12nm$ [38, 88].

Taking these results together, and comparing them with investigations of other glass formers, it seems that the polar DGEBA interacts more strongly with the untreated pores than glass formers such as salol and toluene (some of the most commonly investigated low molecular weight materials in confinement) [45, 37, 82, 42, 39]. The model of a core and shell structure of the resin within the untreated pores with distinct glass transitions was established for these materials. However a much smaller increase or even a decrease of

the glass transition temperature of the core compared to the bulk material was observed in comparison to the presented results on confined DGEBA. It is therefore possible that for DGEBA in confinement, the dynamics are a mixture between distinct areas and a broad distribution of relaxation rates. Other investigations of confined glass formers could not distinguish separate transitions but merely one largely smeared change in dynamics [89, 30].

To really limit the surface interactions it would be interesting to substitute the porous glass with a porous structure of polymerized DGEBA and then investigate the filling with DGEBA. This could be achieved by filling silica pores with the DGEBA-DETA mix for polymerization and after the filler has hardened, leaching the silica resulting in a porous epoxy matrix. Going even further, the confinement of polymerized DGEBA could provide more insight into how the glass transition restricted geometrically is dependent on molecular weight.

A hitherto undiscussed aspect of the behavior of the composite is the observation of a significant change in slope of the thermal expansion independent of the glass transition. Above this slope change the glass former can flow macroscopically through the porous matrix during expansion as it adapts its density to the changes in temperature given by the experiment. As the system is cooled the flow is frozen while the DGEBA is still liquid. This incurs a contraction of the composite as the negative pressure from the mismatch of the thermal expansion coefficients of the components is not equilibrated anymore by the flow and the DGEBA then exerts forces on the pore matrix. For the native pores such a flow transition is apparent for both the core and shell layer and even distinguished in the heat capacity. Similar to the glass transition, decreasing confinement causes the flow transition to occur earlier, i.e. at higher temperatures than in the largest pores.

The same behavior for the flow was also seen in silanized pores. In the smallest pores ($d \leq 20nm$) the flow transition is still shifted to higher temperatures though the glass transition is the same or even decreased compared to the larger pores. Especially interesting is the case of DGEBA in the 20nm silanized pores where the glass transition is not yet influenced by finite size effects but is already hindered in its flow at higher temperatures than for pores $\geq 40nm$. These facts indicate that the flow is independent of both the surface treatment and the glass transition and influenced more strongly by the confinement size than the glass transition. This means that the flow is hindered by the geometrical restrictions which fits the interpretation that the flow transition coincides/can be identified with a change from a constant pressure regime to a constant volume regime in the pores at lower temperatures.

A corresponding variation in the thermal expansion can be seen in previous analysis of salol in porous glasses though it was not evaluated in the context of flow [22, 23]. However the idea of confinement and negative pressure affecting the density of the confined glass former has long been discussed in the context of the reduction of the glass transition temperature [29, 84, 48, 82]. Direct measurements of the density by neutron scattering [40, 82] and estimations of the negative pressure [23, 45, 90] showed evidence of a decrease in density compared to the bulk though not of a magnitude and scale needed to influence the glass transition. Investigations of how the time scale of the temperature changes affects the density changes [91] showed that, as could be expected, the density could equilibrate the temperature variations much better for significantly slowed measurements with heating rates of $0.01K/\text{min}$. This could affect the flow transition, though such a small heating rate could as yet not be implemented due to experimental constraints.

The behavior of the liquid is impacted at much higher temperatures than previously assumed indicating that the filling process and experiments need to be adjusted and possibly include a much broader temperature regime and slower heating rates. In light of this new information about the flow of a glass forming liquid it would be interesting to note what happens with the expansion and flow in other systems. As yet there are not many investigations of the thermal expansion of glass formers in porous systems which can prove valuable in completing the picture of all the different effects.

Bibliography

[1] C.T. Kresge, M.E. Leonowicz, W.J. Roth, J.C. Vartuli, and J.S. Beck. Ordered mesoporous molecular sieves synthesized by a liquid-crystal template mechanism. *nature*, 359(6397):710–712, 1992. 5

[2] R. Ryoo, S.H. Joo, and J.M. Kim. Energetically favored formation of MCM-48 from cationic-neutral surfactant mixtures. *The Journal of Physical Chemistry B*, 103(35):7435–7440, 1999. 5

[3] P. Yang, T. Deng, D. Zhao, P. Feng, D. Pine, B.F. Chmelka, G.M. Whitesides, and G.D. Stucky. Hierarchically ordered oxides. *Science*, 282(5397):2244–2246, 1998. 5

[4] Thomson Reuters. Science watch, tracking trends and performance in research since 1989, 2014 predictions of nobel prize chemistry laureates, 2014. 5

[5] P.W. Anderson. Through the glass lightly. *Science*, 267(5204):1615–1616, 1995. 5

[6] G. Adam and J.H. Gibbs. On the temperature dependence of cooperative relaxation properties in glassforming liquids. *The journal of chemical physics*, 43(1):139–146, 1965. 5, 9

[7] S.K. Bhatia and D. Nicholson. Molecular transport in nanopores. *Journal of Chemical Physics*, 119(3):1719–1730, 2003. 6

[8] S.K. Bhatia and D. Nicholson. Transport of simple fluids in nanopores: Theory and simulation. *AIChE Journal*, 52(1):29–38, 2006. 6

[9] P. Huber, S. Grüner, C. Schäfer, K. Knorr, and A. V. Kityk. Rheology of liquids in nanopores: A study on the capillary rise of water, n-hexadecane and n-tetracosane in mesoporous silica. *European Physical Journal-Special Topics*, 141:101–105, 2007. 6, 7, 44

[10] S. Grüner, T. Hofmann, D. Wallacher, A.V. Kityk, and P. Huber. Capillary rise of water in hydrophilic nanopores. *Physical Review E*, 79(6), 2009. 6

[11] D.H. Bangham and N. Fakhoury. The expansion of charcoal accompanying sorption of gases and vapours. *Nature*, 122:681–682, 1928. 6, 7

[12] M. Erko, D. Wallacher, and O. Paris. Deformation mechanism of nanoporous materials upon water freezing and melting. *Applied Physics Letters*, 101(18):4, 2012. 6

[13] G. Guenther, J. Prass, O. Paris, and M. Schoen. Novel insights into nanopore deformation caused by capillary condensation. *Physical Review Letters*, 101(8), 2008. 6

[14] M. Schoen, O. Paris, G. Guenther, D. Müter, J. Prass, and P. Fratzl. Pore-lattice deformations in ordered mesoporous matrices: experimental studies and theoretical analysis. *Physical Chemistry Chemical Physics*, 12(37):11267–11279, 2010. 6, 8

[15] R. Lucas. Über das zeitgesetz des kapillaren aufstiegs von flüssigkeiten rate of capillary ascension of liquids. *Kolloid Z*, 23(15):15–22, 1918. 7, 44

[16] E.W. Washburn. The dynamics of capillary flow. *Physical review*, 17(3):273, 1921. 7, 44

[17] D.H. Bangham. The gibbs adsorption equation and adsorption on solids. *Transactions Faraday Society*, 33:805–811, 1937. 7

[18] P. Huber, K. Knorr, and A.V. Kityk. Capillary rise of liquids in nanopores. *Material Research Society Symposium Procedures*, 899E(N7.1), 2006. 8

[19] G.H. Findenegg, S. Jaehnert, D. Müter, J. Prass, and O. Paris. Fluid adsorption in ordered mesoporous solids determined by in situ small-angle x-ray scattering. *Physical Chemistry Chemical Physics*, 12(26):7211–7220, 2010. 8

[20] F. Audonnet, N. Brodie-Linder, D. Morineau, B. Frick, and C. Alba-Simionesco. From the capillary condensation to the glass transition of a confined molecular liquid: Case of toluene. *Journal of Non-Crystalline Solids*, 2014. 8, 13, 21

[21] J. Koppensteiner and W. Schranz. Dynamic mechanical analysis of confined glass-forming liquids. *Phase Transitions*, 83(9):744–757, 2010. 8, 17

[22] W. Schranz, M.R. Puica, J. Koppensteiner, H. Kabelka, and A.V. Kityk. Heterogeneous relaxation dynamics of nano-confined salol probed by dma. *Europhysics Letters*, 79(3):360031–360036, 2007. 8, 101

[23] J. Koppensteiner, W. Schranz, and M.R. Puica. Confinement effects on glass forming liquids probed by dynamic mechanical analysis. *Physical Review B*, 78(5):542031–542039, 2008. 8, 44, 101

[24] E. Donth. The size of cooperatively rearranging regions at the glass-transition. *Journal of Non-Crystalline Solids*, 53(3):325–330, 1982. 9, 10, 83

[25] J. H. Gibbs and E. A. DiMarzio. Nature of the glass transition and the glassy state. *The Journal of Chemical Physics*, 28(3):373–383, 1958. 9

[26] K Schröter. Characteristic length of glass transition heterogeneity from calorimetry. *Journal of non-crystalline solids*, 352(30):3249–3254, 2006. 10, 13

[27] C.L. Jackson and G.B. McKenna. The melting behavior of organic materials confined in porous solids. *Journal of Chemical Physics*, 93(12):9002–9011, 1990. 11

[28] D. Sappelt and J. Jackle. The cooperativity length in models for the glass transition. *Journal of Physics A: Mathematical and General*, 26(24):7325, 1993. 11, 83

[29] C.L. Jackson and G.B. McKenna. The glass-transition of organic liquids confined to small pores. *Journal of Non-Crystalline Solids*, 131:221–224, 1991. 11, 13, 52, 72, 90, 101

[30] R. Richert. *Dynamics of Nanoconfined Supercooled Liquids*, volume 62 of *Annual Review of Physical Chemistry*, pages 65–84. Annual Reviews, Palo Alto, 2011. 11, 67, 100

[31] B. Jerome, E. Cecchetto, N. R. de Souza, and A. L. Demirel. Relaxation dynamics in confined glasses. *Journal De Physique Iv*, 10(P7):227–232, 2000. 11

[32] C. Alba-Simionesco, B. Coasne, G. Dosseh, G. Dudziak, K.E. Gubbins, R. Radhakrishnan, and M. Sliwinska-Bartkowiak. Effects of confinement on freezing and melting. *Journal of Physics-Condensed Matter*, 18(6):R15–R68, 2006. 11

[33] F. Kremer. *Dynamics in Geometrical Confinement*. Springer, 2014. 11, 12

[34] S. Napolitano, S. Capponi, and B. Vanroy. Glassy dynamics of soft matter under 1d confinement: How irreversible adsorption affects molecular packing, mobility gradients and orientational polarization in thin films. *European physical journal E, Soft matter*, 36(6):9875–9875, 2013. 11

[35] G. Barut, P. Pissis, R. Pelster, and G. Nimtz. Glass transition in liquids: Two versus three-dimensional confinement. *Physical Review Letters*, 80(16):3543–3546, 1998. PRL. 11, 12

[36] P. Pissis, A. Kyritsis, G. Barut, R. Pelster, and G. Nimtz. Glass transition in 2- and 3-dimensionally confined liquids. *Journal of Non-Crystalline Solids*, 235:444–449, 1998. 11, 13

[37] O. Trofymluk, A.A. Levchenko, and A. Navrotsky. Interfacial effects on vitrification of confined glass-forming liquids. *Journal of Chemical Physics*, 123(19):1945091–1945098, 2005. 11, 99

[38] J.Y. Park and G.B. McKenna. Size and confinement effects on the glass transition behavior of polystyrene/o-terphenyl polymer solutions. *Physical Review B*, 61(10):6667–6676, 2000. 12, 78, 79, 99

[39] M. Arndt, R. Stannarius, W. Gorbatschow, and F. Kremer. Dielectric investigations of the dynamic glass transition in nanopores. *Physical Review E*, 54(5):5377–5390, 1996. 12, 13, 52, 99

[40] D. Morineau, Y. Xia, and C. Alba-Simionesco. Finite-size and surface effects on the glass transition of liquid toluene confined in cylindrical mesopores. *Journal of Chemical Physics*, 117(19):8966–8972, 2002. 12, 13, 101

[41] C. Le Quellec, G. Dosseh, F. Audonnet, N. Brodie-Linder, C. Alba-Simionesco, W. Haeussler, and B. Frick. Influence of surface interactions on the dynamics of the glass former ortho-terphenyl confined in nanoporous silica. *European Physical Journal-Special Topics*, 141:11–18, 2007. 12

[42] F. Kremer and R. Stannarius. Molecular dynamics of liquids in confinement. *Lecture Notes in Physics*, 634:275–300, 2004. 12, 13, 99

[43] J. Zhang, G. Liu, and J. Jonas. Effects of confinement on the glass transition temperature of molecular liquids. *The Journal of Physical Chemistry*, 96(8):3478–3480, 1992. 12

[44] S. L. Simon, J. Y. Park, and G. B. McKenna. Enthalpy recovery of a glass-forming liquid constrained in a nanoporous matrix: Negative pressure effects. *European Physical Journal E*, 8(2):209–216, 2002. 12

[45] J. Koppensteiner, W. Schranz, and M.A. Carpenter. Revealing the pure confinement effect in glass-forming liquids by dynamic mechanical analysis. *Physical Review B*, 81(2):242021–242028, 2010. 12, 99, 101

[46] J. Schuller, Y. B. Melnichenko, R. Richert, and E. W. Fischer. Dielectric studies of the glass-transition in porous-media. *Physical Review Letters*, 73(16):2224–2227, 1994. 13

[47] A. Huwe, M. Arndt, F. Kremer, C. Haggenmuller, and P. Behrens. Dielectric investigation of the molecular dynamics of propanediol in mesoporous silica materials. *Journal of Chemical Physics*, 107(22):9699, 1997. 13, 17

[48] E. Hempel, A. Huwe, K. Otto, F. Janowski, K. Schräter, and E. Donth. Characteristic length of glass transition from calorimetry for benzoin isobutylether in a series of nanometer pores. *Thermochimica Acta*, 337(1-2):163–168, 1999. 13, 73, 84, 99, 101

[49] Dow Chemicals. D.e.r. 331 product specification sheet. 15

[50] D. Enke, F. Janowski, and W. Schwieger. Porous glasses in the 21st century a short review. *Microporous and mesoporous materials*, 60(1):19–30, 2003. 15

[51] W.E.S. Turner and F. Winks. *The Influence of Borix Oxide on the Properties of Chemical and Heat-resisting Glasses.* Department of Glass Technology, University of Sheffield, 1926. 16

[52] P. Levitz, G. Ehret, S.K. Sinha, and J.M. Drake. Porous VYCOR glass - the microstructure as probed byelectron-microscopy,direct energy-transfer,small-angle and molecular adsorption. *Journal of Chemical Physics*, 95(8):6151–6161, 1991. Times Cited: 220. 16

[53] F. Janowski and D. Enke. Porous glasses. *Handbook of porous solids*, pages 1432–1542, 2002. 16

[54] A. Schönhals, H. Goering, and C. Schick. Segmental and chain dynamics of polymers: from the bulk to the confined state. *Journal of Non-Crystalline Solids*, 305(1-3):140–149, 2002. 17

[55] G. Blum, F. Kremer, T. Juworek, and G. Wegner. Molecular dynamics of poly (γ-octadecyl-co-methyl-l-glutamate) in ultrathin films and in the bulk. *Advanced Materials*, 7(12):1017–1020, 1995. 18

[56] S. Lowell. *Characterization of porous solids and powders: surface area, pore size and density*, volume 16. Springer, 2004. 18

[57] S. Brunauer, L.S. Deming, W.E. Deming, and E. Teller. On a theory of the van der waals adsorption of gases. *Journal of the American Chemical Society*, 62(7):1723–1732, 1940. 19

[58] J.H. De Boer, D.H. Everett, and F.S. Stone. The structure and properties of porous materials. *Butterworths, London*, 10:68, 1958. 19

[59] S. Brunauer, P. H. Emmett, and E. Teller. Adsorption of gases in multimolecular layers. *Journal of the American Chemical Society*, 60(2):309–319, 1938. 19

[60] I. Langmuir. Modelisation of adsorption. *Physical Revieuw*, 6:79–80, 1915. 19

[61] E. P Barrett, L. G Joyner, and P. Halenda. The determination of pore volume and area distributions in porous substances. i. computations from nitrogen isotherms. *Journal of the American Chemical society*, 73(1):373–380, 1951. 21

[62] R. Evans, U.M.B. Marconi, and P. Tarazona. Capillary condensation and adsorption in cylindrical and slit-like pores. *Journal of the Chemical Society, Faraday Transactions 2: Molecular and Chemical Physics*, 82(10):1763–1787, 1986. 21

[63] P.I. Ravikovitch, G.L. Haller, and A.V. Neimark. Density functional theory model for calculating pore size distributions: pore structure of nanoporous catalysts. *Advances in colloid and interface science*, 76:203–226, 1998. 21

[64] L.D. Gelb and K.E. Gubbins. Characterization of porous glasses: simulation models, adsorption isotherms, and the brunauer-emmett-teller analysis method. *Langmuir*, 14(8):2097–2111, 1998. 21

[65] T. Young. An essay on the cohesion of fluids. *Philosophical Transactions of the Royal Society of London*, pages 65–87, 1805. 23

[66] M. Reading, B.K. Hahn, and B.S. Crowe. Method and apparatus for modulated differential analysis, 1993. 24

[67] B. Wunderlich, Y. Jin, and A. Boller. Mathematical description of differential scanning calorimetry based on periodic temperature modulation. *Thermochimica acta*, 238:277–293, 1994. 24

[68] J. Schawe, T. Hütter, C. Heitz, I. Alig, and D. Lellinger. Stochastic temperature modulation: a new technique in temperature-modulated dsc. *Thermochimica Acta*, 446(1):147–155, 2006. 24, 25

[69] I. Fraga, S. Montserrat, and J.M. Hutchinson. Topem, a new temperature modulated dsc technique. *Journal of thermal analysis and calorimetry*, 87(1):119–124, 2007. 26

[70] F. Kremer and A. Schönhals. *Broadband dielectric spectroscopy*. Springer, 2003. 30

[71] P Debye. Part i. dielectric constant. energy absorption in dielectrics with polar molecules. *Trans. Faraday Soc.*, 30:679–684, 1934. 30

[72] S. Havriliak and S. Negami. A complex plane analysis of α-dispersions in some polymer systems. In *Journal of Polymer Science Part C: Polymer Symposia*, volume 14, pages 99–117. Wiley Online Library, 1966. 30

[73] K.S. Cole and R.H. Cole. Dispersion and absorption in dielectrics i. alternating current characteristics. *The Journal of Chemical Physics*, 9(4):341–351, 1941. 30

[74] D.W. Davidson and R.H. Cole. Dielectric relaxation in glycerol, propylene glycol, and n-propanol. *The Journal of Chemical Physics*, 19(12):1484–1490, 1951. 30

[75] X. Li, X. Fan, and S. Brandani. Difference in pore contact angle and the contact angle measured on a flat surface and in an open space. *Chemical Engineering Science*, 117(0):137–145, 2014. 38

[76] J. Baller, N. Becker, M. Ziehmer, M. Thomassey, B. Zielinski, U. Müller, and R. Sanctuary. Interactions between silica nanoparticles and an epoxy resin before and during network formation. *Polymer*, 50(14):3211–3219, 2009. 39

[77] R. Sanctuary, J. Baller, J.K. Krüger, D. Schäfer, R. Bactavatchalou, B. Wetzel, W. Possart, and P. Alnot. Complex specific heat capacity of two nanocomposite systems. *Thermochimica Acta*, 445(2):111–115, 2006. 39

[78] A. Budkowski, I.W. Hamley, and T. Koike. *ADVANCES IN POLYMER SCIENCE V148.: Interfaces crystallization viscoelasticity*, volume 148. Springer, 1999. 40

[79] S. Corezzi, M. Beiner, H. Huth, K. Schröter, S. Capaccioli, R. Casalini, D. Fioretto, and E. Donth. Two crossover regions in the dynamics of glass forming epoxy resins. *The Journal of chemical physics*, 117(5):2435–2448, 2002. 41, 96

[80] A. Kusmin, S. Grüner, A. Henschel, O. Holderer, J. Allgaier, D. Richter, and P. Huber. Evidence of a sticky boundary layer in nanochannels: A neutron spin echo study of n-Hexatriacontane and Poly(ethylene oxide) confined in porous silicon. *Journal of Physical Chemistry Letters*, 1(20):3116–3121, 2010. 44

[81] A. Schönhals, H. Goering, C. Schick, B. Frick, M. Mayorova, and R. Zorn. Segmental dynamics of poly(methyl phenyl siloxane) confined to nanoporous glasses. *European Physical Journal: Special Topics*, 141(1):255–259, 2007. 52, 72, 99

[82] C. Alba-Simionesco, G. Dosseh, E. Dumont, B. Frick, B. Geil, D. Morineau, V. Teboul, and Y. Xia. Confinement of molecular liquids: Consequences on thermodynamic, static and dynamical properties of benzene and toluene. *European Physical Journal E*, 12(1):19–28, 2003. 67, 99, 101

[83] E. Hempel, S. Vieweg, A. Huwe, K. Otto, C. Schick, and E. Donth. Characteristic length of glass transition from calorimetry in different confinements. *Journal De Physique IV*, 10(P7):79–82, 2000. 73, 84

[84] W. Zheng and S.L. Simon. Confinement effects on the glass transition of hydrogen bonded liquids. *Journal of Chemical Physics*, 127(19):11, 2007. 78, 101

[85] C. Schick. Glass transition under confinement-what can be learned from calorimetry. *European Physical Journal: Special Topics*, 189(1):3–36, 2010. 80

[86] A. Schönhals, H. Goering, C. Schick, B. Frick, and R. Zorn. Glass transition of polymers confined to nanoporous glasses. *Colloid and Polymer Science*, 282(8):882–891, 2004. 90, 99

[87] M. Henkel, M. Pleimling, and R. Sanctuary. *Ageing and the glass transition*, volume 716. Springer Science & Business Media, 2007. 94

[88] S. Cerveny, J. Mattsson, J. Swenson, and R. Bergman. Relaxations of hydrogen-bonded liquids confined in two-dimensional vermiculite clay. *Journal of Physical Chemistry B*, 108(31):11596–11603, 2004. 99

[89] A. Schönhals, H. Goering, C. Schick, B. Frick, and R. Zorn. Glassy dynamics of polymers confined to nanoporous glasses revealed by relaxational and scattering experiments. *European Physical Journal E*, 12(1):173–178, 2003. 100

[90] J. Koppensteiner and W. Schranz. Dynamic mechanical analysis of confined glass-forming liquids. *Phase Transitions*, 83(9):744–757, 2010. 101

[91] T. Blochowicz, E. Gouirand, S. Schramm, and B. Stuhn. Density and confinement effects of glass forming m-toluidine in nanoporous vycor investigated by depolarized dynamic light scattering. *The Journal of chemical physics*, 138(11):114501–114501, 2013. 101

Acknowledgements

I am especially grateful to my supervisors Roland Sanctuary and Jörg Baller for the possibility of doing my thesis in this interesting field. Thank you for your help, patience and guidance over the years. Especially Jörg also for all our nice discussions about physics and food!

I would like to thank Patrick Huber for being in my CET committee, as well as Christiane Alba-Simionesco and Andreas Michels for completing my jury. I hope you did not groan too much while reading my thesis!

To Carlo DiGiambattista and Rick Dannert: thank you so much for your moral support and discussions acting as my sounding boards for any ideas and problems. Also to Ulrich Müller and Jan Krüger, thank you for your guidance and always having an open ear for me.

Thank you to Jörg Schmauch and Marlena Filimon for your help with the SEM Measurements, and Benjamin Henx for Microscopy assistance.

Thank you Astrid for looking after me and all our administrative needs and so much more.

A big thank you goes to the whole LPCMAM team and the Physics Department for a fun time during my years with you all. Additionally to those already mentioned I am especially grateful to: Rymma Sushko, Olga Asthasheva, Robert Wagner, Ernest Apel for moral and technical support.

Many thanks also goes to my friends for support and encouragement, especially Johanna, Matthias, Sandra, Gregor and Andrej.

Thanks to my sisters, parents, and our extended family for everything. Merci Rabia for help, support, understanding and much more.